2009

Parametric study and optimization of diesel engine operation for low emissions using different injectors

Prashanth Kumar Karra
Iowa State University

2009

Parametric study and optimization of diesel engine operation for low emissions using different injectors

Prashanth Kumar Karra
Iowa State University

Parametric study and optimization of diesel engine operation for low emissions using different injectors

by

Prashanth Kumar Karra

A dissertation submitted to the graduate faculty

In partial fulfillment of the requirements for the degree of

DOCTOR OF PHILOSOPHY

Major: Mechanical Engineering

Program of Study Committee:
Song-Charng Kong, Major Professor
Terry Meyer
Michael Olsen
Hui Hu
Stuart Birrell

Iowa State University

Ames, Iowa

2009

TABLE OF CONTENTS

LIST OF FIGURES

LIST OF TABLES

ABSTRACT

The objective of this research was to develop advanced diesel combustion strategies for emissions reduction in a multi-cylinder diesel engine. The engine was equipped with an electronically-controlled, common-rail fuel injection system, and an exhaust gas recirculation (EGR) system. This experimental setup allowed a wide range of operating conditions to be explored.

Effects of various injector parameters with various EGR levels on emissions were studied. Injector parameters included the injector flow number, nozzle hole geometry (straight, convergent), and nozzle arrangement (6-hole, 10-hole, 16-hole). The included spray angle was kept constant at 133 deg. Other engine parameters included the EGR rate (0-41%), injection pressure (150-225 MPa), start of injection (SOI) (-20 to 5 ATDC), start of pilot injection (-40 to -15 ATDC), and pilot fuel percentage (0-25%).

For single injection operations, a simultaneous reduction of NOx and particulate matter (PM) was achieved by using high EGR (30%) with late injection timing (0 to 5 ATDC) at high injection pressures (150 MPa). For double injection operations, NOx and PM emissions were reduced using 30% EGR, 15% pilot injection at an early pilot timing (-30 ATDC) and late main injection (5 ATDC).

Injectors with low flow numbers were able to produce low emissions at high EGR levels (>35%) and high injection pressures (>150 MPa). The combustion was stable at these high EGR levels as the SOI was held at 0 ATDC. On the other hand, injectors with high flow numbers were not able to produce stable combustion at such high EGR levels with late SOI.

Small nozzle holes in the 10-hole injector helped reduce NOx and PM emissions significantly. However, a 16-hole injector with a similar nozzle hole diameter produced very high PM emissions due to poor air utilization.

To improve the speed of optimization for lower emissions, particle swarm optimization (PSO), a stochastic, population-based evolutionary optimization algorithm, was applied to both engine experiments and numerical simulation. The algorithm was tested using test functions that were used in the field of optimization to ensure reaching a global optimum. A merit function was defined to help reduce multiple emissions simultaneously. The PSO was found to be very effective in finding the optimal operating conditions for low emissions. The optimization usually took 40-70 experimental runs to find the optimum. High EGR levels, late main injection, and small pilot amount were suggested by the PSO. Multiple emissions were reduced simultaneously without a compromise in the brake specific fuel consumption. In some cases, the NOx and PM emissions were reduced to as low as 0.41 and 0.0092 g/kW-h, respectively. The operating conditions at this point were 34% EGR, 5 ATDC main SOI, -24 ATDC pilot SOI, and 5% pilot fuel.

The PSO was also integrated with an engine simulation code and applied to engine optimization numerically. The results showed that optimization of engine combustion using PSO with numerical simulation was an effective means in the development of future emission reduction strategies.

ACKNOWLEDGEMENTS

I would like to take this opportunity to express my gratitude to my major professor and adviser Dr.Song-Charng Kong for providing me an opportunity to work under his supervision. I also would like to thank him for providing timely help, feedback, and for motivating me to pursue my interests. I am also thankful to my POS committee members Dr. Terry R. Meyer, Dr. Michael G. Olsen, Dr. Hui Hu, and Dr. Stuart J. Birrell for serving in my dissertation committee, giving special effort and time to review my dissertation and providing useful suggestions and comments.

I would also like to acknowledge the financial and material support by John Deere. Their help in identifying the problem and setting up the laboratory is greatly appreciated.

This section would not be complete without acknowledging many people who have helped me in finishing this work. I would like to thank Jim Dautremont for his help in building the test cell and for providing valuable suggestions. In addition, I also would like to thank undergraduate students Travis Whigham, Derek Mullins, Nathan Uelner, Lukas Jon Shea for their dedicated work in the engines lab spending countless hours building the test cell. This work would not have been possible without their efforts. I would like to specially thank Noah Van Dam for his diligent work related to PSO and model calibrations. Finally, I would like to thank all members of Dr.Kong's research group and my colleagues at Iowa State University for all the help they have provided.

CHAPTER 1. INTRODUCTION

1.1 Background

Since its invention in late 1800s, the internal combustion (IC) engine has had a significant impact on society and has been the foundation for the successful development of many commercial technologies. It is reported that approximately 301 million automobiles are powered by IC engines worldwide in 2008 [1]. IC engines can deliver power in the range from 0.01 kW to approximately $20X10^3$ kW, based on their displacement. This flexibility allows IC engines to be used in various applications such as automobiles, trucks, locomotives, marine, aircrafts, and power generation. Because of its widespread applications and ages, the IC engine industry is very large and competitive [2].

Population and economic growth are usually the fundamental drivers of the energy demand. The overall energy need can be divided into four demand sectors. They are power generation, transportation, industrial, and residential. It was reported that each of these major demand sectors will experience considerable growth through 2030 [3]. The anticipated volume growth is the highest for the power generation sector followed by transportation sector. In the transportation sector, personal transportation, transportation of goods, non-road works such as construction and agriculture are mostly provided by IC engines. As the environmental concern rises and the demand for low-emissions vehicles increases, it has become a priority for the industry and scientific community to meet these challenges.

The diesel, i.e., compression-ignition (CI), engine is the prime power source in the transportation sector as it offers better fuel economy, power, and durability over the gasoline, i.e. spark-ignition (SI), engines. Approximately 94 percent of all freights in the U.S. are

moved by diesel power. Diesel engines are also the primary power source for non-road equipment including construction and agricultural equipment, marine vessels, and locomotives. While diesel engines are known for their efficiency and durability, they have certain environmental disadvantages over gasoline engines.

1.2 Motivation

The United States is the world's biggest consumer of oil, and over half of the oil is imported. Such dependence on foreign oils can lead to the national security issue. Thus, improving IC engine efficiency is important in reducing foreign oil dependency. Improving engine efficiency can also help reduce emissions of carbon dioxide (CO_2), which is a greenhouse gas although it is a complete combustion product.

Four major engine exhaust pollutants are carbon monoxide (CO), nitrogen oxides (NOx), hydrocarbons (HC), and particulate matter (PM) (also called soot). Of these emissions, SI engines emit significantly less PM than CI engines as fuel-air mixture in SI engines is homogeneous and combustion is stoichiometric. A three-way catalyst can be used to convert about 90-95% of CO, HC and NOx into CO_2, H_2O, and N_2. On the other hand, non-homogeneous combustion in CI engines results in a diffusion flame that leads to high NOx emissions, and the fuel rich region inside the jet leads to PM formation. However, CI engines do not emit as much CO and HC as SI engines because CI engines are operated in overall lean conditions and there is oxygen available to prevent incomplete combustion.

Research found that PM are carcinogenic and can elevate lung cancer rates in occupational groups exposed to diesel exhaust [4, 5]. NOx emissions can form nitric acid which contributes to acid rain. NOx will also react with volatile organic compounds in the

presence of sunlight to form ozone, a key component of smog. It was also reported that NOx can deplete the ozone layer at high altitudes and make the earth vulnerable to many kinds of harmful solar rays [6]. Regulations on engine exhaust emissions and fuel economy are now enforced around the world. The emission standards have been categorized according to the type of the engine, engine size, and its application.

There have been many studies on in-cylinder combustion to reduce diesel engine emissions. Simultaneous reduction of PM and NOx emissions from diesel engines is the biggest challenge faced by the industry. In order to reduce the NOx emissions, the local combustion temperature has to be kept below 2200 K, but PM emissions will increase at these reduced temperature levels. However, when the temperature is below 1650 K, both NOx and PM can be reduced simultaneously. This concept is referred to as low temperature combustion (LTC). Fuel injection plays an important role in determining the emissions. Oftentimes, the combustion is not sustainable and the brake power is reduced significantly when the engine is operating under LTC regimes. Modifying the fuel injection can improve the combustion stability while operating under LTC regimes. This study will explore LTC operation in diesel engines using various fuel injection strategies for reducing exhaust emissions while maintaining comparable engine efficiency.

1.3 Objectives

The objective of this research is to investigate the effect of different fuel injection strategies and engine operating parameters on diesel emissions. This study will also develop a methodology to optimize the operating parameters in order to meet the future emissions standards.

Previous studies showed that, depending on the injection strategy, exhaust gas recirculation (EGR) could be used to reduce NOx emissions [7]. Multiple fuel injections in conjunction with EGR was also found to reduce PM and NOx emissions simultaneously [8]. However, only limited literature is available on the effects of injector geometry on engine performance.

In this study, several approaches are introduced to improve the diesel combustion pattern to reduce primarily NOx and PM emissions. First, engine experiments were performed on a multi-cylinder diesel engine using baseline injectors. Then injectors with various nozzle geometries and sizes were tested to study their effects on emissions reduction. Performance of different injectors under various EGR, injection pressure, and double injection conditions was evaluated.

Response surface equations for NOx, PM and brake specific fuel consumption (BSFC) were derived to study effects of different variables on emissions. Interactions between these variables were also studied to determine the combined effect of variables on emissions. While response surfaces can predict the trend of emissions, they often failed to find the global optimum particularly when the surface is multi-dimensional. As it is impossible to test all the possible operating conditions on an engine, a particle swarm optimization (PSO) method will be used to optimize the operating conditions to reduce emissions.

CHAPTER 2. LITERATURE REVIEW

Diesel engines can offer better fuel economy and durability as compared to gasoline engines. While the high efficiency of diesel engines can benefit CO_2 emissions reduction, their PM and NOx emissions are subject to legislative limits due to their adverse effects on human health and environment. In the mean time, legislations also mandate the emissions of CO and HC [9].

Diesel combustion can be manipulated by many parameters such as EGR, injection pressure, and the injection profile. All these parameters will affect the combustion process, which in turn determines the emissions levels. Parameters which affect the combustion process are briefly explained below, followed by discussions on methods of optimizing engine performance for emissions reduction.

2.1 Exhaust Gas Recirculation (EGR)

A fraction of the exhaust gas are re-circulated from the exhaust to the intake system. This recycled exhaust is mixed with fresh intake air before the intake air enters the cylinder. It has been shown by previous studies that EGR can reduce NOx emissions by reducing the combustion temperature [10]. The NOx emissions are formed inside the cylinder at high temperature regions. According to the equation $Q= m.C_p.\Delta T$, the total temperature increase (ΔT) is affected by the specific heat (C_p) of the constituents of the gas. If the specific heat of the gas is higher, then the temperature increase of the gas will be reduced to keep the total heat release (Q) constant. The specific heat of water vapor (H_2O) and carbon dioxide (CO_2) are considerably higher than the specific heat of fresh air. When exhaust gas (containing H_2O and CO_2) is introduced into the cylinder, a lower gas temperature can be obtained leading to

a lower local combustion temperature and a reduction in total NOx. In the same time, oxygen availability is reduced when EGR is used. Reduced oxygen availability also reduces the NO formation as explained by Eq. (2.1), (2.2), and (2.3) below. The formation of NOx emissions can be described by the extended zeldovich mechanisms [11].

$$O + N_2 \longrightarrow NO + N \qquad (2.1)$$

$$N + O_2 \longrightarrow NO + O \qquad (2.2)$$

$$N + OH \longrightarrow NO + H \qquad (2.3)$$

The combined effect of equivalence ratio (Φ) and temperature (T) on soot and NOx formation was explained by Kamimoto and Bae [12] based on detailed chemistry modeling. In this study, a quantitative Φ-T map was created for NOx and soot by performing 0-D chemical kinetics calculations. The NOx and soot formation with respect to Φ and T are depicted in Figure 2.1. It can be seen that soot formation occurs under rich conditions ($\Phi > 2$) and temperature between 1700 and 2100 K. On the other hand, NOx is formed when combustion temperature is above 2200 K for $\Phi < 2$.

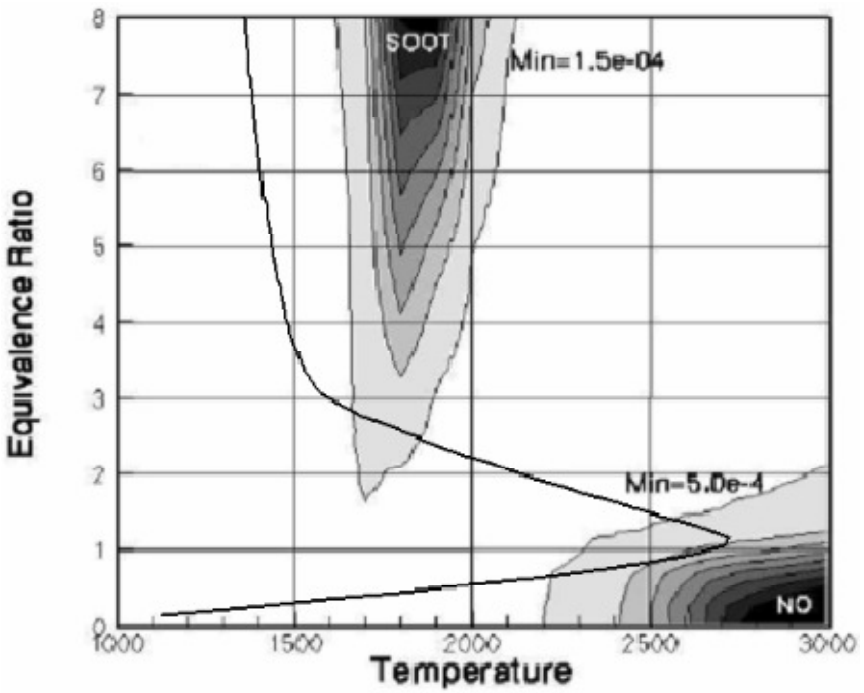

Figure 2.1 Soot and NO concentrations without EGR as a function of the equivalence ratio and temperature. Soot is in g/m^3, NO in mole fractions, and temperature in K.

The line in Figure 2.1 corresponds to the adiabatic flame temperature of diesel fuel with respect to the equivalence ratio. It can be noted from the figure that the adiabatic flame temperature needs to be less than 2200 K to avoid the NO formation at low equivalency ratios. At higher equivalence ratios, the temperature needs to be further reduced to avoid the formation of soot. If the temperature is kept below 1650 K, both NOx and soot formation can be avoided regardless of equivalence ratio. Figure 2.2 shows three adiabatic flame temperature paths for different compression ratios with 60 % EGR. The adiabatic flame temperatures shifted towards left with the use of EGR. As it can be seen from Figure 2.2, both NOx and soot are avoided by reducing the adiabatic flame temperature.

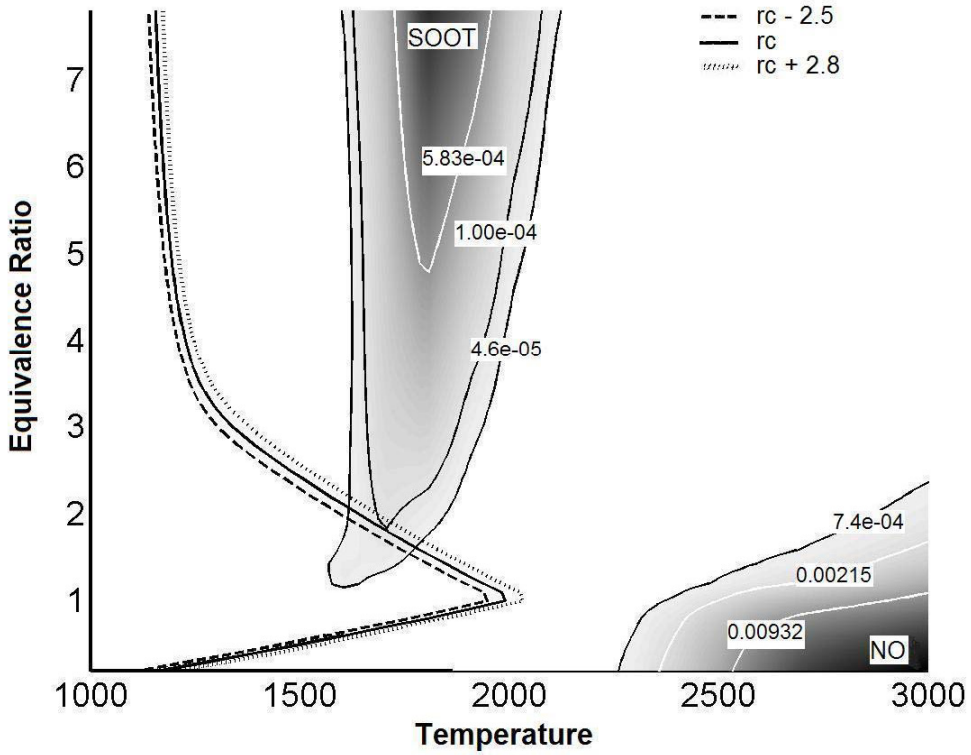

Figure 2.2 Soot and NO concentrations with 62% EGR as a function of equivalence ratio and temperature. Soot is in g/m^3, NO in mole fractions and temperature in K.

Exhaust gases (primarily CO_2 and H_2O) have higher specific heat (C_p) compared to the fresh intake air. This effectively reduces the combustion temperature and reduces the formation of NOx. There have been many studies on the effect of EGR on NOx and PM emissions in diesel engines. It was shown experimentally that EGR can reduce the oxygen flow rate to the engine [13]. This results in a reduced local flame temperature during combustion and, thus a reduced rate of NOx formation.

In addition to lowering the combustion temperature, EGR was also found to retard the start of combustion and alter the emission characteristics [14]. The delayed ignition has two advantages. It can reduce the cylinder pressure rise rates, which can reduce the combustion

noise as well as increase the mixing time, which can create more homogeneous mixture for PM reduction [15, 16].

2.2 Injection Pressure

The use of ultra high injection pressure can reduce the PM emissions. High injection pressure combined with micro-hole nozzle increases turbulent mixing for better fuel vaporization and PM reduction [17]. High injection pressure reduces the injection duration. Reduction in injection duration allows more time for fuel-air mixing to obtain a more homogeneous mixture. Better mixing leads to higher oxidation of PM and a reduction in the total PM emissions [18, 19]. However, due to high combustion temperatures associated with using high injection pressures, NOx formation increases. The use of EGR along with high injection pressure can reduce NOx formation while reducing PM [20]. Due to better atomization, CO and HC emissions can also be reduced. A small increase in BSFC was observed when high injection pressure was used. This is due to the increase in pump losses as the fuel pump is needed to increase the rail pressure.

2.3 Injector Geometry

The geometry of the nozzle in an injector plays an important role in controlling diesel spray atomization and combustion. Several nozzle parameters such as the nozzle hole diameter, the length-to-diameter ratio, and the roundness of the nozzle inlet will affect fuel atomization characteristics and combustion [21, 22]. The importance of the nozzle flow and its effects on spray atomization were discussed by Bergwerk [23]. Internal flow phenomena such as the velocity distribution inside the nozzle, turbulence, and cavitation inside the

nozzle can determine the disturbance level in the liquid jet at the nozzle exit [24, 25]. These initial disturbances will affect the liquid breakup, penetration, spray evaporation, and eventually ignition and combustion. Figure 2.3 depicts a typical combustion chamber and a piston in a diesel engine together with a high speed image of diesel spray.

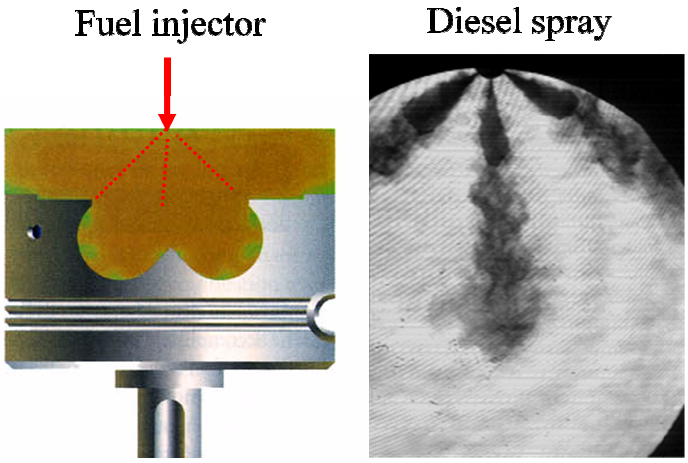

Figure 2.3 Fuel injector and diesel spray in a diesel engine.

Nozzles with large diameters are less efficient in atomizing fuel sprays compared to those with smaller diameters. However, small nozzles require a longer injection duration which could reduce combustion efficiency [26]. High injection pressures (150 – 200 MPa) can reduce the injection duration of small diameter nozzles by increasing the injection velocity.

The nozzle size will influence the fuel–air mixing process and therefore engine performance and emissions [27]. Pickett and Siebers [17] investigated the effects of nozzle hole diameter on PM formation in diesel engine environments. Nozzles with different diameters were tested in a constant volume chamber. It was found that PM formation can be reduced as the nozzle diameter was reduced. Numerical modeling using detailed chemistry also revealed that PM formation can be closely related to the lift–off length of the diesel

spray [28]. Meanwhile, the PM–NOx trade–off can be overcome by using high exhaust gas recirculation (EGR) to achieve low temperature combustion.

Another important characteristic of a nozzle is the variation in the nozzle cross–sectional area along its length. This geometrical characteristic can be defined by the conicity of the nozzle which is also called K–factor,

$$K = 100 \cdot \frac{(D_i - D_o)}{L} \qquad (2.3)$$

where D_i is the inlet diameter, D_o outlet diameter, and L the length of the nozzle.

Various studies have showed that the variation in the nozzle geometry can produce different fuel spray characteristics [21, 22, 29, 30]. Nurick [31] investigated the effect of nozzle inlet geometry on the nozzle flow. It was found that cavitation can be prevented by using a round–edge inlet nozzle with the ratio of inlet radius to nozzle diameter (R/D) larger than 0.14. Benajes et al. [32] conducted an experimental study to analyze the influence of different orifice geometries (conical and cylindrical) on the injection rate of a common–rail fuel injection system. It was found that the discharge coefficient was higher in the conical nozzle than that in the cylindrical nozzle. In addition, the flow in the cylindrical nozzle collapsed at high injection pressures due to cavitation that was not observed in the conical nozzle.

Literature on the effects of nozzle conicity on spray related issues such as cavitation and injection velocity is limited. Desantes et al. [33] tested three injector nozzles with different conicity (K = –0.2, 0, 1.1) for cavitation under different injection pressures and ambient pressures. Fuel flow rates and momentum fluxes at the nozzle exit were measured. The injection pressure was varied between 2 and 160 MPa.

It was found that, as K–factor increased, the tendency towards cavitation was reduced [33]. Cavitation was not evident for K=1.1. The mass flow rate can be reduced due to cavitation at high injection pressures. The momentum flux did not change as the K–factor of the nozzle changed, i.e., cavitation did not influence the momentum flux. Hence, the exit velocity was increased to compensate the reduced mass flow rate due to cavitation.

2.4 Double Injections

Splitting the injected fuel into a number of pulses can cause a change in the combustion characteristics. Appropriate configurations of multiple injections have shown to decrease PM emissions without a significant increase in NOx emissions. The availability of local oxygen can be improved greatly when fuel is injected multiple times. This is due to an increase in mixing time of air and fuel. An increase in local oxygen concentrations increases the oxidization of PM, leading to reduced PM emissions. Some optimal injections were found to have more fuel in early injections and less in subsequent injections [34-36]. These findings agree with results of Benajes et al. [37] who demonstrated that by using a post injection strategy, reduction in PM could be achieved without compromising NOx emissions or fuel consumption. Optimal injection strategies can be different for different operating conditions.

2.5 Optimization

Optimization is a process of maximizing or minimizing a mathematical function, an output of a process, or an objective function based on input variables that affect the process. Depending on the complexity of the function, many different types of optimizations can be

used. If the function can be expressed in the form of a mathematical function, differential calculus can be used to minimize or maximize the function [38]. However, there are several problems whose topology cannot be expressed in the form of a mathematical function. In such cases, methods such as response surface method (RSM), genetic algorithm (GA), and particle swarm optimization (PSO) can be used to examine the peaks and valleys of the design hyperspace.

Internal combustion engine operation is a good example of a system where the interaction between engine operating parameters (also called design variables) is so intertwined that a reliable response surface model is not available [39]. Particle swarm optimization (PSO) is a stochastic, population based evolutionary algorithm which can be used to find the maximum or minimum of a given function. RSM, GA, and PSO are explained below.

2.5.1 Response Surface Method

Response surface methodology comprises a group of statistical techniques for building of empirical models and model exploitation. By careful analysis of experiments, it creates a response, or a mathematical equation depicting the design variables and their interactions [40]. Once the response is created, search of the objective function hyperspace is started from one point to another. The direction of the optimization is determined by the direction of steepest decent for minimizing the objective function [41, 42]. This method is also called gradient search method.

Gradient search methods are applied to the response surface model to determine the path of steepest decent, which points in the direction of reducing the objective function value.

By following this path, the objective function will eventually downturn after reaching a local valley. At the valley, another factorial is applied to again investigate the local terrain. If another hyper plane with a discernable gradient can be applied, the optimization continues. If the response surface no longer appears planar, or appears relatively non-sloped, a local minimum is likely to exist nearby, and additional experiments with high resolution are performed to develop a curved surface model which is more accurate than the original model. This surface can then be searched with traditional mathematical methods [43].

This method is effective in finding a local minimum. However, it does not promise a global minimum. A good judgment on the part of the user is required to start the process at a good starting point. Starting at a poor point may result in finding only a local minimum if there is one in the vicinity [44]. In a study performed using response surface to optimize the engine emissions, it was reported that a good starting point was chosen which lies near the previously known optimum point [45]. In this study, a mathematical expression consisting of the several emissions is used as an objective function. This simplified the complicated problem of reducing different emissions into a search for maximization of the objective function.

2.5.2 Genetic Algorithm

Genetic algorithm is a search technique used to find exact or approximate solution of a given optimization problem. GA is a class of evolutionary algorithms inspired by evolutionary biology such as mutation, selection and crossover. A population that includes randomly selected citizens is allowed to evolve under pre-determined selection rules to maximize the fitness. Each citizen representing the input factor level is represented as a

sequence of 0's and 1's (binary encoding). Fitness value of each citizen is evaluated and fittest citizens are allowed to breed with some randomness to generate a new generation of citizens [46, 47].

Based on the differences in the application of mutation, GA can be divided into two distinct types, the simple GA and the micro-GA (μGA). The simple GA utilizes a population size of around 200 citizens in each generation [46]. If this type of GA is used, then few generations would require thousands of function evaluations. This method would be prohibitive when each function evaluation takes significant amount of time for experimental engine runs or 3-D computer simulations. A μGA on the other hand utilizes only around 5 individual citizens in each generation. The population is expected to converge relatively quickly. Several modifications such as elitism are used in combination with μGA to increase the likelihood of finding a global optimum while exploring throughout the search space.

The μGA was used by some researchers to reduce the engine emissions by optimizing the engine operating conditions. These studies included using the μGA on an experimental engine and 3D computer simulations. An experimental study done by Thiel et al. was able to meet the 2002/2004 emissions levels in a single cylinder experimental diesel engine [48]. In a similar study done by Liechty et al. in 2004, a single cylinder engine was coupled with μGA using a computer interface to automate the experiments. Several input variables including start-of-injection, EGR, boost pressure, multiple injection parameters were optimized to reduce the emissions. The optimum point was found in 31 generation with 5 citizens in each generation. The optimum resulted in emissions that had 2 times higher PM and NOx emissions compared to the 2007 EPA standards, but with an 8% reduction in fuel consumption [49].

2.5.3 Particle Swarm Optimization

Particle swarm optimization (PSO) is a stochastic, population based evolutionary algorithm for problem solving. This method was proposed in 1995 by social-psychology major James Kennedy and electrical engineer Russell Eberhart. PSO has roots in two main component methodologies. One is its ties to artificial life in general, and to bird flocking, fish schooling, and swarming theory in particular [50]. It is also related to evolutionary computation, and has ties to both genetic algorithms and evolutionary programming. Implementing PSO is computationally inexpensive in terms of memory and speed as it requires only primitive mathematical operators. Early tests have found the implementation of PSO to be effective with several kinds of problems. PSO has also been demonstrated to perform well on test functions used for validating genetic algorithm optimization [50, 51].

In theory, individual members of a school or a swarm can profit from discoveries and previous experience of all other members during search for food. During the original experiments with PSO, birds exhibited “flocking” characteristics such as synchronously changing direction and scattering and regrouping. This suggests that social sharing of information among co-existing members offer an evolutionary advantage [52, 53]. This hypothesis is fundamental to the development of PSO.

This model also contains an attraction factor to a roosting area. In these simulations, birds will begin to fly around without a particular destination and then spontaneously form flocks. This goes on until one bird fly over the roosting area. When the programmed “desire to roost” is higher than the “desire to stay in flock”, the bird will pull away and land.

A swarm of members is analogous to a set of design points and a design space. The position of a design point is influenced by defined neighbors. The "velocity" (speed and direction) of a design variable at the beginning of an iteration is given by:

$$V_{i+1} = V_i + C_1R_1 (Pbest_i - X_i) + C_2R_2 (Gbest - X_i) \quad (2.4)$$

The "velocity" will be used to determine the new value of a design variable as given below:

$$X_{i+1} = X_i + V_{i+1} \quad (2.5)$$

X is a design variable, i is the design variable number, R_1 and R_2 are random numbers between 0 and 1, C_1 and C_2 are constants (generally 2.0), $Pbest_i$ is the best value found by the design variable i, and Gbest is the best value in all previous iterations of any design variable (i.e. swarm member).

Attributes of particles are given as follows:

- Location of particle in the design space (i.e. co-ordinate or design variable value)
- Objective function value
- Velocity vector value
- Pbest
- Pbestold (Pbest from previous iteration)

The search for the optimal value is controlled in PSO by three different expressions.

$$V_{i+1} = V_i + C_1R_1 (Pbest_i - X_i) + C_2R_2 (Gbest - X_i) \quad (2.6)$$

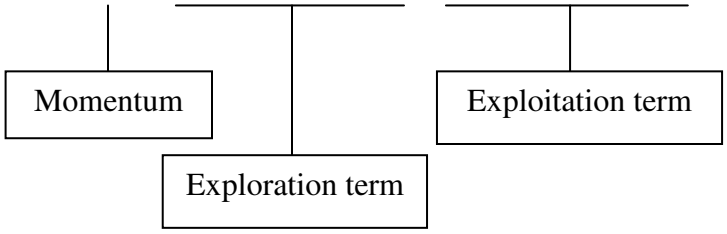

The momentum term keeps the velocity (value of design variable in the next iteration) from changing abruptly. The exploration term (Pbest) learns from its own experience from previous iterations. The exploitation term (Gbest) term learns from collaboration from all other members and all previous iterations. A limit on velocity (V) is enforced (Vmax) to restrict the value of design variable from going beyond the range of that design variable.

An inertia weight has been applied to Eq. (2.4) to control the impact of a particle's previous velocity on the calculation of the current velocity vector. The modified equation is shown in Eq. (2.7).

$$V_{i+1} = W_{iner}(V_i + C_1R_1\ (Pbest_i - X_i) + C_2R_2\ (Gbest - X_i)) \qquad (2.7)$$

A large value for W_{iner} facilitates global exploration, which is particularly useful for problems with complex design spaces. A small value allows for more localized searching, which is useful as the swarm moves toward the neighborhood of the optimum [54, 55]. A large value of 0.729 calculated using constriction factor method was used in this study to facilitate a global exploration of search space. The flow chart of PSO is given in Figure 2.4.

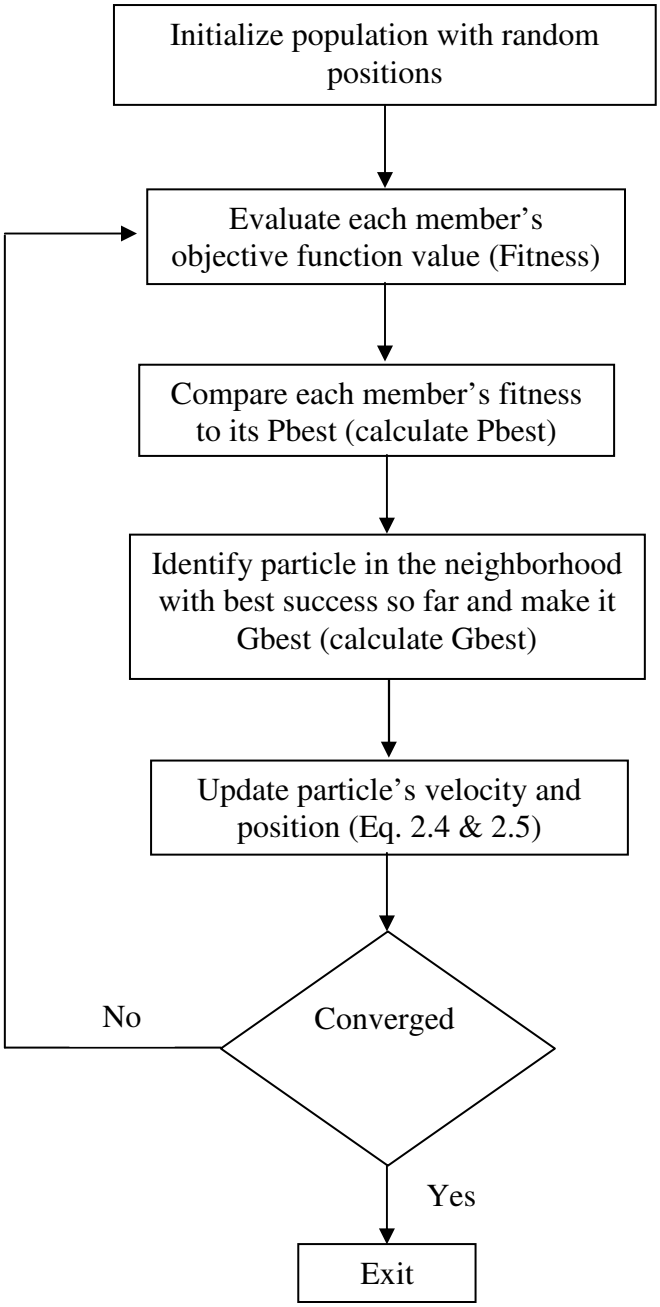

Figure 2.4 Flow chart of PSO optimization methodology.

CHAPTER 3. EXPERIMENTAL SETUP

Experiments were performed in this study using a John Deere 4045HF475 off-road four-cylinder 4.5 L engine. The engine is rated at 129 kW at 2400 rpm. Detailed engine parameters are given in Table 3.1.

Table 3.1 Engine specifications

Engine	John Deere 4045 HF475 4-cylinder 4-valve direct injection
Bore and Stroke (mm)	106 x 127
Total engine displacement (L)	4.5
Compression Ratio	17.0:1
Valves per Cylinder	2 / 2
Firing Order	1-3-4-2
Combustion System	Direct Injection
Engine Type	In-line, 4-stroke
Aspiration	Turbocharged (located on engine)
Injection System	Common Rail
Piston	Bowl-in-piston

3.1 System Layout

The layout of the experimental setup used to conduct the experiments is shown in Figure 3.1. The exhaust line was divided into two pipes to drive the EGR. A suction pump that is placed in the EGR loop sucks the exhaust into the EGR line. The engine was controlled by the DevX software provided by John Deere. The engine was coupled with a DC dynamometer manufactured by GE and controlled by a standalone dynamometer controller. Details of the system components will be discussed in the following sections.

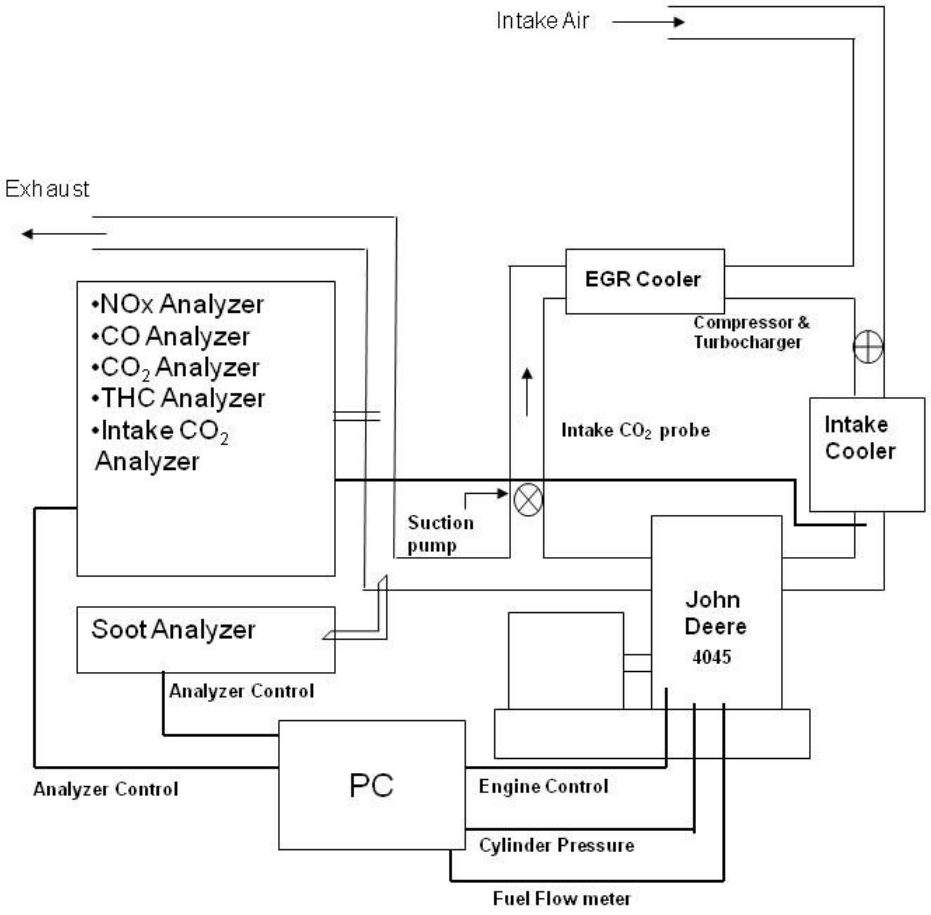

Figure 3.1 Schematic of the engine test facility.

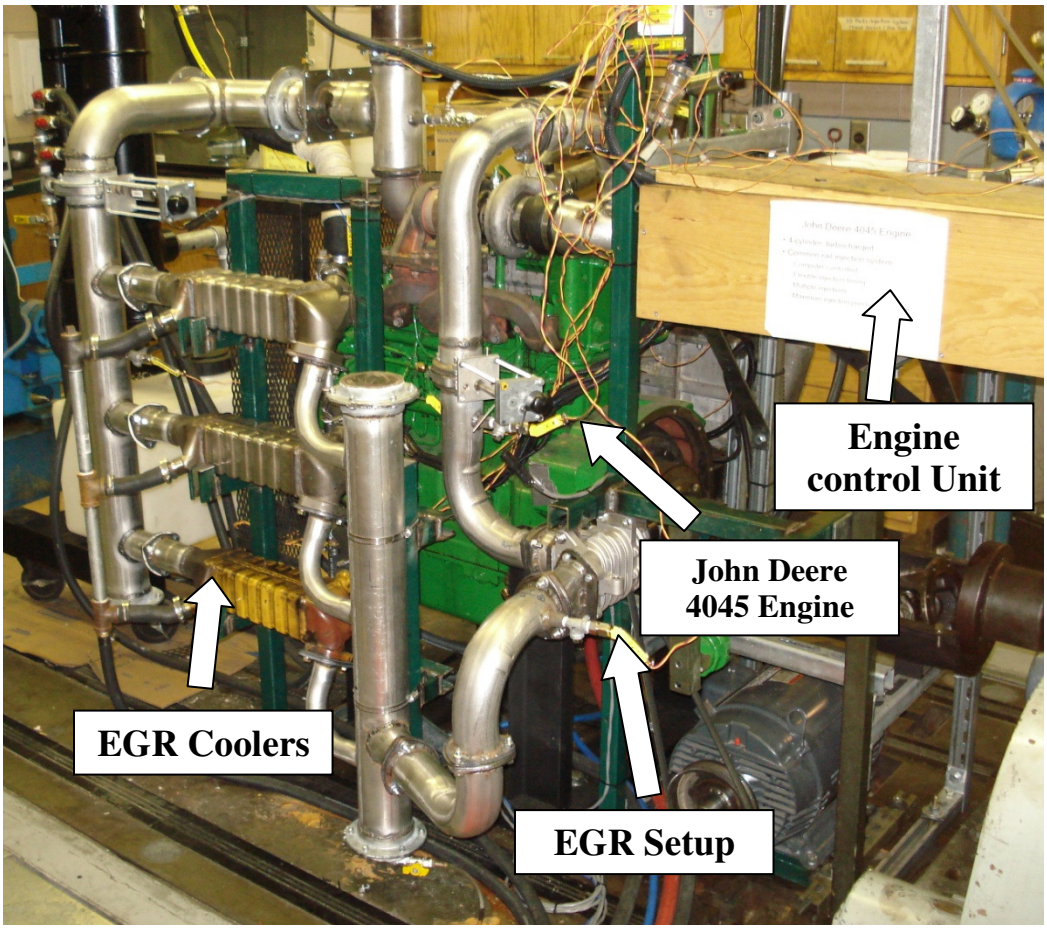

Figure 3.2 Picture of the engine facility.

3.2 Measurement Techniques

The following sections explain the instruments and procedures used for measuring the various performance parameters. All the experiments were performed at steady-state conditions when there was no change in engine oil temperatures and exhaust gas temperatures. The engine was warmed up at the beginning of each test to reach steady-state conditions.

3.1.1 Intake Air Flow Rate Measurement

The intake air flow to the engine was measured using a Meriam laminar flow element (LFE) model 50MC2-4. The calibration on the unit was performed according to NIST standards. The calibration data were standardized to an equivalent dry gas flow rate at 70º F and 29.92 in Hg absolute (101.3 kPa abs). The LFE measures the actual volumetric flow rate. To obtain the actual volumetric flow rate, the differential pressure (DP) across the LFE to the LFE was measured. The flow rate was obtained by substituting the DP value into Eq.(3.1).

$$\text{Flow rate (CFM)} = \mathrm{B} * \mathrm{DP} + \mathrm{C} * \mathrm{DP}^2 \qquad (3.1)$$

where B is 5.3518E+01 and C is -9.64278E-02.

3.1.2 Cylinder Pressure Measurement

An uncooled and ground insulated engine pressure transducer manufactured by Kistler (6125 A) was used to measure the cylinder pressure during engine operation. The cylinder pressure acts on the diaphragm which converts the pressure into a proportional force inside the sensor. This force is then transferred to the quartz package, which produces an electrostatic charge under load. An electrode taps off this charge and feeds it to the connector, where it is converted into a voltage by a charge amplifier connected in series. The crank shaft position was measured using an optical encoder attached to the engine crank shaft wheel. The resolution of the optical encoder was set to 0.25 crank angle degree (CAD) resolution. A trigger was used to synchronize the cylinder pressure measurement and the crank shaft position.

The cylinder pressure at the first data point was taken as a reference voltage each time the cylinder pressure was measured at BDC of the intake stroke, where it was assumed that

the cylinder pressure was equal to the intake boost pressure. The remaining voltage data were collected in reference to this first point. If the cylinder pressure at a certain point is greater than the first point, then the voltage at that point would be higher than the reference voltage. The following equation was used to convert the voltage data into absolute pressure.

$$P_i = (V_i - V_1) * C.C + P_{int} \quad (3.2)$$

where P_i is the cylinder pressure at point i in psi, V_i is the voltage recorded at point i in volts, V_1 is the voltage at a reference point in volts, C.C is the calibration constant for the cylinder pressure transducer (psi/volt), P_{int} is the intake boost pressure (also the pressure at the reference point) in psi. To calculate the ensemble average, the data points for all the acquired engine cycles that were associated with each crank angle were added and averaged for over 50 cylinder cycles.

3.1.3 Gas Emissions Measurement

The gaseous emissions were measured using the HORIBA 7100 DEGR emissions analyzer. The analyzer and exhaust gas flow inside each unit were controlled by the main control unit (MCU). CO, CO_2, and EGR CO_2 emissions were measured using AIA-722 series analyzers. These analyzer use a non-dispersive infrared absorption (NDIR) method for measuring CO and CO_2. A non-heated exhaust gas sample was dried in the sample handling system before flowing into the analyzer. In the NDIR analyzer, two equal-energy infrared beams are directed through two parallel optical cells. One of them is for reference and another for sample measurement. When the sample is flown through the analyzer, certain wavelengths in the infrared beam are absorbed by the component of interest in the sample

gas. The quantity of infrared radiation that is absorbed is proportional to the component concentration.

NO_x was measured using a chemiluminescence sensor (CLD) (CLA-720MA). Before the sample is sent to the analyzer, the sample is led through a catalyst which converts NO_2 in the sample to NO. After the conversion, the sample is exposed to ozone which results in a chemiluminescent reaction yielding NO_2 and oxygen. This reaction produces light which has intensity proportional to the mass flow rate of NO into the reaction chamber. The light is measured by means of a photodiode and associated amplification electronics.

The total hydrocarbons (HC) were measured using a heated flame ionization detector (FID) analyzer (FIA-725A). The ionization mechanism in the analyzer is carried out in two phases. In the first step, organic compounds in the sample are cracked to form CH, CH_2, and CH_3 radicals. In the second step, these radicals react with oxygen to form CHO^+ and an electron (e^-). The electrometer in the analyzer measures the current generated by the ionization of the carbon atoms in the flame fueled by a 40% hydrogen (in helium) and air mixture. The current generated is proportional to the total hydrocarbon content in the sample.

3.1.4 PM Measurement

An AVL smoke meter (415 S) was used to measure PM in the exhaust. The heated sample probe takes the sample from the exhaust pipe into the analyzer. The sample is then passed through a filter paper. The degree to which the filter paper is blackened indicates the PM content in the sample. The paper blackening is measured using an optical reflectometer head. PM in the sample is zero for white filter paper and 10 for completely black paper. The

paper blackening increments are linear between white and black. The filter soot number (FSN) is calculated by the instrument using Eq.(3.3).

$$\mathrm{FSN} = 10 \cdot (1 - \frac{R_B}{R_W}) \qquad (3.3)$$

Based on the FSN and the volume of the sample taken, FSN is converted by the instrument using built-in correlations to mg/m^3.

3.1.5 EGR Measurement

A low pressure loop was used to re-circulate the exhaust gas into the intake manifold. The exhaust gas was driven into the intake using the vacuum created by a suction pump. The exhaust gas was cooled using an intercooler before it reaches the vacuum pump. The exhaust gas is allowed to mix with intake air. The mixture then goes through the compressor of the turbocharger. The supercharger was driven using an AC motor whose speed was controlled by a frequency inverter. The EGR level in the intake was measured using following formula.

$$\mathrm{EGR}\ \% = \frac{[CO_2]_{\mathrm{intake}} - [CO_2]_{\mathrm{atm}}}{[CO_2]_{\mathrm{Exhaust}} - [CO_2]_{\mathrm{atm}}} \qquad (3.4)$$

3.1.6 Exhaust Flow Rate Calculation and PM Unit Conversion

As mentioned above, PM was measured in the units of mg/m^3. Tier 4 emissions standards set by environmental protection agency (EPA), however, mandate all emissions in g/kW-h. This necessitates the conversion of PM emissions from mg/m^3 to g/kW-h. Exhaust volumetric flow rate ($\dot{V}_E$) is required to do such a conversion. The exhaust mass flow rate was calculated by adding the flow rates of intake air and fuel. The ideal gas law was used to calculate the volume flow rate of the exhaust. PM was then calculated using following formula.

$$\text{PM (g/kW} - \text{h)} = \text{PM (g/m}^3) * \dot{V}_E * \left(\frac{1}{\text{brake power}}\right) \qquad (3.5)$$

Exhaust temperature measured after the turbocharger was used in the ideal gas law equation. Universal gas constant was calculated using $R = 8.314/MW_E$. Molecular weight of exhaust (MW_E) was calculated using the concentrations of the gases recorded by the Horiba analyzers in order to evaluate the universal gas constant.

3.1.7 Emissions Unit Conversion

During the emissions measurement, a predetermined amount of exhaust sample was fed to the analyzers. The analyzers measure concentration of the emissions in ppm (parts per million). However, the EPA emissions standards require that all emissions are reported in the units of g/kW-h. The SAE standard SAE J1003 recommends a procedure to covert the diesel engine emissions from ppm to g/kW-h. As this standard requires, all emissions are measured at steady state operating conditions. Exhaust flow rate was used to convert the units of emissions from ppm to g/h. This was divided by the brake power of the engine to convert the units to g/kW-h. Equations 3.6-3.11 were used to convert the units of emissions from ppm to g/kW-h.

$$\text{HC (g/h)} = \frac{(\text{DHC}/10^4) * M_F}{(\text{DCO}/10^4) + \text{DCO}_2 + (\text{DHC}/10^4)} \qquad (3.6)$$

$$\text{CO (g/h)} = \frac{M_{CO}(\text{DHC}/10^4) * M_F}{(M_c + \alpha M_H)\,[(\text{DCO}/10^4) + \text{DCO}_2 + (\text{DHC}/10^4)]} \qquad (3.7)$$

$$\text{NO}_x\text{ (g/h)} = \frac{M_{NO_2}(\text{DNO}_x/10^4) * M_F}{(M_c + \alpha M_H)\,[(\text{DCO}/10^4) + \text{DCO}_2 + (\text{DHC}/10^4)]} \qquad (3.8)$$

$$\text{BSHC} = \frac{\text{HC (g/h)}}{\text{brake power}} \tag{3.9}$$

$$\text{BSCO} = \frac{\text{CO (g/h)}}{\text{brake power}} \tag{3.10}$$

$$\text{BSNO}_x = \frac{\text{NO}_x\text{ (g/h)}}{\text{brake power}} \tag{3.11}$$

3.1.8 Heat Release Rate Calculation

Heat release rate (HRR) inside the cylinder was calculated based on the principle that the apparent net heat release rate, which is the difference between the apparent gross heat release rate and the heat transfer rate to the walls, equals the sum of rate at which work is done on the piston and the rate of change of sensible internal energy of the cylinder contents. The following three assumptions were made in calculating the HRR. First, the gas mixture inside the cylinder is assumed to be homogeneous. Second, the gases inside the cylinder obey the ideal gas law. Third, the specific heat (γ) of the charge mixture is constant throughout the combustion. The heat transfer to the wall was calculated by assuming the cylinder wall temperature as 600 K. The HRR was calculated using Eq.(3.12).

$$\frac{dQ_n}{d\theta} = \frac{\gamma}{\gamma-1} \cdot p \cdot \frac{dV}{d\theta} + \frac{1}{\gamma-1} \cdot V \cdot \frac{dp}{d\theta} + \text{HL} \tag{3.12}$$

where $\frac{dQ_n}{dt}$ is the net heat release rate, γ is the ratio of specific heats (C_p/C_v), V is the instantaneous cylinder volume, $\frac{dV}{d\theta}$ is the rate of change of cylinder volume with respect to crank angle, p is the instantaneous cylinder pressure, $\frac{dp}{d\theta}$ is the rate of change of cylinder pressure with respect to crank angle, HL is the heat loss to the wall.

CHAPTER 4. METHODS AND PROCEDURES

All the experiments were performed at 1400 rpm which is the engine speed that produces the peak torque. Ultra-low sulfur No. 2 diesel fuel was used for all the engine experiments. Table 4.1 gives detailed descriptions and respective ranges of the engine operating variables that were tested. The start of injection (SOI) is denoted in degrees after Top Dead Center (ATDC). Most of, but not all, the combinations were tested, as either combustion did not sustain at certain cases or it was not necessary to test certain conditions due to apparently high emissions. A fuel mass of 50 mg/injection was injected. The engine was controlled and monitored using DevX software provided by John Deere.

Table 4.1 Variables tested and their ranges

Main SOI	-20 to 5 ATDC	Start of Injection
Pilot SOI	-40 to -15 ATDC	Start of Pilot Injection
EGR	0% to 40%	% of EGR
Injection pressure	100 to 200 MPa	Pressure at which fuel is injected
Pilot fuel	15%, 25%, 40%	% of total fuel that was injected during pilot injection.

4.1 Injector Selection

An injector is identified by three numbers, eg., 6X133X800. The first number indicates the number of holes in the injector. The idea behind using multiple nozzles in an injector was to utilize the air in the cylinder more effectively. Multiple holes can also increase the total fuel injected at a given injection pressure. The nozzles on the tip of the injector are uniformly distributed in a circular fashion.

The second number is the included spray angle. Typically wide spray angles are used in diesel engines in order to spread the fuel to utilize sufficient air for combustion.

Nonetheless, narrow spray angles are also of interest because they allow early injection without fuel spray impinging on the cylinder wall.

The third number indicates the flow number of the injector. Flow number is the total fuel volume injected under standard injector test conditions. Flow number is directly proportional to the total area of the nozzles in an injector. An injector denoted by 6X133X800 has 6 holes, 133 degrees included spray angle, and 800 flow number. An example of a 6X133X800 injector is given in the Figure 4.1.

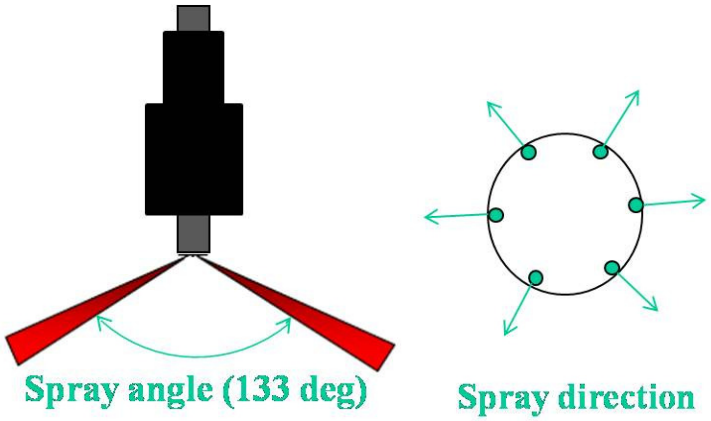

Figure 4.1 A schematic of the 6X133X800 injector.

Table 4.2 gives the details of the injectors evaluated in this study. A convergent nozzle was also used in an injector. The definition of the K-factor is given in Eq.(2.3). The length of nozzle, L that is used in the definition of K factor, was 0.8 mm for the injectors that were tested.

Table 4.2 Injector specifications

Notation	Details	Individual Nozzle diameter
6X133X800	Baseline, 6-holes, 133 degree spray angle, 800 flow number	148 µm
6X133X800 K=3	Convergent nozzle	148 µm
10X133X800	Same flow number, more nozzles, but reduced nozzle diameter.	115 µm
16X133X800	Same flow number, more nozzles, but reduced nozzle diameter.	91 µm
6X133X480	Lower flow number, reduced nozzle diameter	115 µm
10X133X500	Lower flow number, reduced nozzle diameter	91 µm

4.2 Tier 4 Emissions

The emissions standards set by the EPA to be met by diesel engine manufacturers by the year of 2014 for off-road application are comprehensive and stringent. Table 4.3 gives the comparison of emissions standards for off-road diesel engines rated between 75 and 130 kW. For the Tier 4 emissions, the emissions standards are for diesel engines rated between 56 and 130 kW. All emissions are measured in g/kW-h. The Tier 4 emissions standards will be used as the targets in this study.

Table 4.3 Emissions standards for off-road diesel engines rated between 75 and 130 kW (unit: g/kW-h)

Tier	Year	CO	HC	NMHC+NOx	NOx	PM
Tier 1	1997	-	-	-	9.2	-
Tier 2	2003	5.0	-	6.6	-	0.3
Tier 3	2007	5.0	-	4.0	-	0.3
Tier 4	2012-2014	5.0	0.19	-	0.4	0.02

4.3 EGR Limitations

EGR was primarily used to reduce the combustion temperature to help reduce the NOx emissions. However, as the EGR increased, the PM emissions also increased. When a high level of EGR (around 60% EGR) was used, both NOx and PM can be reduced. At these high levels of EGR, the combustion may not be sustainable and the brake power output of the engine will be reduced significantly. This will increase the fuel consumption of the engine which is not desirable. Due to combustion instability and high fuel consumption, EGR levels were limited to 40% in this study.

Other effects of EGR include the reduction of intake oxygen concentration. At 0% EGR, the exhaust contains about 11.5% oxygen. With the introduction of EGR, exhaust with lower oxygen concentration replaces the air which has 20.94% oxygen. Thus introduction of EGR reduces the overall oxygen concentration in the intake. Table 4.4 and Figure 4.2 compare the oxygen concentration in the intake at EGR levels ranging between 0 and 35%. As the EGR increased, the intake oxygen concentration reduced almost linearly. Also, when the intake temperature was increased to 40 °C, the intake oxygen concentration reduced at same EGR level. Relatively more intake air was replaced with EGR with the increase in intake temperature leading to a reduction in overall oxygen concentration.

Table 4.4 Variation of intake O_2 concentration with EGR % at intake temperature 23°C and 40° C

EGR %	O2 % (23 °C Intake)	O2 % (40 °C Intake)
0	20.94	20.94
10	20.14	19.94
20	18.64	18.24
30	16.74	16.64
35	15.54	15.14

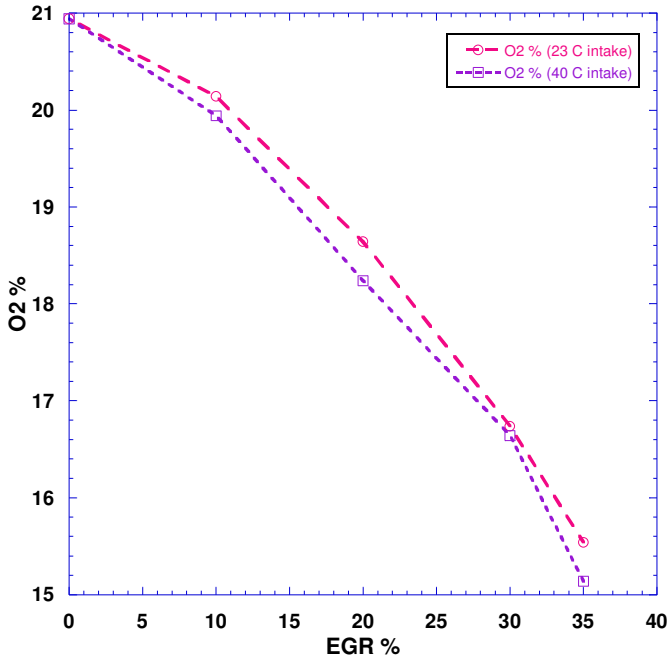

Figure 4.2 Comparison of intake O2 concentration for different EGR levels at intake temperatures of 23 °C and 40 °C

4.4 PSO Optimization

The PSO algorithm used in this study was designed to include any number of engine variables as needed. The lower limits, upper limits, and resolutions were defined in a single file *engine.txt*. The resolutions were set based on the capabilities of the experimental setup. The following equation was used to round the value of the variable to the nearest possible resolution point in each iteration.

$$X_i = LL_i + round\left(\frac{X_i - LL_i}{res_i}\right) * res_i \qquad (4.1)$$

where X_i is the value of the variable i, LL_i is the lower limit of the variable i, res_i is the resolution of the variable i.

Random numbers used in this optimization were generated using the MATLAB function sum(100*clock). This function generates the random numbers based on the current

time and date. The random number generator was tested to ensure that the random numbers generated are uniformly distributed between 0 and 1.

All the necessary data that need to be passed on to the next iteration were saved into three files: *pnew.txt, pbest.txt,* and *gbest.txt*. Files that are passed on to the next iteration were inserted with iteration number in the file name for easy tracking.

Depending on the number of engine variables and the type of problem, the optimization process can take several days to produce a solution. The program was designed to facilitate the cessation of optimization after any iteration and resumption at a later time.

The operating conditions generated by the program were saved into the file *rundata**i**.txt* where 'i' is the iteration number. The merit function which will be defined in the next section includes NOx, HC, CO, PM, and BSFC. The NOx, HC, CO, PM, and BSFC data that were collected from the experiments were saved into the file *result**i**.txt*. The program then calculates the fitness function values of each of these experiments to determine the operating conditions of next iteration.

4.5 Merit Function Definition

It is well known that diesel emissions have a trade-off. As we reduce NOx emissions by using the EGR, PM emissions increase. To account for this trade-off problem, a merit function was used in this study to reduce several emissions simultaneously. An example of the merit function is shown in Eq. (4.2). The emissions are included in the denominator of the merit function. The Tier 4 emissions mandates are included in the fitness function as the targets. As the emissions and BSFC reduced as the optimization process progresses, the

fitness function value increases. The numerator of the fitness function was chosen as 1000 to keep the fitness function value easily readable.

All the BSFC and emissions in the merit function are in g/kW-h. When the BSFC and NOx, HC, CO emissions targets are met, the value of the fitness function would reach 200.

$$Fitness = \frac{1000}{\left(\frac{NOx}{w_1 * NOxt}\right)^2 + \left(\frac{PM}{w_2 * PM_t}\right)^2 + \left(\frac{HC}{HC_t}\right) + \left(\frac{CO}{CO_t}\right) + \frac{BSFC}{BSFC_t}} \qquad (4.2)$$

The subscript t denotes the target and w_1 and w_2 are weighting factors for NOx+HC and PM, respectively. The values of w_1 and w_2 were set to 1 in this study.

CHAPTER 5. RESULTS OF PARAMETRIC STUDY

5.1 Parameters Affecting the Emissions in Diesel Combustion

The emissions of diesel engines can be controlled either through in-cylinder combustion control or through exhaust aftertreatment. This study investigated the in-cylinder combustion control approach to reduce emissions. There are several important parameters that can affect the diesel engine emissions. Among these parameters, the important ones are SOI, EGR, injection pressure, and fuel allocation in different injection pulses. These parameters can be used in combination with others to produce desired emission levels. Experimental results of the effects of these parameters on emissions are presented in the following sections.

5.2 Effect of SOI on Engine Performance

5.2.1 Effects on NOx and PM

Other parameters being constant, the trade-off between NOx and PM can be observed by varying the SOI. By injecting the fuel late in the engine cycle (retarded SOI), both the amount of premixed burn and the peak in-cylinder combustion temperatures are reduced. As shown in Figure 5.1, NOx emissions were reduced as SOI was retarded. However, as the SOI was first retarded, there was an increase in PM emissions. This trade-off can cause a challenge to reduce both emissions simultaneously. When the SOI was further retarded to near TDC, soot emissions were reduced because the combustion temperature was relatively low such that less soot was formed. This feature is referred as “low temperature combustion”

as seen in Figure 2.1 As a result, at late SOI, both NOx and PM can be simultaneously reduced.

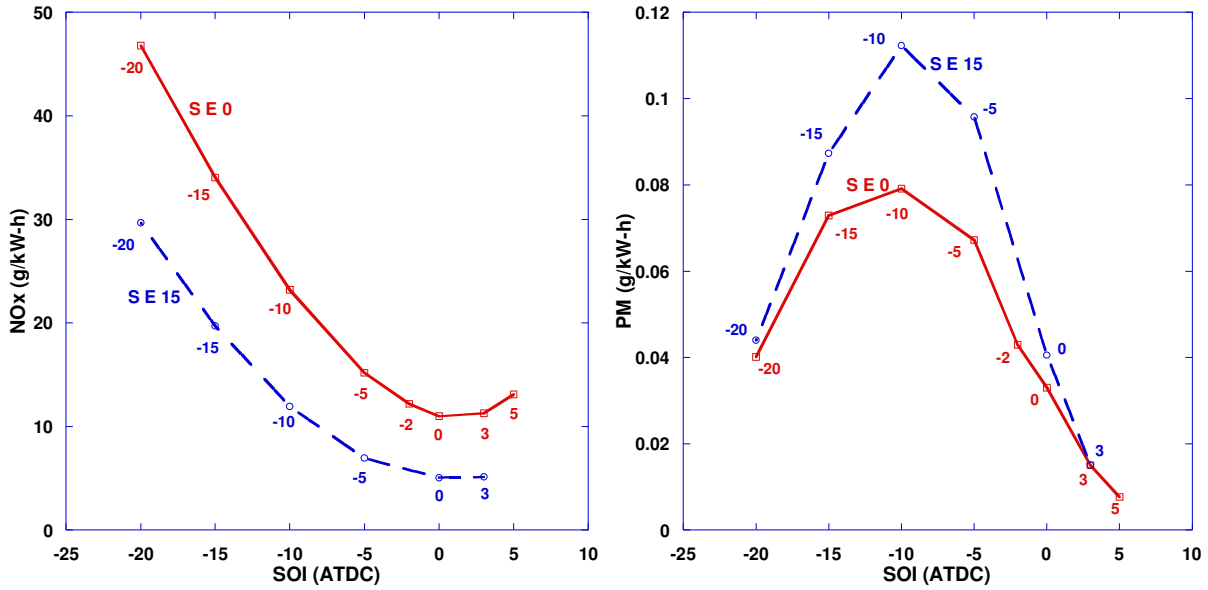

Figure 5.1 Effect of SOI on NOx and PM emissions at EGR levels 0 and 15% and 150 MPa injection pressure. The number next to each data point is the corresponding SOI.

5.2.2 Effects on CO, HC, and BSFC

Cylinder pressures and heat release rates for different SOIs are presented in Figures 5.2 and 5.3, respectively. As the SOI was retarded, the peak cylinder pressure reduced. A similar trend was observed in heat release rate data. As the SOI was retarded, the premixed combustion was reduced, leading to a reduction in the peak heat release rate. As with NOx and PM, SOI had significant effect on CO and HC emissions. CO emissions were the lowest between -10 and -15 CAD ATDC. As the SOI was moved towards TDC, CO emissions increased significantly as the fuel had relatively less time and lower temperature to burn completely. A similar trend was observed when the EGR was increased to 15%. HC emissions on the other hand were the highest when the SOI was at -20 ATDC. The BSFC values at both EGR levels followed a similar trend as shown in Figure 5.5. The BSFC values

were the lowest at -10 ATDC. BSFC deteriorated due to high HC and/or CO emissions at early or late injection timings.

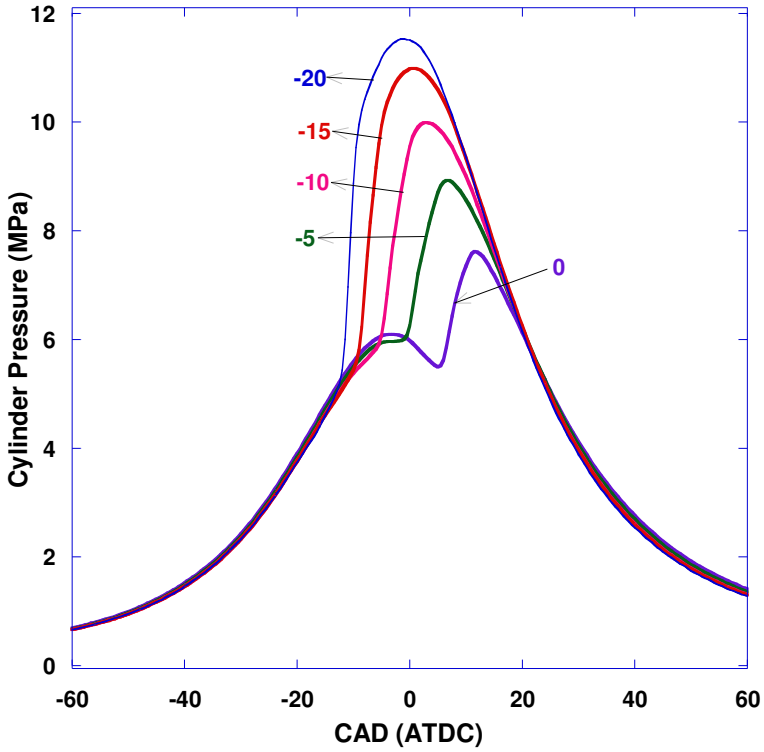

Figure 5.2 Cylinder pressure history for SOI between -20 and TDC, 0% EGR.

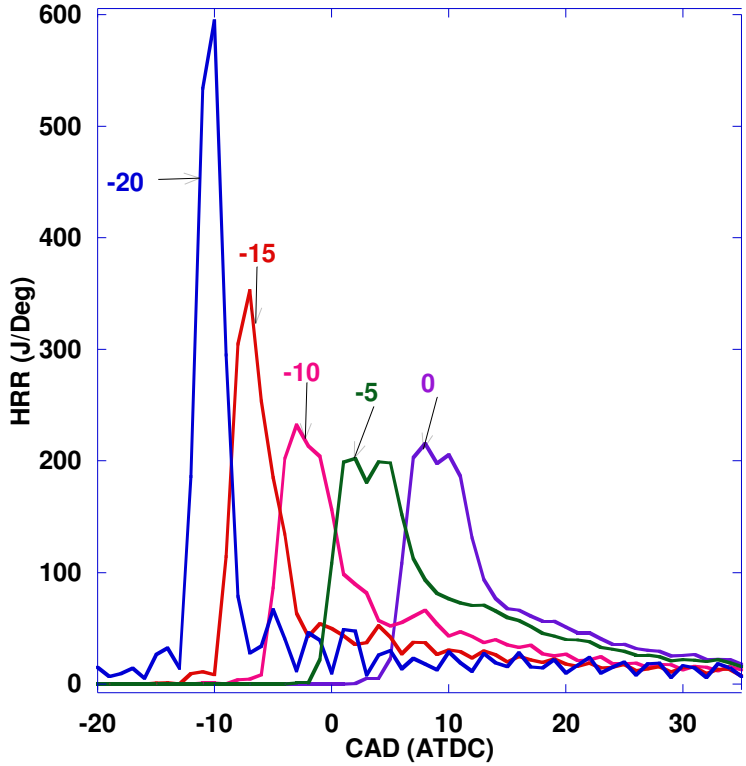

Figure 5.3 Heat release rate history for SOI between -20 and TDC, 0% EGR

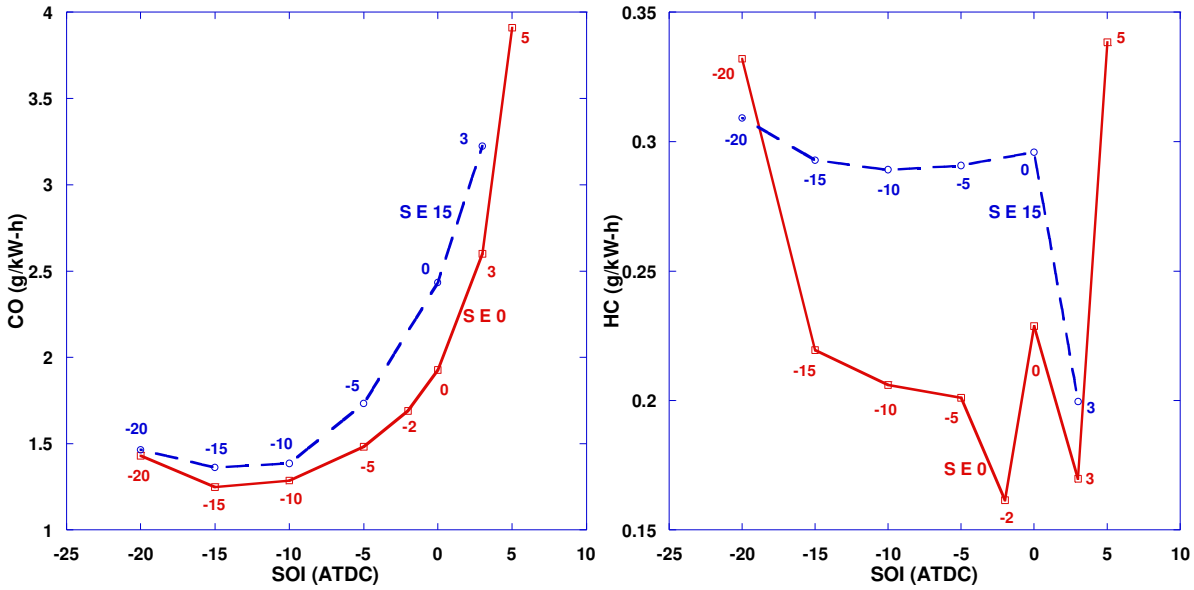

Figure 5.4 Effect of SOI on CO and HC emissions at EGR levels 0 and 15% and 150 MPa injection pressure

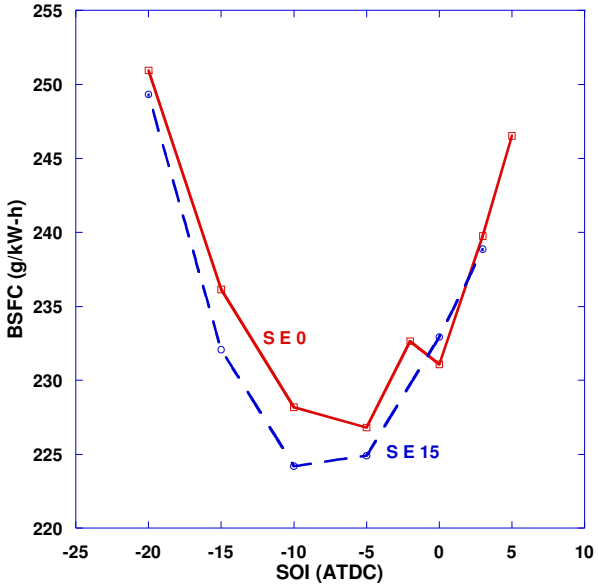

Figure 5.5 Effect of SOI on BSFC at EGR levels 0 and 15%

5.2.3 Effects on Combustion Stability

Despite that simultaneous reduction of NOx and PM can be achieved by retarding the injection timing, the operating range is limited due to the problems associated with combustion stability. At retarded timings, the fuel does not have enough time to mix with oxygen which reduces the combustion efficiency. This can also be observed from the HC emissions presented in Figure 5.2. If the SOI is further retarded, combustion may not be sustainable and the engine may misfire.

5.3 Effect of Multiple Injections

5.3.1 Problems with Very Early Pilots

Figure 5.6 shows the path of pilot injection fuel inside a diesel engine cylinder. The pilot SOI of -30 ATDC marks the earliest of the conventional diesel injection timing. Injection timing has a pronounced effect on fuel spray movement [56]. Between the injection

timings of TDC and -30 ATDC, a counter clockwise in-cylinder flow is established. The fuel spray hits the piston bowl and moves along the piston into the open space above the piston bowl. This movement will enable the fuel to mix with sufficient air providing enough oxygen for the fuel to burn. As the injection timing is advanced beyond -30 ATDC, before the establishment of the counter clock wise in-cylinder flow, instead of moving up into the cylinder, the fuel starts to move toward the bottom of the piston. This seriously reduces the interaction of fuel and air resulting in incomplete combustion and high PM and HC formation.

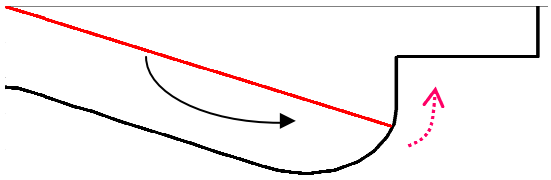

Figure 5.6 Fuel spray path at pilot SOI of -30 ATDC

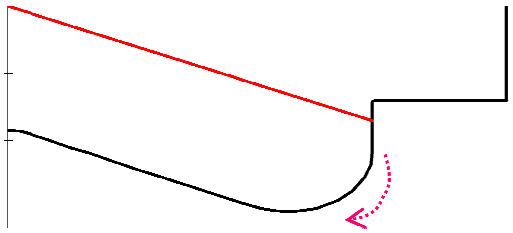

Figure 5.7 Fuel spray path at pilot SOI of -45 ATDC

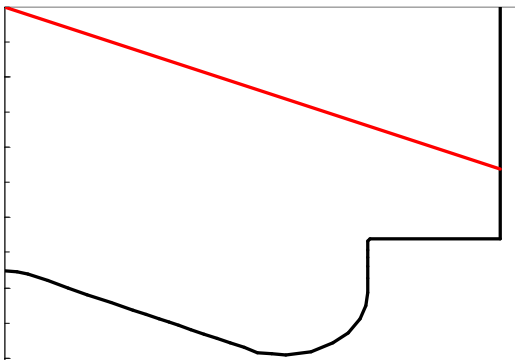

Figure 5.8 Fuel spray path at pilot SOI of -60 ATDC

Spray-wall impingement at very advanced SOI (e.g., -60 ATDC) is shown in Figure 5.8. The very early fuel injection causes the fuel to miss the piston bowl and hit directly the cylinder wall. Spray-wall impingement must be avoided to avoid lubrication oil dilution by unburnt fuel. In early injection cases, a portion of poorly targeted fuel adheres to the cylinder wall and eventually enters the crankcase where it reduces the viscosity of the lubricating oil.

5.3.2 Possibility of Late Main Injection

Main injection timing, along with pilot injection timing, plays an important role in minimizing the emissions and BSFC. While the pilot injection needs to minimize the wall impingement and maximize the time for mixing, the main injection timing needs to assure that stable combustion is sustained. The late injection timings, as mentioned in the above sections, would limit the NOx production from the main injection, while also continuing to ensure proper mixing for PM oxidation.

5.3.3 Effects on NOx and PM Trends

The amount of fuel injected in the pilot injection affects the premixed combustion which, in turn, will affect the NOx and PM emissions. Figure 5.9 shows the effects of pilot fuel amount (percentage of total fuel) on NOx and PM emissions at different pilot SOI. The main injection was kept constant at 5 ATDC. In the absence of EGR, the pilot fuel amount alone can also affect the NOx emissions. As the EGR was increased to 30%, the difference between NOx emissions for 15% pilot and 25% pilot injections reduced. However, the same trend was not observed in PM emissions. The PM emissions at 25% pilot injection increased significantly over the PM emissions at 15% pilot. It is also worth noting that the PM

emissions increased at 25% pilot as the pilot SOI was advanced from -20 ATDC to -35 ATDC.

The cylinder temperatures were lower as the pilot SOI was retarded. This reduced the oxidation of PM resulting from pilot fuel combustion, and resulted in higher total PM emissions. The engine noise levels were also considerably less compared to the single injection cases. This pilot combustion causes a mild increase in cylinder pressure and shortens the ignition delay of min combustion, leading to a reduction in engine noise.

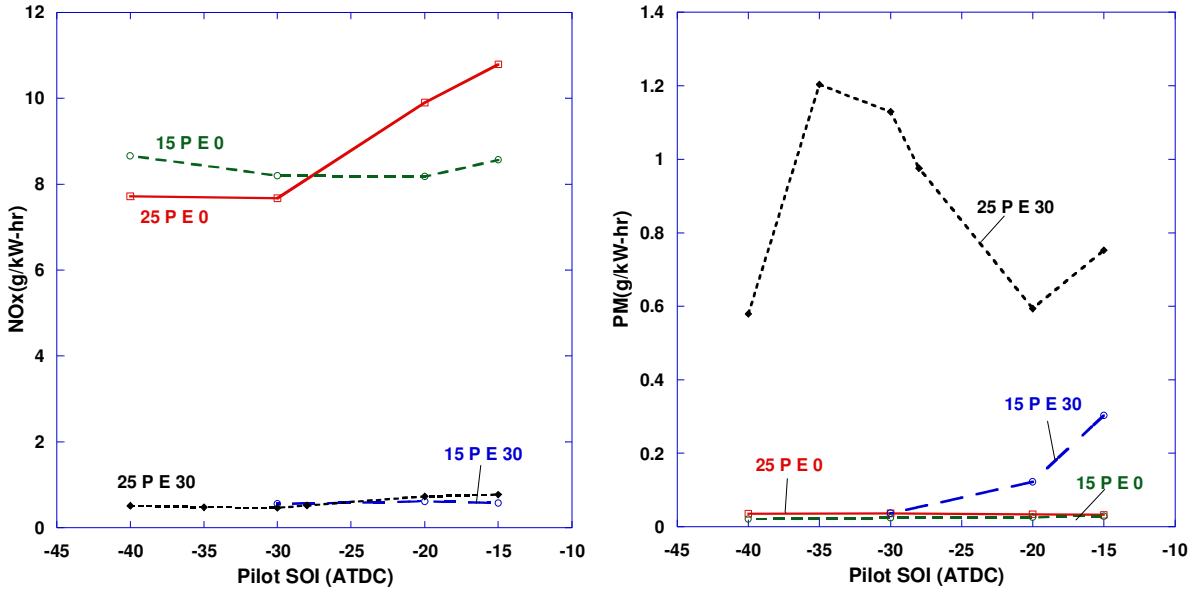

Figure 5.9 Effect of pilot injections (15% and 25%) on NOx and PM emissions (Main SOI 5 ATDC). Note that "15PE30" means 15% pilot fuel with 30% EGR.

5.3.4 Effects on CO, HC, and BSFC

Advancing the pilot injection timing has increased the CO, HC and BSFC values as can be seen in Figures 5.10 and 5.11. At 0% and 30% EGR levels, both CO and HC increased between -30 ATDC and -40 ATDC SOI at 25% pilot injection. At 0% EGR, 25% cases appeared to cause higher CO and HC emissions while at 30% EGR, 15% pilot cases have caused higher CO and HC emissions. Results were not conclusive in terms of the pilot

fuel amount. At 30% EGR, the ignition delay is relatively long. Under such conditions, 15% pilot fuel might spread out too lean in the cylinder and cause incomplete combustion and high CO and HC emissions. It is also evident from BSFC results in Figure 5.11.

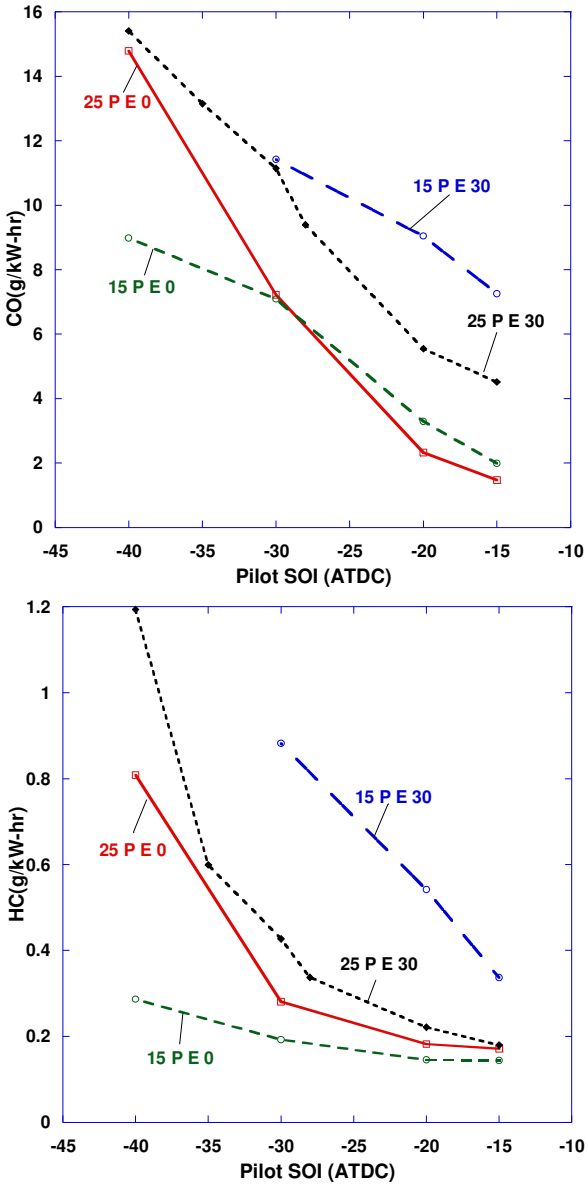

Figure 5.10 Effect of pilot injections (15% and 25%) on CO and HC emissions (Main SOI 5 ATDC)

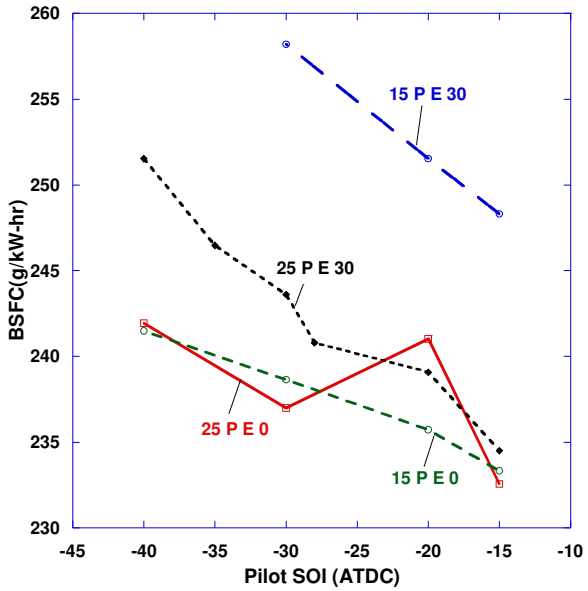

Figure 5.11 Effect of pilot injections (15% and 25%) on BSFC (Main SOI 5 ATDC)

Figures 5.12 and 5.13 compared the cylinder pressures and heat release rates at 25% and 40% pilot injection for two pilot SOI of -20 and -40 ATDC. There was an increase in the peak cylinder pressure when 40% pilot injection was used. Contrary to the general perception, for the same pilot fuel amount, the cylinder pressure was higher when the pilot SOI was at -20 ATDC compared to the cylinder pressure at -40 ATDC. It is also evident from Figure 5.13 that the pre-mixed combustion was greater when the pilot SOI was at -20 ATDC.

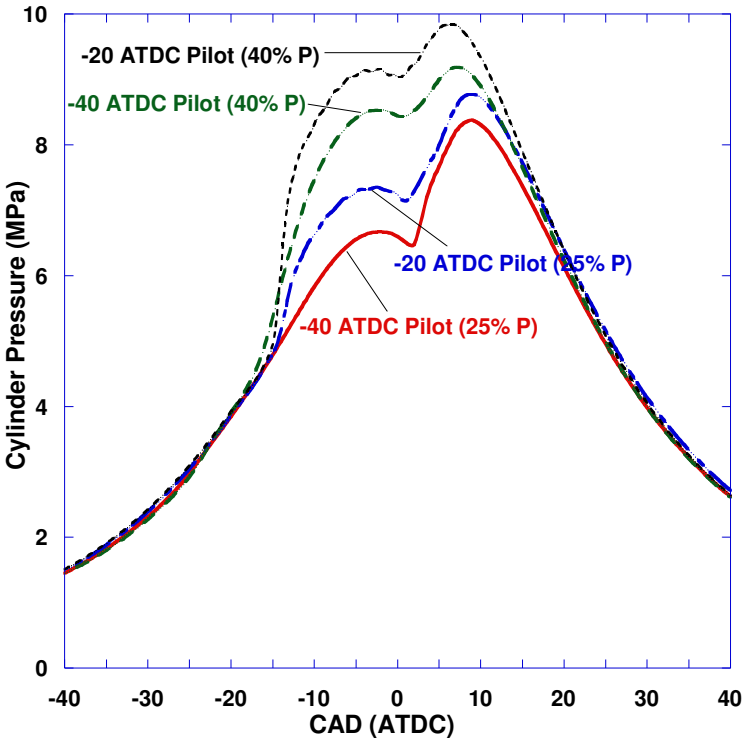

Figure 5.12 Effects of pilot duration and pilot SOI on cylinder pressure

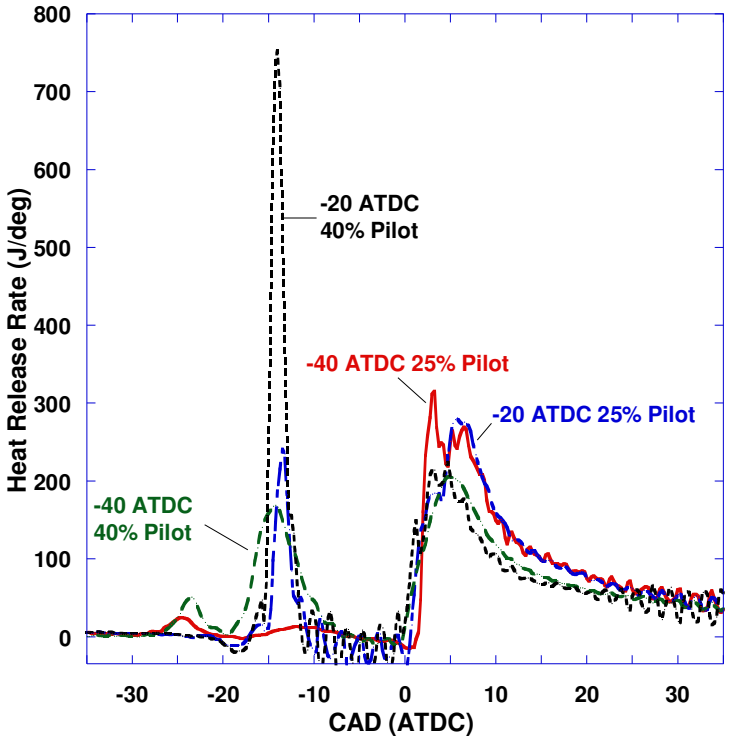

Figure 5.13 Effects of pilot duration and pilot SOI on heat release

5.4 Effect of EGR

5.4.1 Effects on Emissions and BSFC

NOx and PM emissions for single and double injections at three EGR levels (0, 15, and 30%) are shown in Figure 5.14. The CO, HC emissions and BSFC for the same conditions are shown in Figures 5.15 and 5.16. The NOx emissions were significantly reduced as the EGR was increased from 0 to 30% for both single and double injection cases.

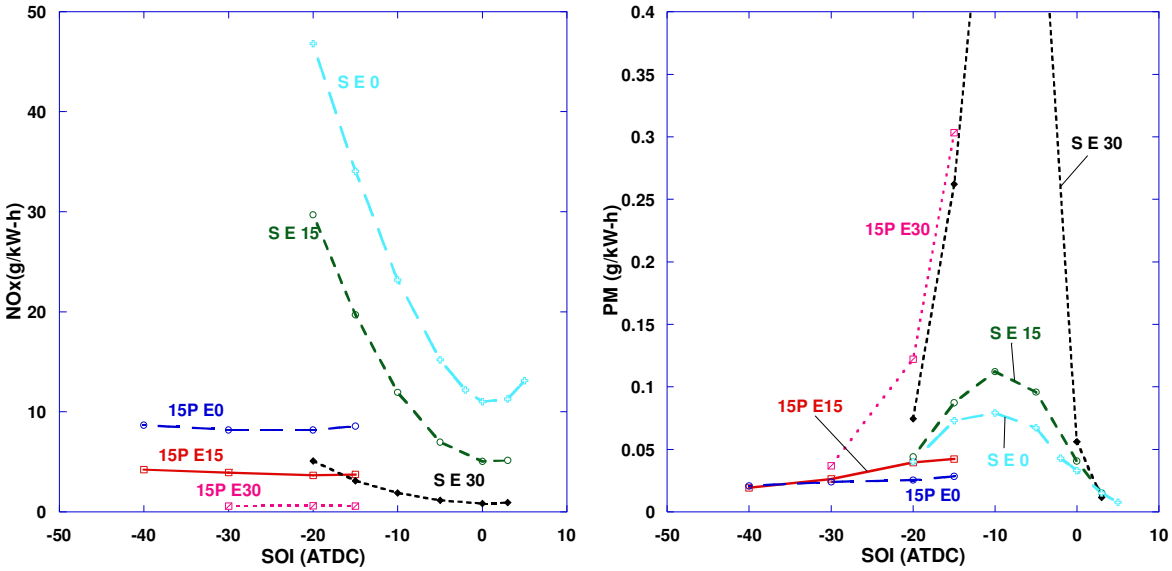

Figure 5.14 NOx and PM emissions at different EGR levels for single and double injection conditions at 150 MPa injection pressure

PM emissions followed the expected trend. As the EGR was increased, the PM emissions increased due to lower combustion temperature. However, for SOI at TDC, the PM emissions were nearly the same at all EGR levels. The PM emissions also rose at higher EGR levels for the cases with pilot injections.

Figures 5.15 and 5.16 show the CO, HC and BSFC trends at three levels of EGR. As expected, CO, HC and BSFC have increased with the increased in EGR for both single and double injection conditions. Overall speaking, the BSFC data were at a similar level for 0%

and 15% EGR cases. However, BSFC increased significantly for 30% EGR cases due to more incomplete combustion (i.e., higher CO and HC emissions).

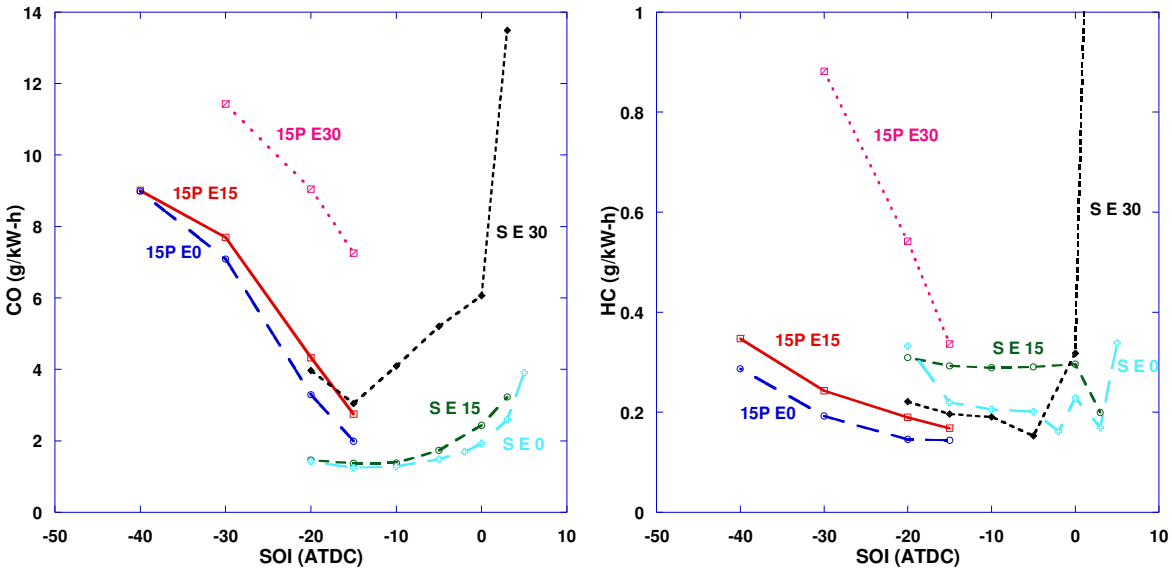

Figure 5.15 CO and HC emissions at different EGR levels for single and double injection conditions at 150 MPa injection pressure

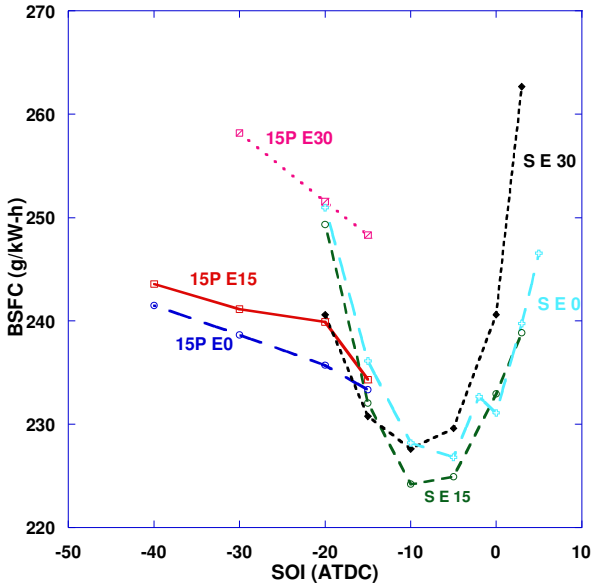

Figure 5.16 BSFC at different EGR levels for single and double injection conditions at 150 MPa injection pressure

5.4.2 Effect of EGR on Cylinder Pressure and HRR

Figure 5.17 shows the effect of EGR on the cylinder pressure and HRR. It can be seen that as the EGR increased, the cylinder pressure reduced. This is due to the lower combustion temperatures associated with high EGR levels. The initial cylinder pressure levels were not the same for the three EGR conditions. This was due to the fact that as EGR was increased, the combustion temperature was reduced such that the exhaust gas energy level was also decreased. As a result, the turbo boost was reduced, causing a lower compression pressure. Note that EGR was cooled and an intercooler was used to maintain a constant intake temperature at 23ºC in the intake manifold. An important effect of EGR is its ability to delay the start of ignition and allow the diffusion-only combustion. From the HRR curves in Figure 5.17, it is clearly evident that as the EGR is increased, the start of ignition has delayed. EGR has also shifted combustion from premixed-diffusion phase to diffusion-only combustion which is useful in simultaneously reducing NOx and PM emissions.

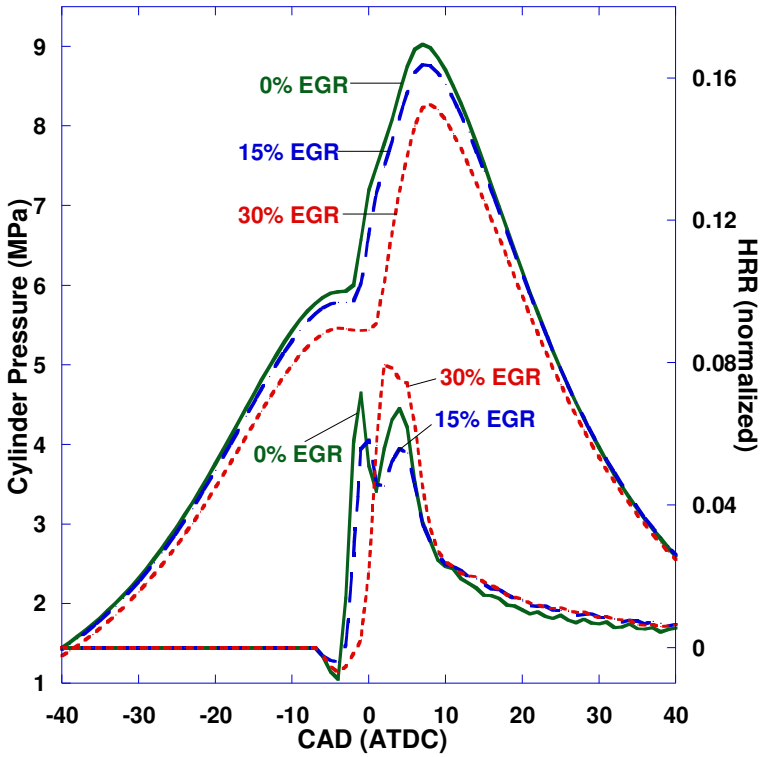

Figure 5.17 Cylinder pressures of using the convergent nozzle with different EGR levels at 150 MPa injection pressure and –5 ATDC SOI

5.5 Effect of Injection Pressure on Emissions

5.5.1 Effects on Emissions and BSFC

Figure 5.18 shows the NOx and PM emissions at different injection pressures for single injection cases. The emissions are presented for three levels of EGR. The increase in injection pressure from 100 MPa to 200 MPa increased NOx emissions. This can be attributed to the increase in spray velocity at higher injection pressures leading to better atomization. Higher injection velocities (because of higher injection pressure) will lead to more rapid premixed burn and a higher local temperature which will increase NOx emissions.

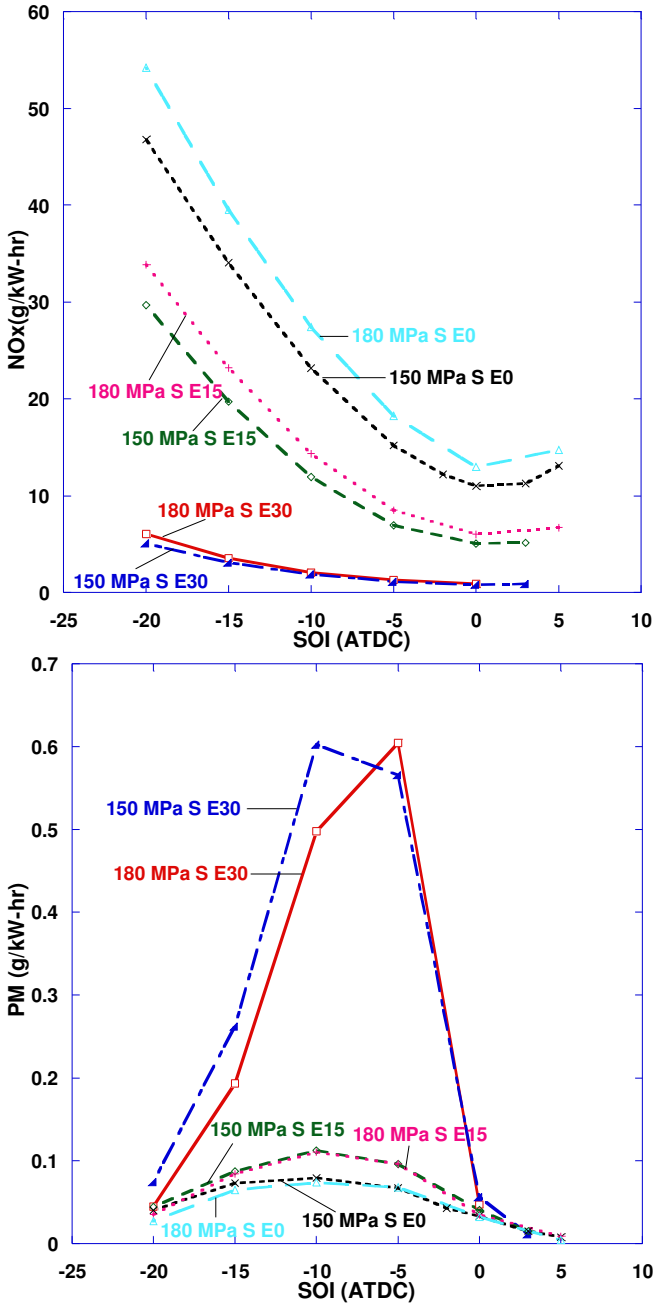

Figure 5.18 Effects of Injection pressure on NOx and PM emissions at different EGR levels

PM emissions were found to be the lowest for the 200 MPa injection pressure. As mentioned earlier, high injection pressures can help attain better combustion of fuel which will result in low PM emissions. It should also be noted that the effect of high injection pressure on NOx emission reduces as the EGR is increased.

Figures 5.19 and 5.20 show the CO, HC emissions and BSFC data for the above mentioned operating conditions. At the same EGR levels, the BSFC was higher at high injection pressures. It should be noted that the present engine used a common rail pump. At high injection pressures, the work required by the pump to maintain high injection pressure was higher. As the pump is run from the power generated by the engine, the net work available at the crankshaft was lower. This has caused an increase in the BSFC which can be seen in Figure 5.20.

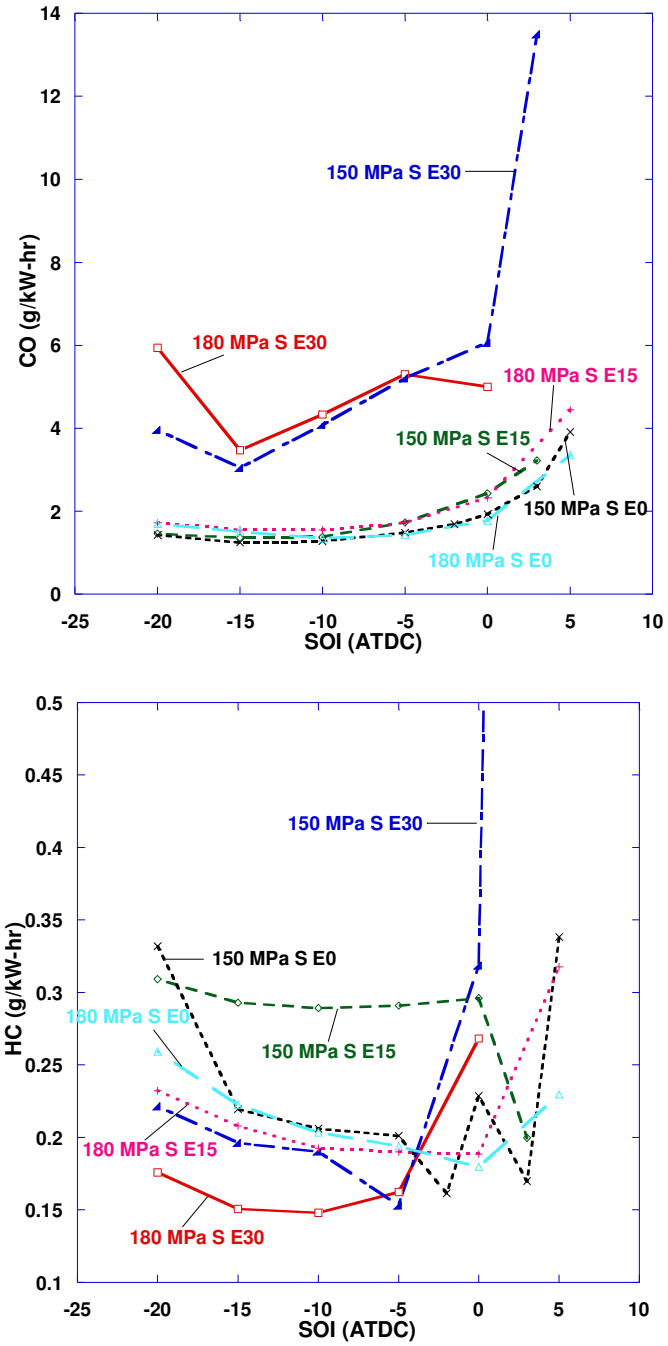

Figure 5.19 Effects of Injection pressure on NOx and PM emissions at different EGR levels

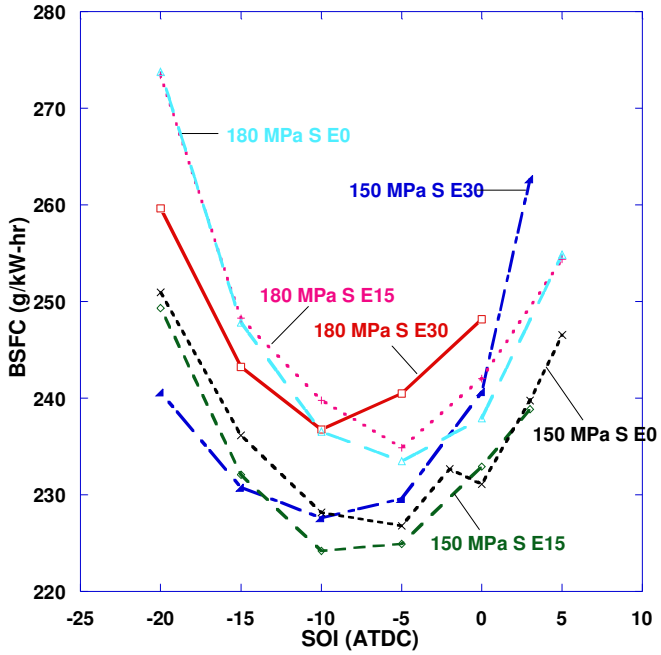

Figure 5.20 Effects of Injection pressure on NOx and PM emissions at different EGR levels

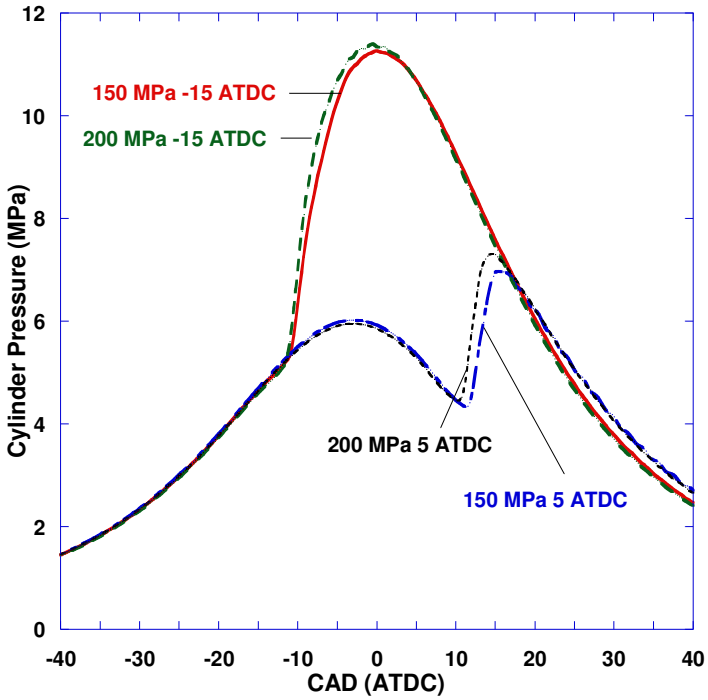

Figure 5.21 Comparisons of cylinder pressure at two injection pressures of 150 and 200 MPa at -15 ATDC and 5 ATDC SOI

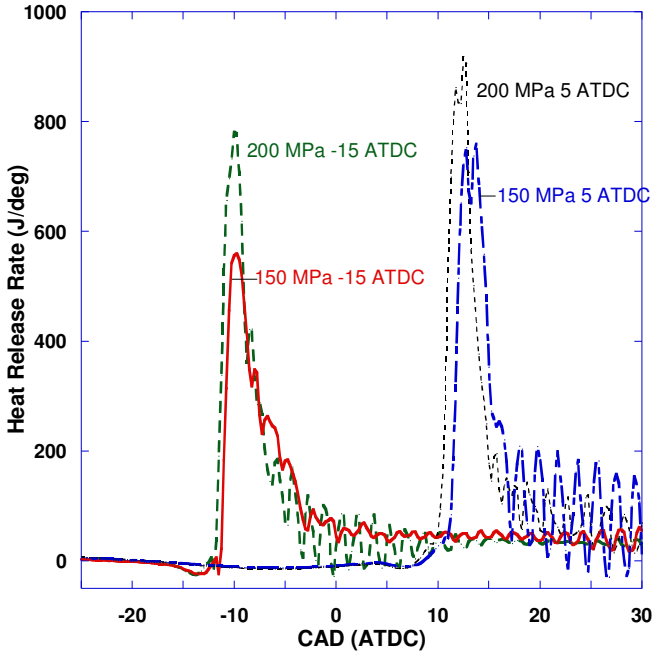

Figure 5.22 Comparisons of heat release data at two injection pressures of 150 and 200 MPa at -15 ATDC and 5 ATDC SOI

Figures 5.21 and 5.22 show the cylinder pressure and heat release rate data for two injection pressures of 150 and 200 MPa for SOI = -15 and 5 ATDC with 30% EGR. It can be seen that higher injection pressures result in slightly earlier ignition and higher cylinder pressures. Figure 5.22 shows that 200 MPa injection pressure also results in a higher heat release rate spike. This is believed to be due to better fuel atomization which, in turn, produces rapid combustion and reduces PM emissions.

5.6 Baseline Injectors (6X133X800)

Most of the results using the "6X133X800" (baseline) injectors have been discussed in previous sections. This section will discuss more on the effects of double injections. Additionally, favorable operating conditions will be summarized for further comparisons with other injectors.

5.6.1 Effects of Double Injections on Emissions and BSFC

Various combinations of injection pressures, EGR rates, injection timings, and fuel allocations were tested to study their effects on emissions with baseline injectors. Previous studies have revealed that a main SOI of 5 ATDC has resulted in least NOx and PM emissions. Thus, for all the double injection cases presented in the following sections, the main SOI was fixed at 5 ATDC and pilot SOI was varied.

Figure 5.23 shows the comparison of NOx and PM emissions at 150 MPa injection pressure using double injections. Two different pilot fuel quantities were tested including 15% and 25%. It is clearly evident from Figures 5.23 that 15% pilot performed better compared to 25% pilot, especially at the retarded pilot timings of -20 and -15 ATDC. Both NOx and PM emissions results show the same trend that the 15% pilot case results in lower emissions. It should be noted that PM data for 25% pilot, 30% EGR are not presented as the PM values were beyond the scale that was chosen (a smaller scale was chosen to present the data more clearly). The NOx and PM emissions in Figure 5.23 were lower for retarded pilot SOI at 15% Pilot. This is likely due to combustion temperature being in low-sooting region [57].

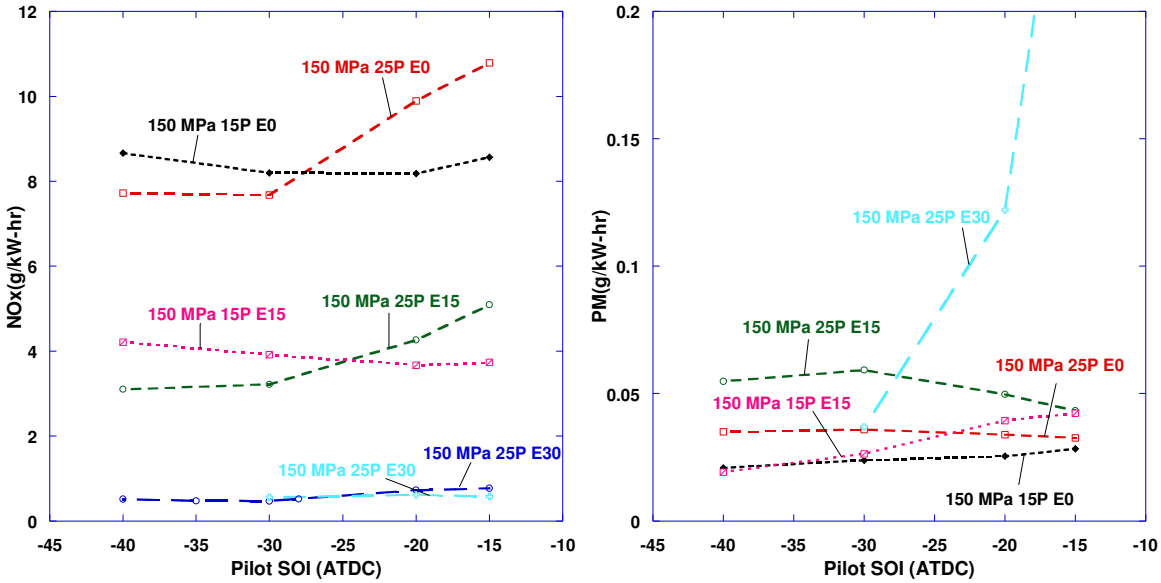

Figure 5.23 NOx and PM vs pilot SOI at 150 MPa injection pressure (main SOI = 5 ATDC) for different pilot fuel quantities and EGR

On the other hand, BSFC was relatively low for the 25% pilot cases compared to that of 15% pilot as shown in Figure 5.24. The 15% pilot with 30% EGR had the highest BSFC. Though BSFC was relatively high for 15% pilot cases, NOx and PM emissions were relatively low. Thus, it was of great interest to further test 15% pilot injection as will be discussed later.

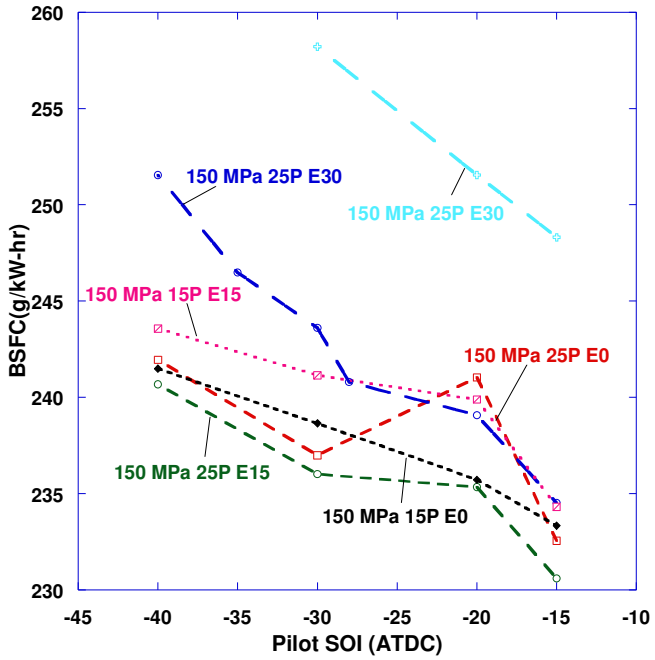

Figure 5.24 BSFC vs pilot SOI at 150 MPa Injection pressure (main SOI = 5 ATDC)

Favorable operating conditions that produced simultaneous PM and NOx emissions are summarized in Figure 5.25 and Table 5.1. Figure 5.25 shows NOx and PM data at 30% EGR, 150 MPa and 180 MPa injection pressures. The box at bottom left corner shows the Tier 4 emissions standard for non-road diesel engines of the present engine category. It can be noted that at 180 MPa injection pressure with 15% pilot injection at -40 ATDC (main SOI = 5 ATDC), PM emissions was 0.0057 g/kW-hr. This is well below the Tier 4 standard. However, NOx emission was 0.561 g/kW-hr which did not meet the standard. During experiments, further advancing pilot SOI would produce high HC emissions to a point that the combustion inside the cylinder was not able to sustain and hence the engine failed to produce power. It should also be noted that by increasing the injection pressure from 150 MPa to 180 MPa, the pilot SOI can be advanced from -30 ATDC to -40 ATDC for further PM reduction. However, BSFC was increased from 258 to 310 g/kW-hr.

Table 5.1 lists the emissions and BSFC results of selected cases shown in Figure 5.25. For low PM and NOx emissions, the favorable operating conditions are using the single injection at a late SOI or using the double injection with early pilot and late main SOI. However, it can be seen that CO and HC (Figure 5.26) emissions are relatively high by using 30% EGR. Further investigations are required for simultaneous emissions reductions.

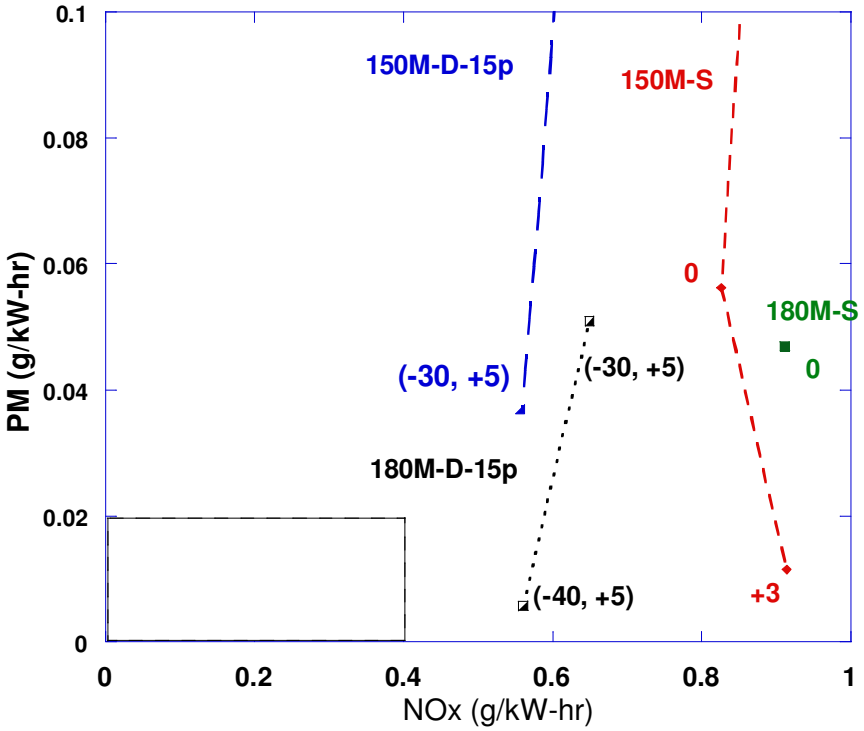

Figure 5.25 NOx vs PM emissions for 150 and 180 MPa injection pressures at 30% EGR for both single and double injection conditions. (Note that (-40, +5) denotes pilot SOI = -40 ATDC and main SOI = + 5 ATDC)

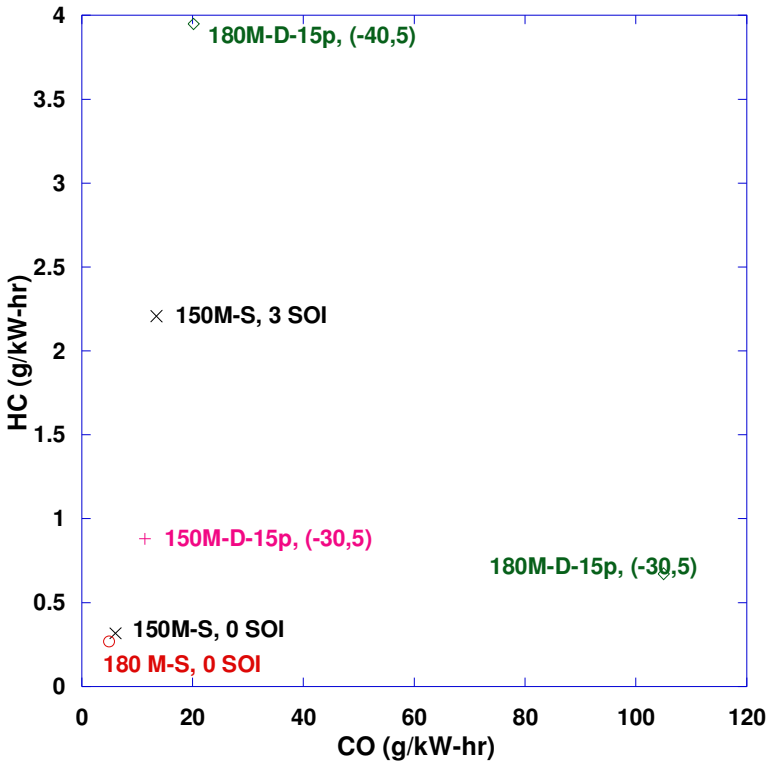

Figure 5.26 CO vs HC emissions for 150 and 180 MPa injection pressures at 30% EGR for both single and double injection conditions. (Note that (-40, +5) denotes pilot SOI = -40 ATDC and main SOI = + 5 ATDC)

Table 5.1 List of emissions and BSFC results for selected cases shown in Figure 5.25. The EGR level was 30% for all the cases tested

P_inj	SOI (ATDC)	NO (g/kW-hr)	PM (g/kW-hr)	BSFC (g/kW-hr)	CO(g/kW-hr)	HC (g/kW-hr)
150	0	0.826	0.056	240	6.06	0.318
150	+3	0.914	0.012	262	13.5	2.21
180	0	0.911	0.047	248	4.99	0.268
150	-30/+5	0.559	0.037	258	11.4	0.88
180	-30/+5	0.649	0.051	269	10.5	0.672
180	-40/+5	0.561	0.005	310	20.19	3.95

5.7 Convergent Nozzle (6X133X800, K=3)

5.7.1 Effects on Emissions and BSFC

The convergent nozzle injector was tested at the same experimental conditions under which the baseline injector was tested. Note that, the maximum allowable injection pressure for the convergent nozzle injector was 200 MPa (compared to 180 MPa for the baseline injectors). Figure 5.27 shows PM and NOx emissions using single injection with 15% and 30% EGR. As with the previous set of injectors, 15% EGR was not effective in reducing NOx emissions. It should be noted that, for 15% EGR at retarded timings between 0 ATDC and 5 ATDC, PM emissions varied between 0.007 g/kW-hr and 0.05 g/kW-hr. When EGR was increased to 30%, as in the case of previous injectors, PM emissions increased initially by retarding SOI timings with a peak at -5 ATDC. Further retarding SOI to 0 and 5 ATDC would reduce PM emissions to reach the Tier 4 standard.

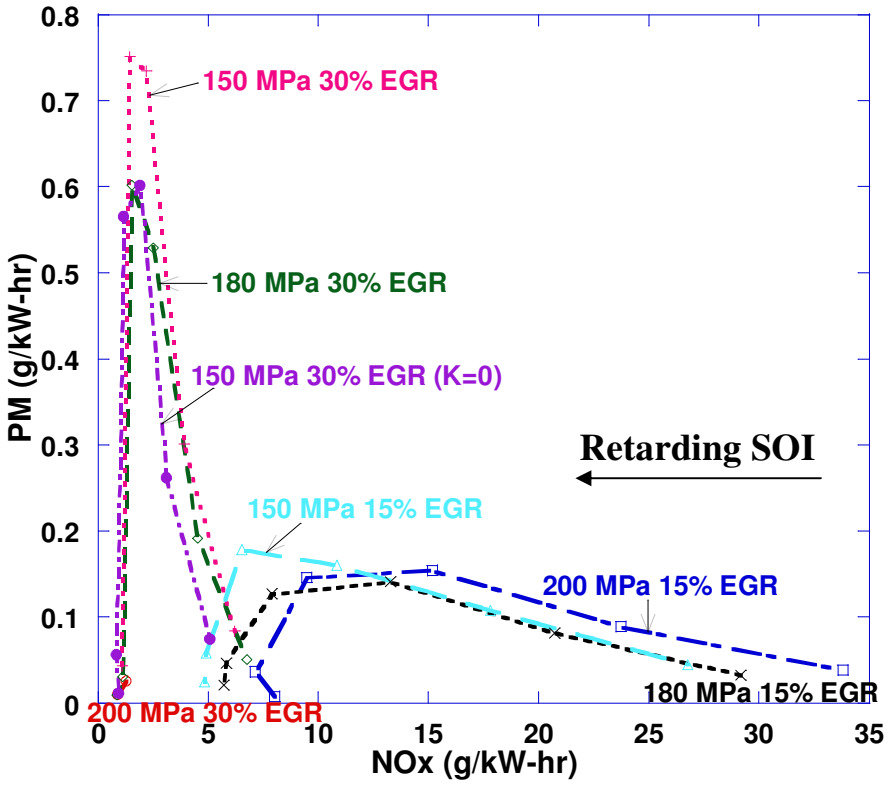

Figure 5.27 PM and NOx emissions using the K=3 nozzle at different conditions

Figure 5.28 shows the comparisons between baseline injectors (K=0) and the injectors with K= 3.0. It can be seen that the injectors with K=3.0 were not significantly different from the baseline injectors in reducing PM emissions. The baseline injectors performed better in reducing NOx emissions compared to the injectors with K=3.0. This could be due to high injection velocity in the case of converging nozzles to produce higher NOx emissions. Figure 5.29 indicates that BSFC of the converging nozzles is also similar to that of the baseline injectors.

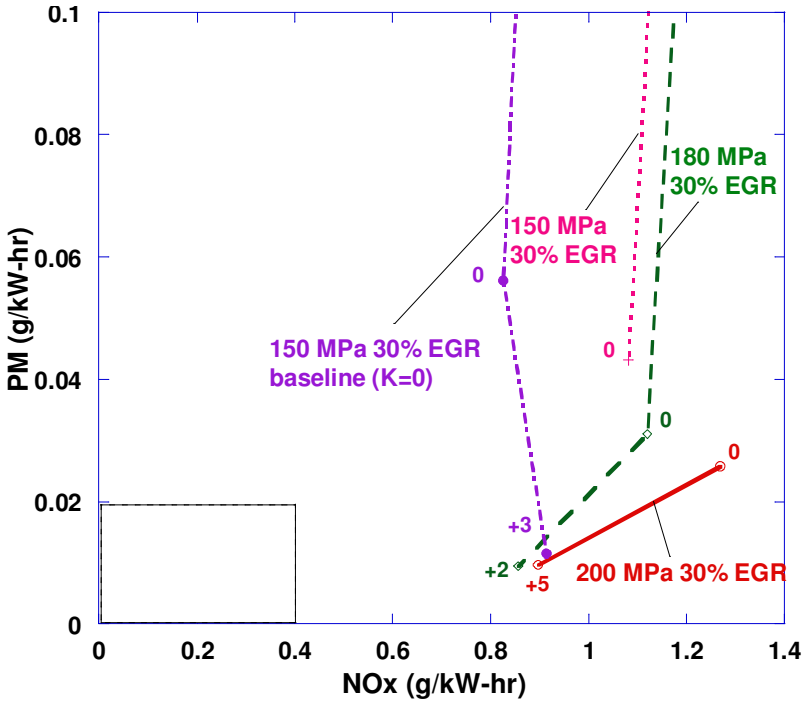

Figure 5.28 PM vs NOx for baseline nozzle (K=0) and the converging nozzle at different conditions

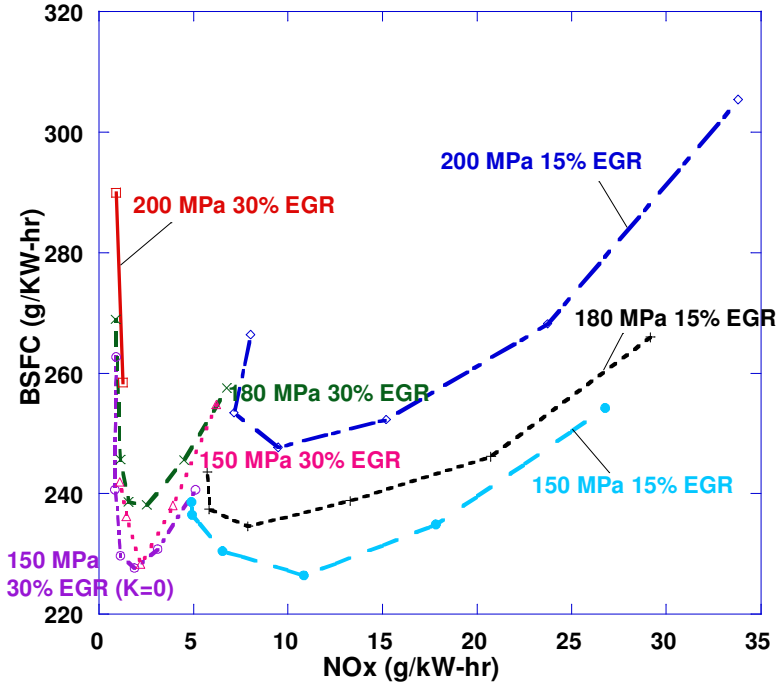

Figure 5.29 BSFC vs NOx for the converging nozzles (K=3) in comparison with the baseline nozzle (K = 0)

Figures 5.30 and 5.31 show the comparisons of NOx and PM emissions for the double injection cases. These tests were performed at 15% pilot fuel with main injection at 5 ATDC. A pilot sweep was performed from -30 ATDC till -15 ATDC. It can be seen that as the pilot SOI is advanced, PM emissions is reduced rapidly for both the baseline and the converging nozzles while NOx emissions remain unchanged in most cases. Though PM emissions is within the limits for Tier 4 standards for an advanced pilot SOI of -30 ATDC, NOx emissions varies between 0.6 g/kW-hr and 1 g/kW-hr which is higher than the standard of 0.4 g/kW-hr.

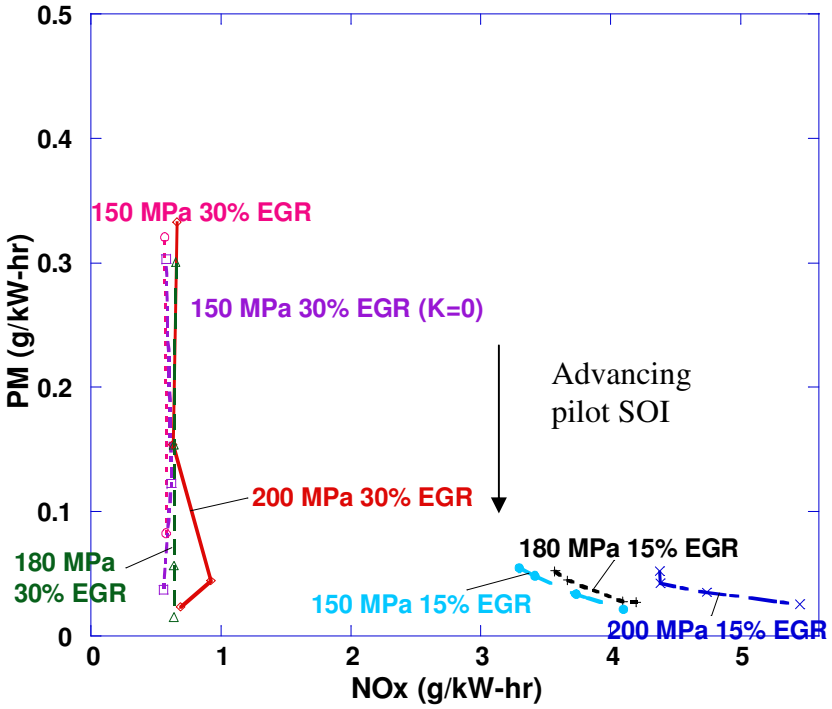

Figure 5.30 PM vs NOx emissions for the converging nozzles under different double injection conditions

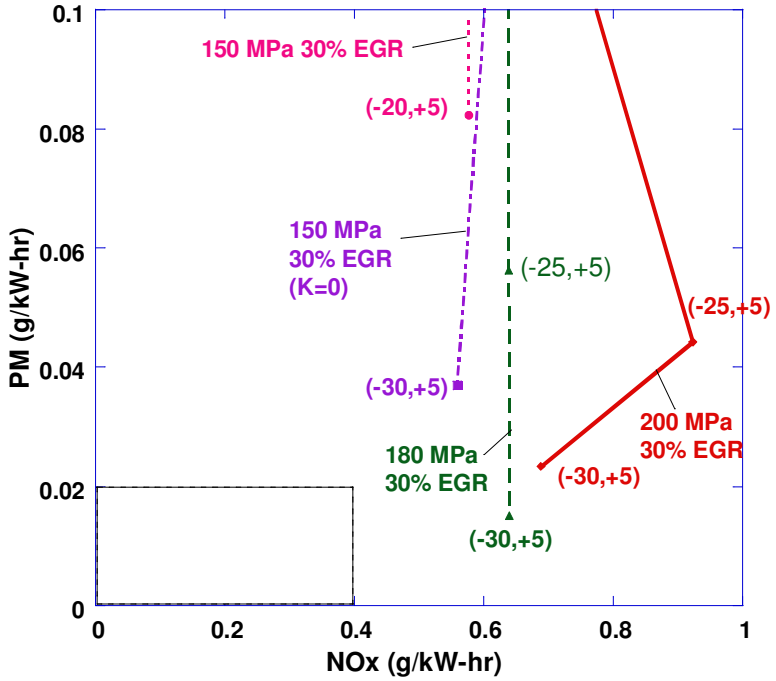

Figure 5.31 A close-up plot of Figure 5.30 with the comparison between the baseline nozzles (K=0) and the converging nozzles

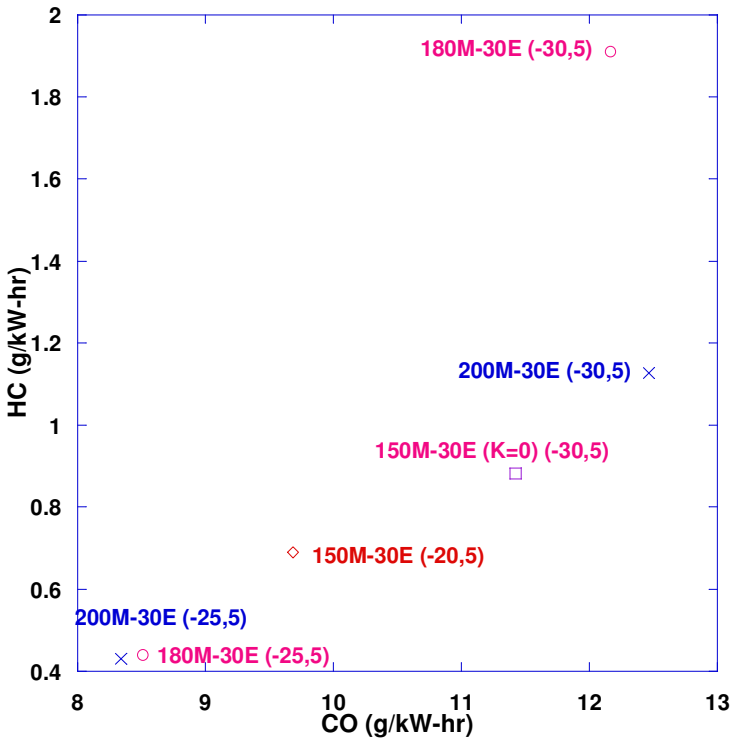

Figure 5.32 CO and HC emissions for the cases shown in Figure 5.31

During the double injection tests, it was observed that the converging nozzle did not allow to use a pilot SOI as early as the one used for the baseline nozzle. For instance, by comparing results in Figures 5.31 and 5.25, for 180 MPa injection, a pilot SOI of -40 ATDC can be used in the baseline injectors. However, engine combustion was not stable using the converging nozzles under the same conditions. It is speculated that the fuel spray has a higher velocity by using the converging nozzles that could result in rapid atomization and vaporization such that the mixture leaned out and ignition failed. The other possibility is that the high velocity fuel jet could escape the piston bowl and result in poor combustion. Nonetheless, for the same injection conditions, e.g., 180 MPa injection pressure with pilot SOI = -30 ATDC, the converging nozzles result in lower PM emissions (see Figure 5.31) as compared to the baseline nozzles (see Figure 5.25). The same is true for 150 MPa injection pressure whose PM emissions was 0.122 g/kW-hr for pilot SOI = -20 ATDC.

Table 5.2 List of emissions and BSFC results for selected cases shown in Figure 5.31 using the converging nozzles. EGR level was 30% for all the cases tested.

P_inj	SOI	NOx (g/kW-h)	PM (g/kW-h)	BSFC(g/kW-h)	CO(g/kW-h)	HC(g/kW-h)
150	0	1.08	0.043	241	5.19	0.29
180	0	1.12	0.031	245	4.60	0.27
180	+2	0.86	0.009	269	11.9	1.61
200	0	1.27	0.026	258	4.77	0.28
200	+5	0.90	0.010	290	13.0	2.27
180	-30/+5	0.64	0.015	277	12.2	1.91
200	-30/+5	0.688	0.023	290	12.5	1.13

The emission data of selected cases were shown in Table 5.2 by using the converging nozzles. By comparing data in Tables 5.1 and 5.2, generally speaking, the emissions are

similar. However, the use of the present converging nozzles (K=3) offers a slight advantage in PM reductions under the same injection conditions.

5.8 10-hole Injector (10X133X800)

5.8.1 Geometry of the Injector

The baseline and convergent nozzle injectors have showed the capability of reducing emissions under certain conditions. As the EGR was increased to reduce the NOx emissions, the PM emissions increased significantly. It was shown from experiments performed in a constant-volume combustion chamber that a smaller nozzle hole can enhance fuel atomization and mixing to reduce PM emissions [17]. Therefore, it is of interest to explore the effects of the nozzle hole size in real engine conditions. On the other hand, the total flow area needed to be kept the same in order to inject the same amount of fuel within the same duration, i.e., same flow number. As a result, a new set of injectors were designed. The new injectors have 10 holes and the size of each hole was reduced. The injectors are denoted as "10X133X800", as described in Table 4.2.

5.8.2 Effects on Emissions

Figures 5.33 and 5.34 show the emissions and BSFC data using the 10-hole injectors at various EGR and injection pressure levels. As expected, the PM emissions were lower compared to the convergent nozzle and baseline injectors at both 150 and 200 MPa injection pressure and 30% EGR. The NOx emissions were similar to that of baseline injectors.

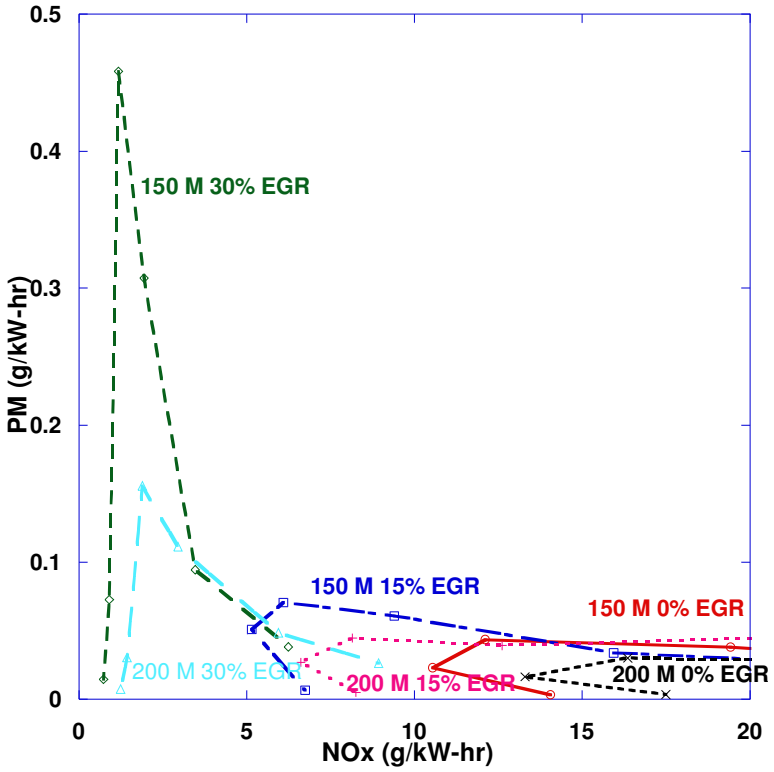

Figure 5.33 NOx vs PM emissions using 10-hole injectors at different EGR levels

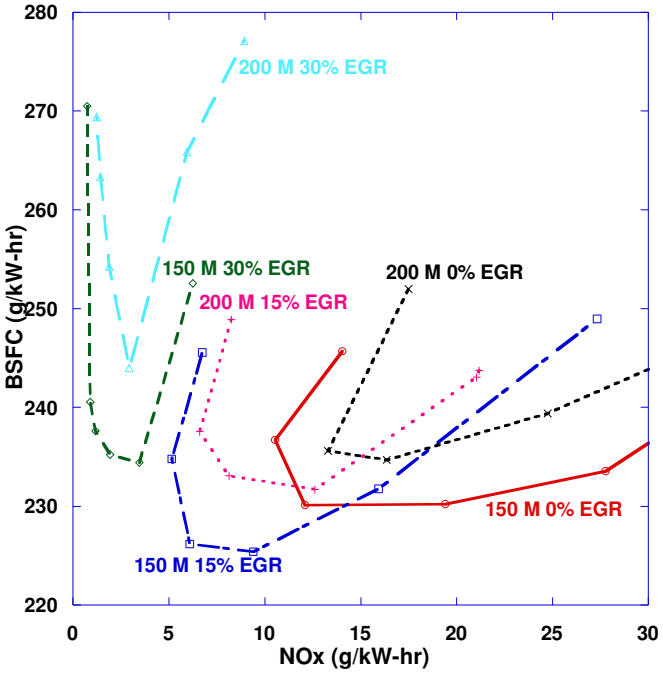

Figure 5.34 NOx vs BSFC emissions using 10-hole injectors at different EGR levels

5.8.3 Comprehensive Comparison of Emissions

In this section, performance of the above three injectors are compared at selected operating conditions, particularly at high EGR conditions.

From Figure 5.35, NOx emissions using the convergent nozzle were comparable with the baseline injector, but PM emissions were significantly higher. It is evident that using the 10-hole injector could reduce PM emissions with very little sacrifice to NOx emissions, in particular, for late injection timings.

The injection pressure was found to have significant effects on NOx and PM emissions at high EGR conditions. NOx levels increased with injection pressures while PM levels reduced for all injectors. It is interesting to observe that although the introduction of EGR reduced the oxygen available to the fuel for most of the injection timings, the BSFC did not vary noticeably between 0% and 30% EGR conditions as can be seen from Figure 5.37. The reason is that the same amounts of fuel were used and the intake charge temperatures were kept constant (i.e., 23 ºC) regardless of the EGR levels.

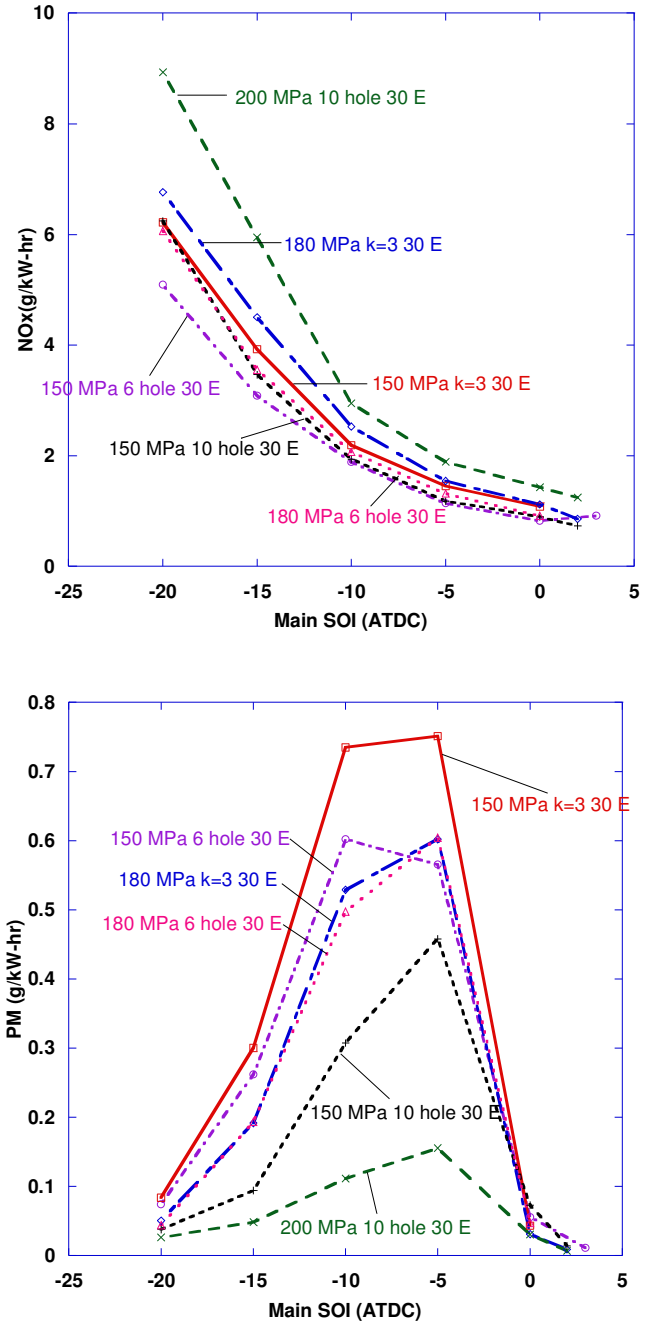

Figure 5.35 NOx and PM emissions of all three injectors at 30% EGR with different injection pressures

Figure 5.36 shows the CO and HC emissions for 30% EGR. It can be readily noticed that at late injection timing (e.g., past TDC), significant CO and HC emissions were produced due to incomplete combustion. As a result, the BSFC increased significantly at late

SOI. Note that the latest allowable injection timing was 3 ATDC for 30% EGR due to the low in-cylinder oxygen levels, as compared to 5 ATDC for 0 and 15% EGR conditions.

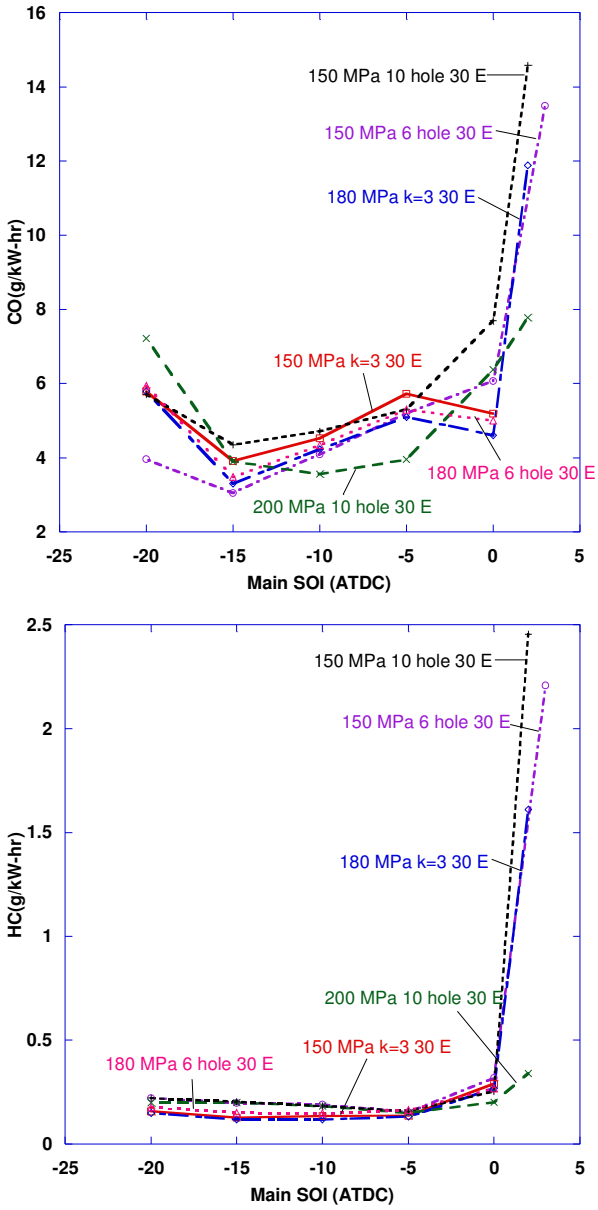

Figure 5.36 NOx and PM emissions of all three injectors at 30% EGR with different injection pressures

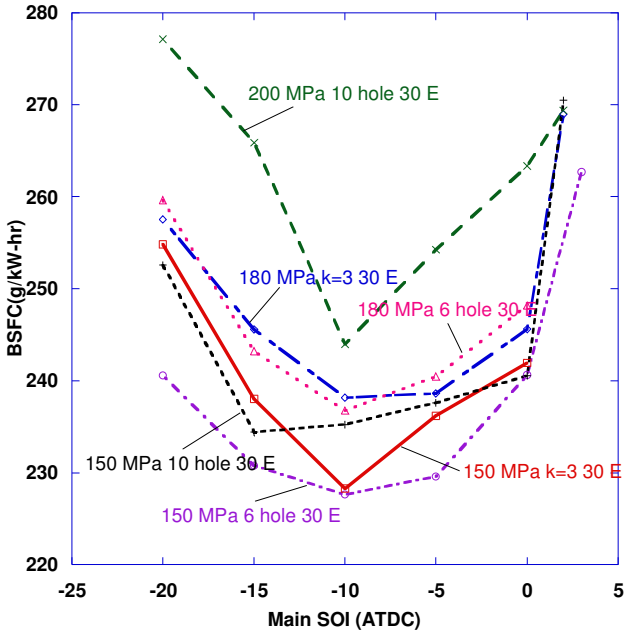

Figure 5.37 BSFC of all three injectors at 30% EGR with different injection pressures

Figure 5.38 shows NOx and PM emissions data from all the cases tested in this study. It appears that higher EGR rates with late SOI are required for simultaneous PM and NOx reductions using single injection. Figure 5.39 shows the same data set in a smaller scale. The box at the left bottom corner indicates the Tier 4 emission requirements for the present class of engines. Among the cases that met PM regulations were the 10-hole injector using 150 MPa injection pressure with SOI at 2 ATDC, the convergent nozzle using 180 MPa injection pressure with SOI at 2 ATDC, and the 6-hole injector using 150 MPa injection pressure with SOI at 3 ATDC. Despite the fact that a 30% EGR rate was used, NOx emissions were still not within the limit of the Tier 4 standards. Further investigations are needed to create a local mixture condition that can prevent NOx production such as using extremely high EGR or other injection schemes.

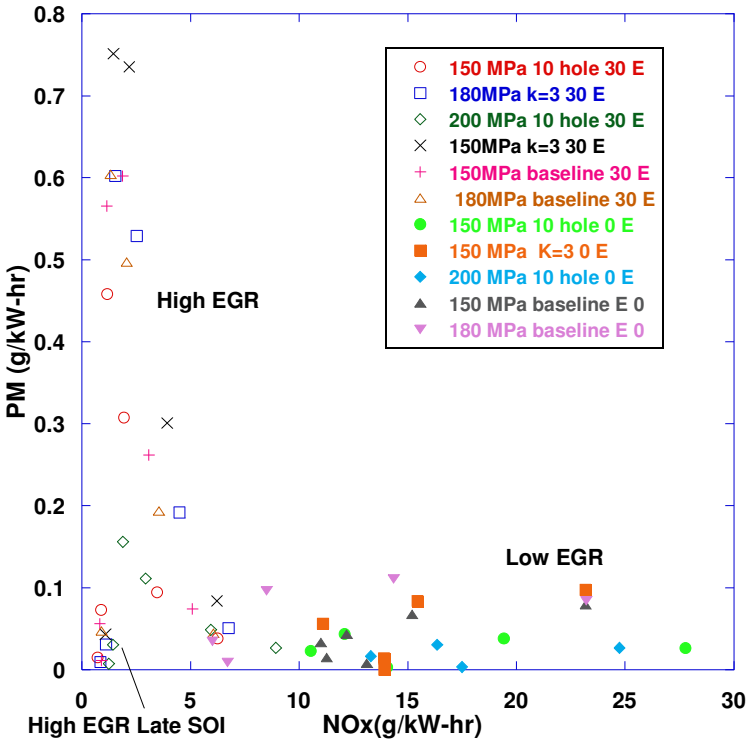

Figure 5.38 PM and NOx emissions for all the cases tested in this study (0%, 15% and 30% EGR for all three injectors at different injection pressures)

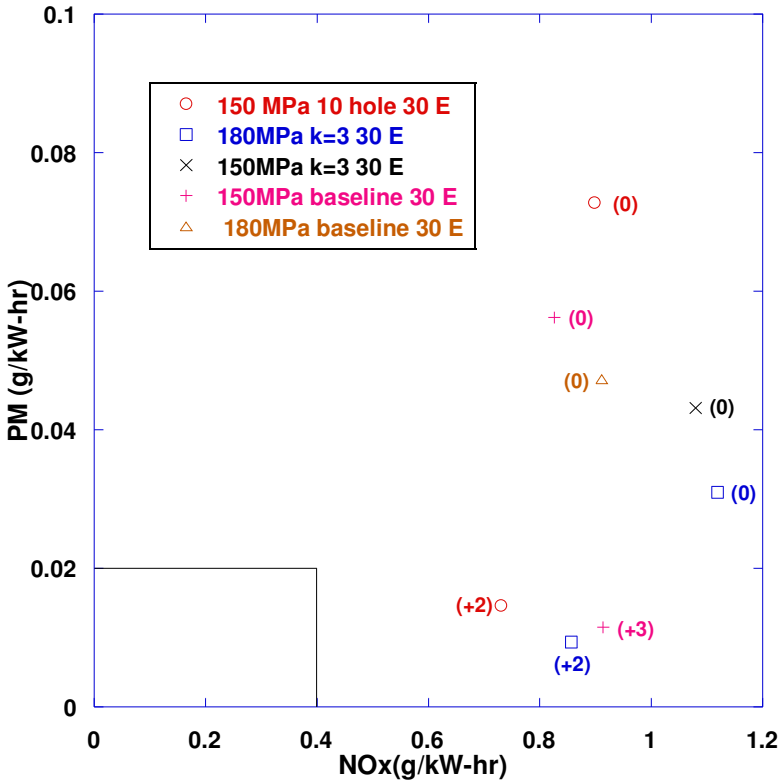

Figure 5.39 PM and NOx emissions for selected cases that produced emission results within the scale shown. The number next to the data point is the SOI timing. The box on left bottom corner shows the Tier 4 standards for NOx and PM emissions

Figure 5.40 shows the cylinder pressure and the normalized heat release rate data for all three injectors at 150 MPa injection pressure, 0 ATDC SOI, and 30% EGR. Note that in a production engine, the turbocharger is driven by exhaust gas and different operating conditions can result in different exhaust gas energy levels. As a result, the compression pressures at TDC differed slightly due to the use of a turbocharger to the extent that the intake boost pressure could not be directly controlled by the operator. All three injectors produced very similar combustion phasing under the same injection timings as can be seen from the heat release data. Under these low temperature combustion conditions, the PM emissions levels using the three injectors were also similar.

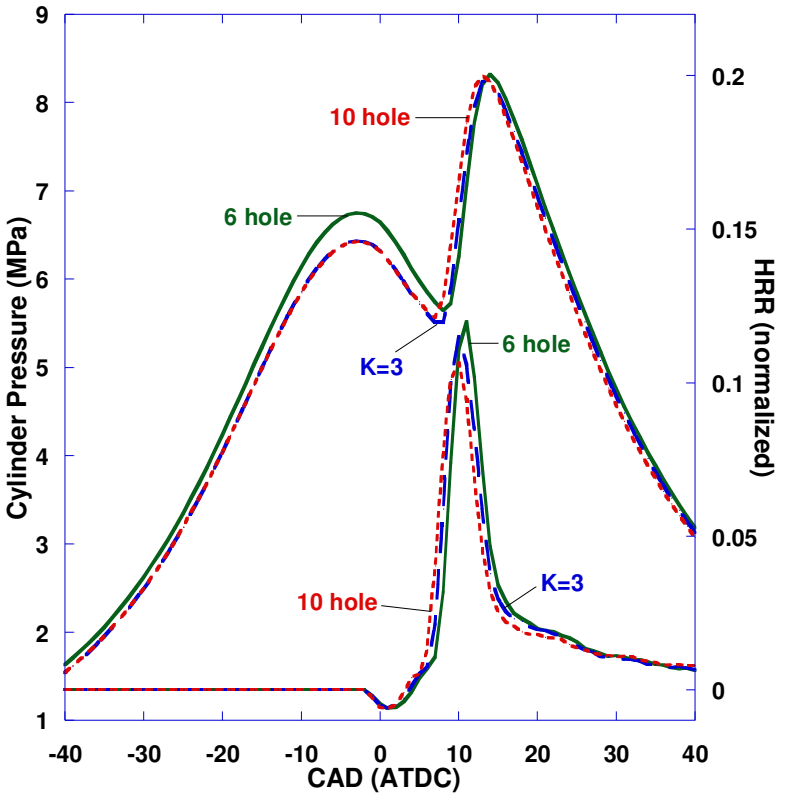

Figure 5.40 Cylinder pressures and normalized heat release rate data for different injectors with 150 MPa injection pressure, 0 ATDC SOI, and 30% EGR

Figure 5.41 shows the cylinder pressure and heat release rate data for the above three cases with low emissions. It can be seen that the ignition delay was relatively long, and the peak cylinder pressure was lower than those in earlier injection timings (Figure 5.40).

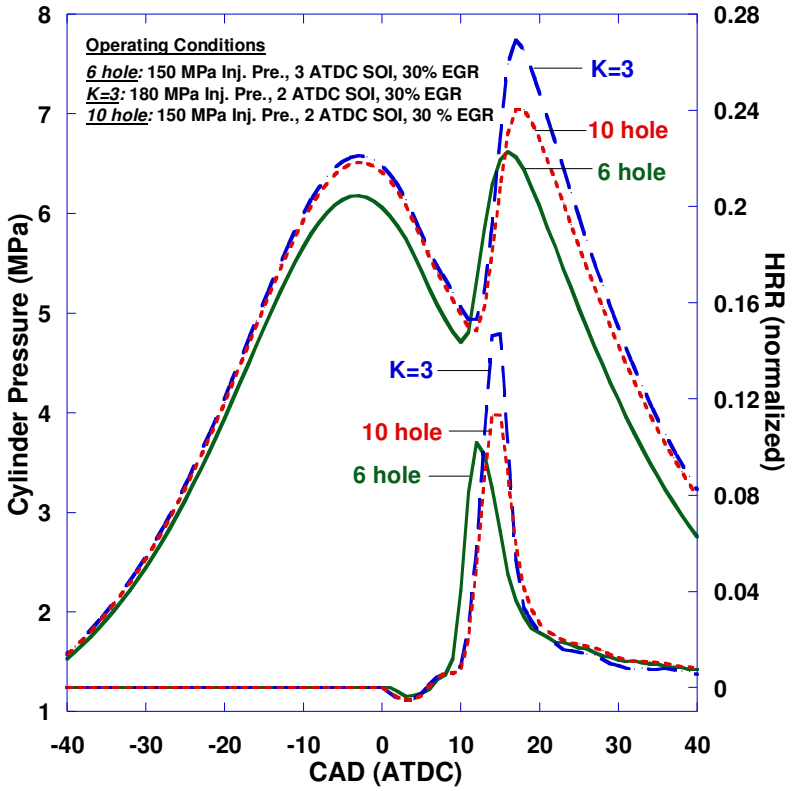

Figure 5.41 Cylinder pressure and heat release rate for 30% EGR, late injection conditions (SOI = 2 and 3 ATDC) that produced low PM emissions shown in Figure 5.39

5.9 16-hole Injector (16X133X800)

5.9.1 Injector Geometry

Following the success of 10-hole injectors, effects of further increasing the number of nozzles on the injector were studied. A new injector with 16 holes on its tip was designed. The flow number was kept the same at 800. This injector has 8 nozzles on each circle. This increase in the number of nozzles reduced the nozzle hole size from 114 µm (10-hole injector) to 91 µm. The graphical representation and spray simulation results using a 45-degree sector mesh are given in Figure 5.42.

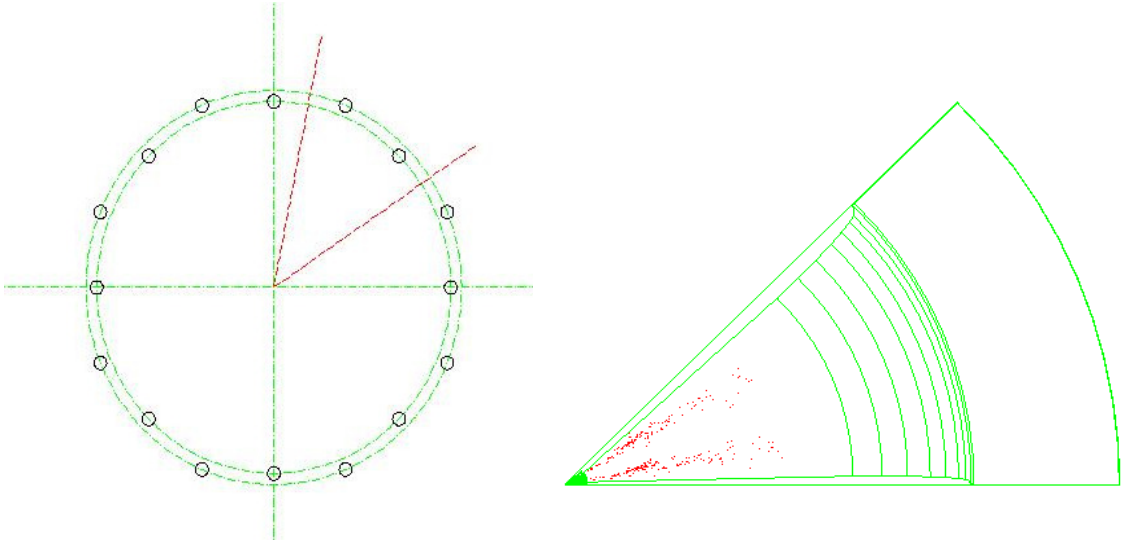

Figure 5.42 16-hole Injector geometry and a 45 degree sector mesh

5.9.2 Effects on Emissions and BSFC

Despite that the nozzle size was reduced, the 16-hole injector did not reduce the PM emissions. On the contrary, there was a huge increase in PM emissions compared to the three injectors previously tested (Figure 5.43). The reason is believed to be due to the limited spray penetration and poor air utilization. In the 10-hole injector, there were 10 holes on the tip of the injector on a single circle, i.e., one nozzle for every 36 degrees on the circle. When the number of holes was increased to 16, there was one nozzle every 22.5 degrees. This reduction in "angular distance" between nozzles led to the close spacing of the fuel sprays. In addition, a smaller nozzle hole can produce small drops that do not have significant momentum to penetrate. As a result, poor air utilization will occur which increases PM emissions. The BSFC values (Figure 5.44) for the 16-hole injectors were also higher compared to other injectors due to poor combustion efficiency.

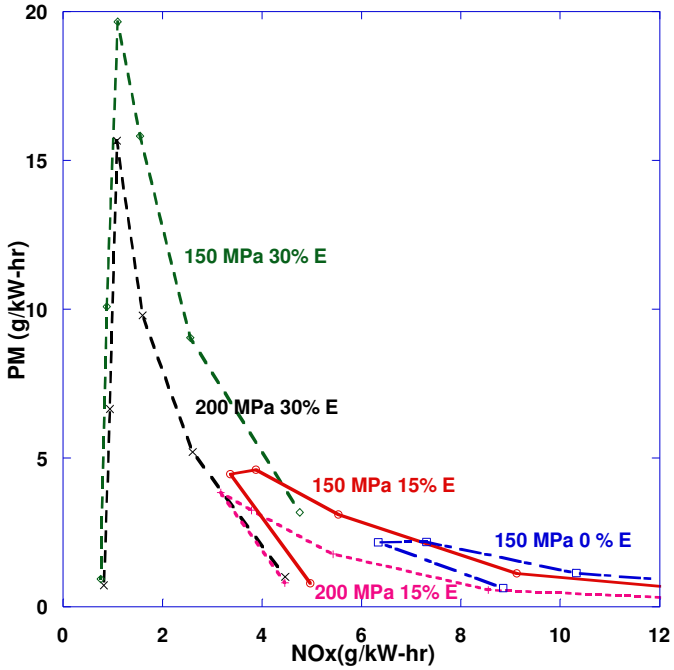

Figure 5.43 NOx vs PM for all the single injection cases for 16 hole injectors

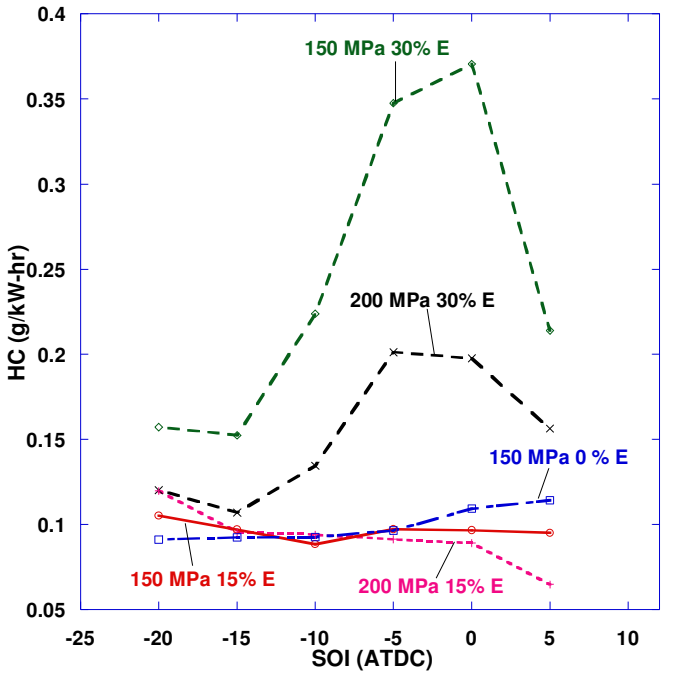

Figure 5.44 NOx vs BSFC for all the cases for 16 hole injectors

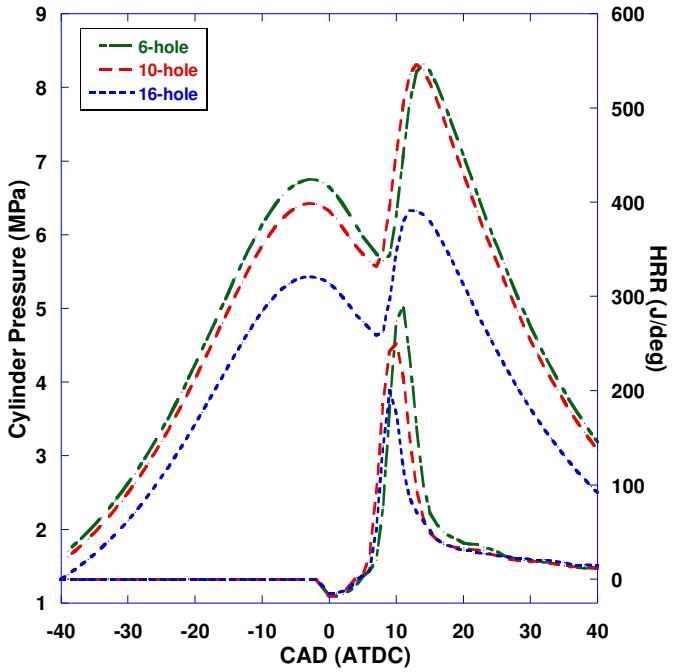

Figure 5.45 Cylinder pressure and HRR for three injectors (6-hole, 10-hole, and 16-hole at 150 MPa injection pressure, 0 ATDC SOI, and 30% EGR

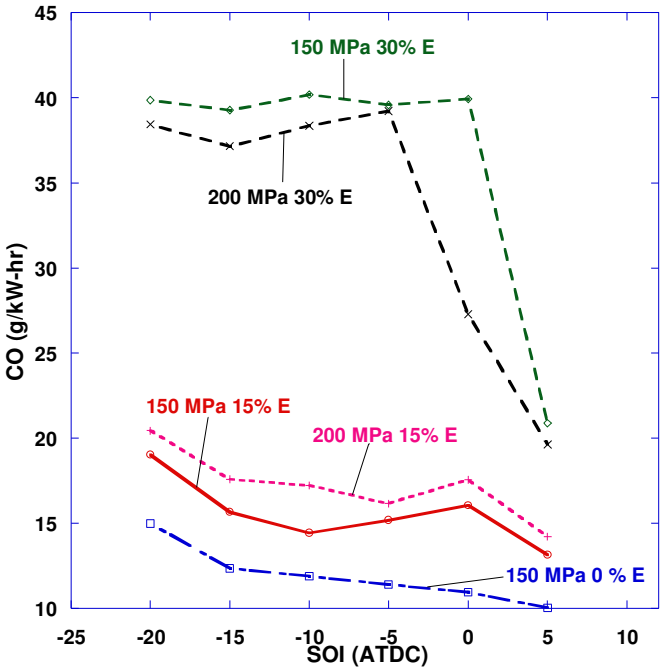

Figure 5.46 CO emissions for all 16-hole injector cases

Comparisons of cylinder pressure and HRR for all three injectors at 150 MPa injection pressure, 0 ATDC SOI, and 30% EGR are shown in Figure 5.45. It should be noted that while fuel injected was 50 mg/stroke for 6-hole and 10-hole injectors, only 45 mg/stroke of fuel was injected for 16-hole injectors. This difference can be seen in both cylinder pressure and HRR curves in Figure 5.45. Though the shapes of the curves look similar, 16-hole injectors produced significantly higher PM and CO emissions over other injectors. The CO emissions at 0% and 15% EGR are well over the CO emissions by other injectors at 30% EGR. As explained above, spray overlap has likely caused the CO emissions to increase.

5.10 6X133X480 Injectors

Some of the strategies mentioned in the above sections can reduce the emissions significantly. However, the PM emissions increased significantly using convergent and baseline nozzles when the EGR was increased above 30%. The BSFC was also increased for EGR higher than 30%. This indicates that the combustion was incomplete. A lower flow number injector will inject the fuel with a lower flow rate for a longer duration. The lower fuel flow rate can make it easier for air-fuel mixing, leading to a reduction in NOx without drastically increasing the PM emissions at high EGR levels (>30%). Therefore, injectors with a lower flow number were made (6X133X480). In this injector, each nozzle has a flow number of 80 instead of 133 as in the case of the baseline injector. The NOx and PM emissions using single injection are given in Figure 5.47. The new injectors allowed the EGR to reach a high level without increase in PM or BSFC (Figure 5.48).

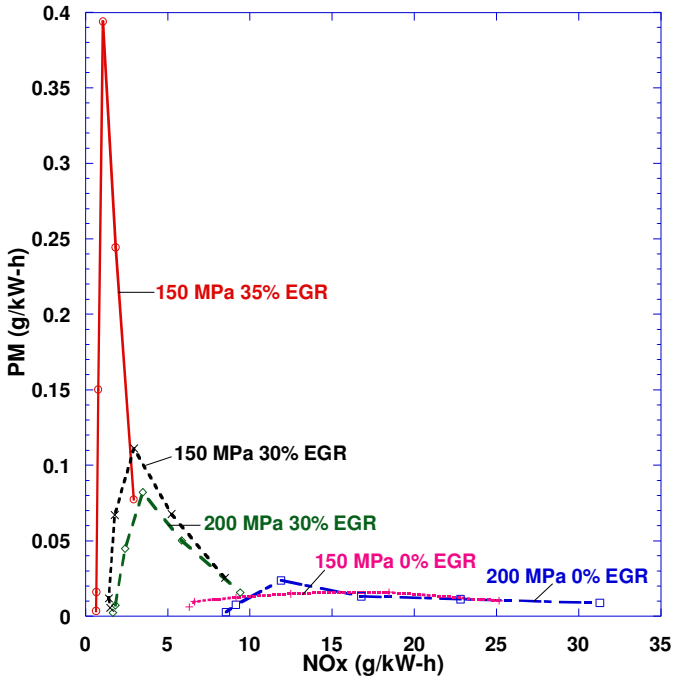

Figure 5.47 NOx vs PM for all the single injection cases using 6X133X480 injectors

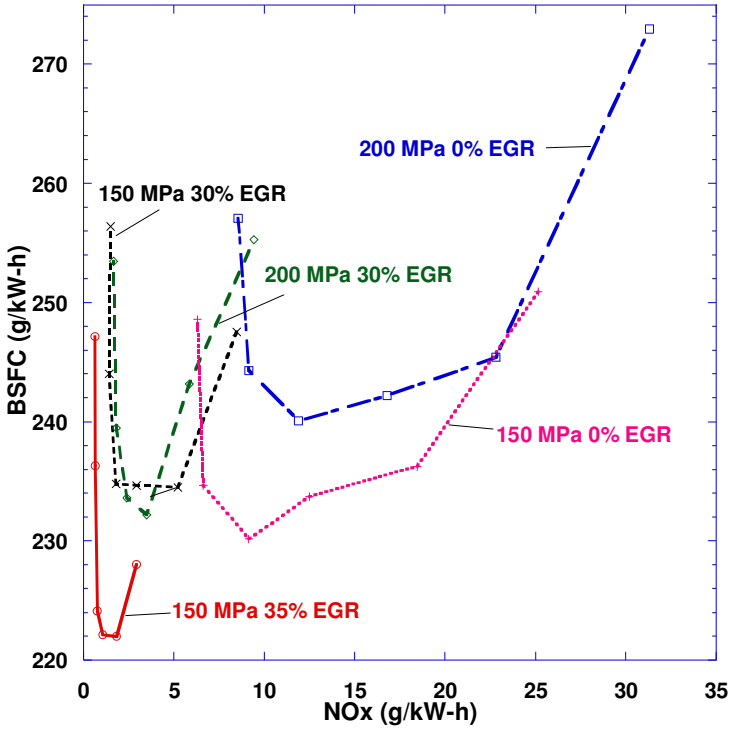

Figure 5.48 NOx vs BSFC for all the single injection cases using 6X133X480 injectors

More tests were performed with higher EGR rates at different injection pressures including 130 MPa, 150 MPa, and 200 MPa. The NOx and PM emissions for conditions using 0 ATDC SOI are shown in Figure 5.49. As can be seen, these injectors were able to meet Tier 4 emissions standards at 200 MPa injection pressure, 0 ATDC SOI, and 41% EGR. The emissions for other high EGR conditions were also relatively close to the Tier 4 standards compared to the results shown in Figure 5.39.

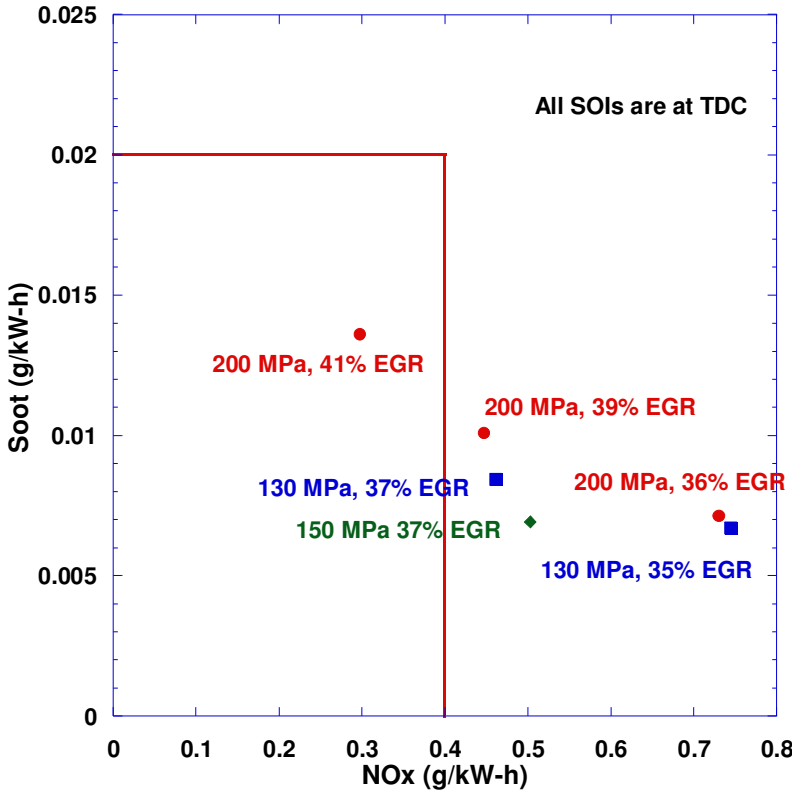

Figure 5.49 PM and NOx emissions for selected cases. The box on left bottom corner shows the Tier 4 standards.

Emissions for all the cases presented in the above figure are given in Table 5.3. For most cases, the BSFC values were under 250 g/kW-h. At the same time, the CO and HC emissions were significantly lower than that of baseline and convergent nozzle injectors mentioned in Tables 5.1 and 5.2. It is premised that longer injection duration with a smaller

nozzle hole size enhanced the oxidation of both CO and HC emissions leading to a reduction in the same.

Table 5.3 Emissions of cases shown in Figure 5.49 at various operating conditions

P_inj	EGR%	NOx (g/kW-h)	PM (g/kW-h)	BSFC (g/kW-h)	CO (g/kW-h)	HC (g/kW-h)
130	35	0.74	0.006	332	11.57	1.36
130	37	0.46	0.0084	247	8.31	0.967
150	37	0.503	0.0069	244	7.63	0.658
200	36	0.73	0.0071	240	4.89	0.29
200	39	0.447	0.001	244	5.80	0.39
200	41	0.2976	0.014	266	12.26	2.42

Further comparisons can be observed from Figure 5.50. In this figure, comparisons of cylinder pressure and HRR of best cases for 6X133X480 and baseline injectors are given. It should be noted that the SOI for baseline case was at 3 ATDC while it was TDC for the other cases. It is evident from HRR curves that despite a 3 ATDC SOI, the ignition delay for the baseline case was much less compared to the other two cases. This shows that the effect of EGR is significant compared the SOI on ignition delay. Also, the peak HRR, which could be associated with the peak cylinder temperature, was significantly higher for the baseline injector. This may have led to higher NOx emissions in the case of baseline injectors.

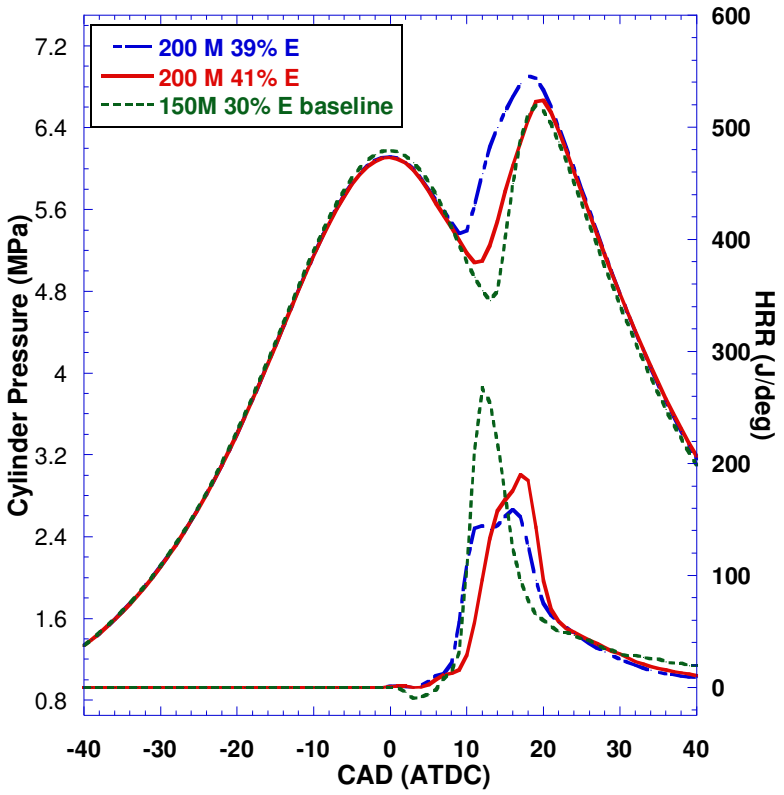

Figure 5.50 Comparison of cylinder pressure and HRR of baseline injector (3 ATDC SOI) and 6X133X480 (TDC SOI) injectors.

5.11 10X133X500 Injectors

Motivated by the success of the 10-hole injectors with 800 flow number, new injectors (10X133X500) with a reduced flow number were designed. Each nozzle on this injector has a flow number of 50. Note that the flow number of the nozzles on the 16-hole injector mentioned in Section 5.9 was also 50. The previous 16-hole injector produced relatively high PM emissions due to poor air utilization since the nozzle holes were crowded. Despite the same flow number per nozzle, the 10X133X500 injectors have proved to be very successful in reducing the PM emissions. This underlines the importance of nozzle arrangement to promote air utilization. Results are shown in Figure 5.51. Despite that a wide range of operating conditions were tested, only results with low emissions are presented.

Three injection pressures, 150 MPa, 200 MPa and 225 MPa, were tested. At 200 MPa injection pressure and 0 ATDC SOI, only 39% EGR was required to meet the Tier 4 standard compared to 41% using the 6-hole injectors mentioned in the previous section.

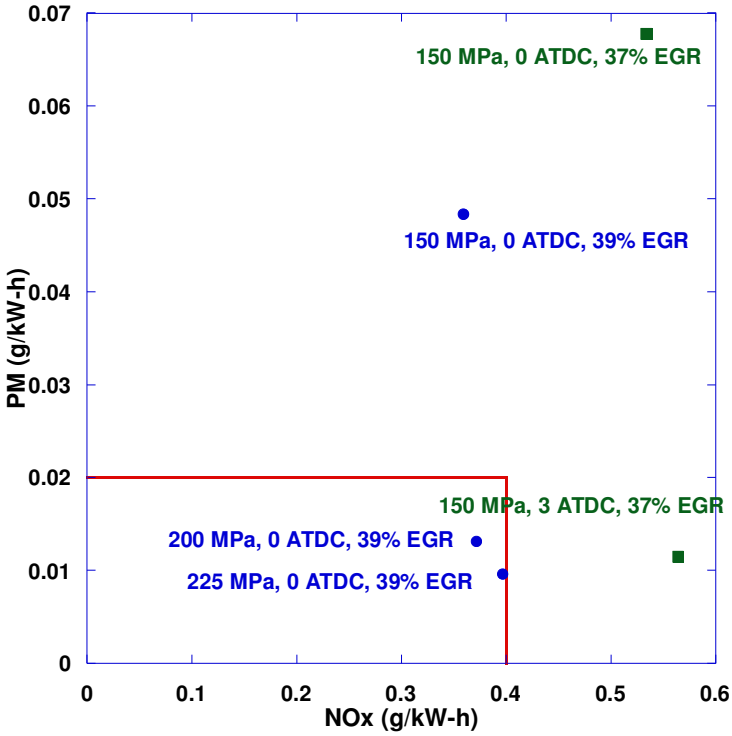

Figure 5.51 PM and NOx emissions for selected cases that produced emission results within the scale shown. The box on left bottom corner shows the Tier 4 standards.

HC and CO emissions along with others for the cases mentioned in Figure 5.51 are given in Table 5.4. As with the case of 6X133X480 injectors, the BSFC levels were well below 250 g/kW-h.

Table 5.4 Emissions of cases shown in Figure 5.51 at various operating conditions

P_inj	EGR%	NOx (g/kW-h)	PM (g/kW-h)	BSFC(g/kW-h)	CO(g/kW-h)	HC(g/kW-h)
150	37% (TDC)	0.534	0.07	237	9.25	0.529
150	37% (3ATDC)	0.56	0.011	263	14.823	4.37
150	39	0.359	0.048	242	10.54	0.837
200	39	0.372	0.013	239	9.07	0.499
225	39	0.397	0.009	245	8.49	0.42

In Figure 5.52, comparisons of cylinder pressure and HRR for the conditions mentioned in the figure are given. Start of injection in both cases was 3 ATDC. The effect of EGR was clearly observed in both cylinder pressure and HRR. The peak cylinder pressure and peak HRR were lower when 10X133X500 injectors were used at 37% EGR. This led to significant reduction in NOx emissions.

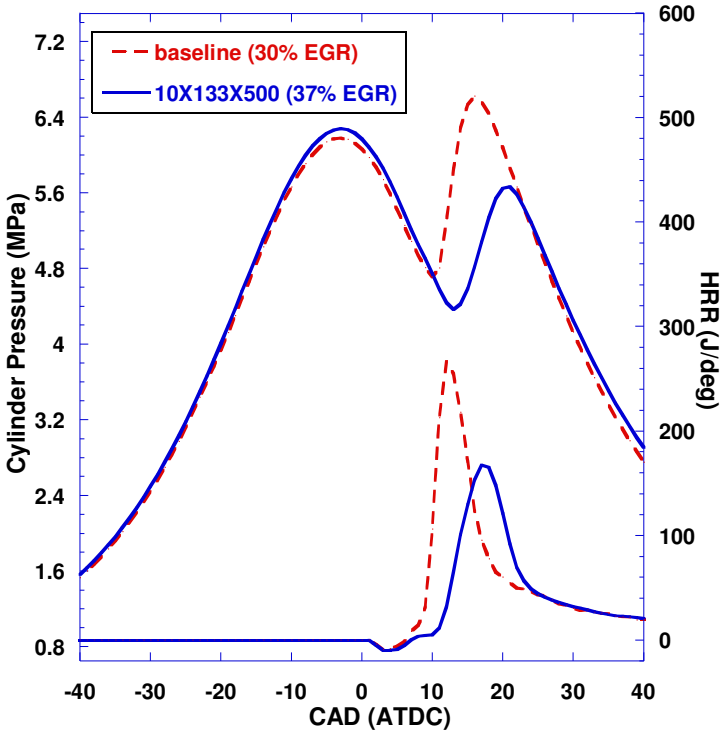

Figure 5.52 Comparison of cylinder pressure and HRR of baseline and 10X133X500 injectors at 150 MPa, and 3 ATDC SOI.

5.12 Summary of Parametric Study

In summary, effects of various parameters on engine emissions were studied. It was found that late main injections could reduce NOx and soot emissions simultaneously. EGR was helpful in further reducing NOx emissions. High injection pressures were found to help reduce soot emissions by enhancing the fuel spray atomization. When the above three variables were used in combination for the baseline injectors, NOx and soot emissions were found to be lower. However, when compared to the Tier 4 emissions, these emissions were still high. When EGR was increased while further retarding the injection timing, the combustion became unstable and the BSFC increased significantly. This indicated that emissions could not be further reduced using current setup. This had led to the development of the low flow number injectors and injectors with more nozzle holes.

A pathway of emissions reduction strategies used in this study is explained in Figure 5.53. The star shown in the figure represents the lowest emissions the baseline injectors could produce. It should be noted that the star's position is not drawn to the scale. The operating conditions at this point were 150 MPa injection pressure, 3 ATDC SOI, and 30% EGR. The injection timing could not be delayed further as the combustion would become unstable. The EGR also could not be increased due to the same reason. With the introduction of the low flow number injectors (smaller injector nozzle diameter), high EGR rate could be used for achieving low NOx emissions. Combustion could remain stable at high EGR levels while producing low emissions. As a result of further increasing EGR and injection pressure, the emissions were pushed into the Tier 4 box. As late injection was avoided, the BSFC could also remain within acceptable limits.

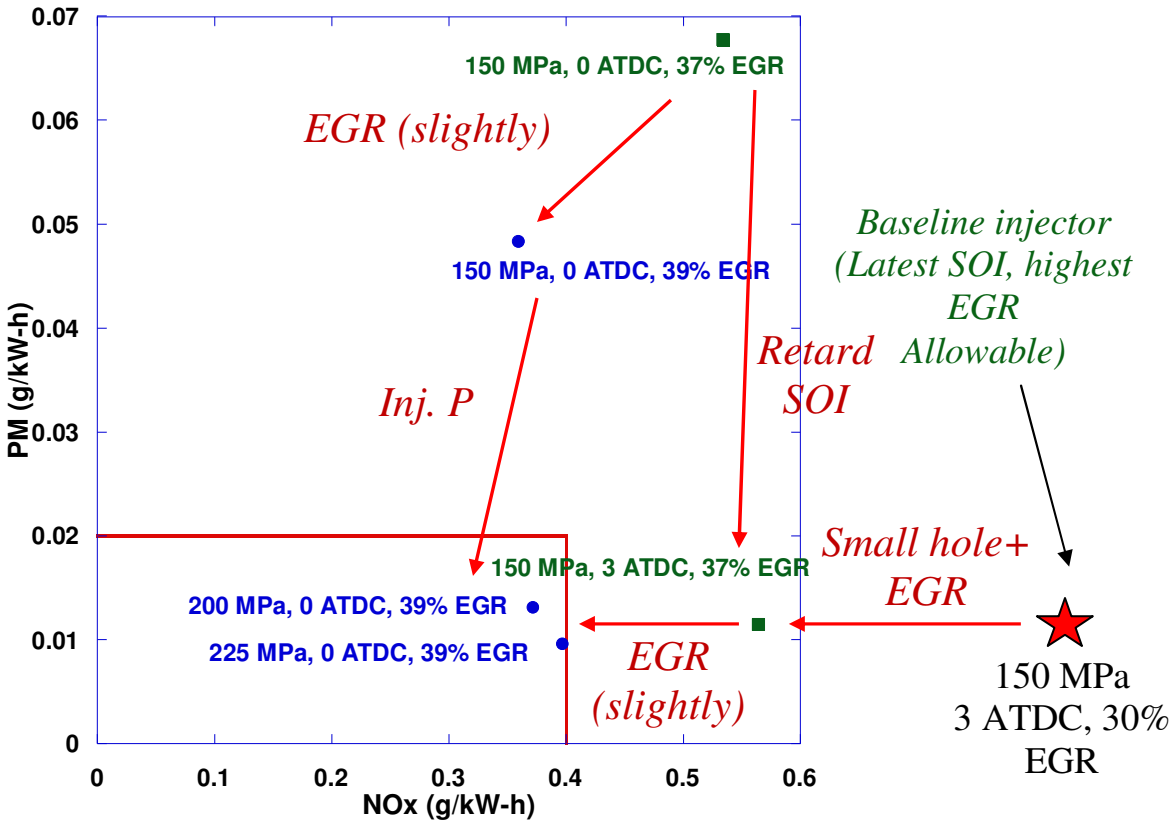

Figure 5.53 Pathway of emissions reduction

CHAPTER 6. RESULTS OF OPTIMIZATION STUDY

6.1 Validation of Particle Swarm Optimization (PSO)

There are many optimization algorithms to minimize or maximize a given problem and their success greatly depends on the type of problem. Many mathematical optimization algorithms require that the surface of the problem is known to the user. Such algorithms were not successful in solving problems with complex response surfaces such as the optimization of diesel engines for reduced emissions. Some algorithms may be trapped at a local minimum. To make sure that the current PSO algorithm does not produce such errors, it was tested using several multimodal (with multiple local minima) test functions that were widely used in the field of optimization.

The surface plots of the Ackley's Path function, Eq. (6.1), is given in Figures 6.1. The lowest function values in each iteration calculated by PSO during optimization are given in Figures 6.2. It was considered that the PSO has achieved the convergence when the function value is equal to the global minimum given in Table 6.1. The PSO was able to find the global minimum in 46 iterations.

$$f(x) = -a.e^{-b.\sqrt{\frac{\sum_{i=1}^{n} x^2}{x}}} - e^{\frac{\sum_{i=1}^{n} \cos(c.x_i)}{x}} + a + e^1 \qquad (6.1)$$

(a =20 ,b=0.2, c=2*π)

Table 6.1 Variable ranges and global minimum for Ackley's Path Function

Variable Name	Variable Range		g min	f(x) at g min
X1	-32.768	32.768	0	
X2	-32.768	32.768	0	0

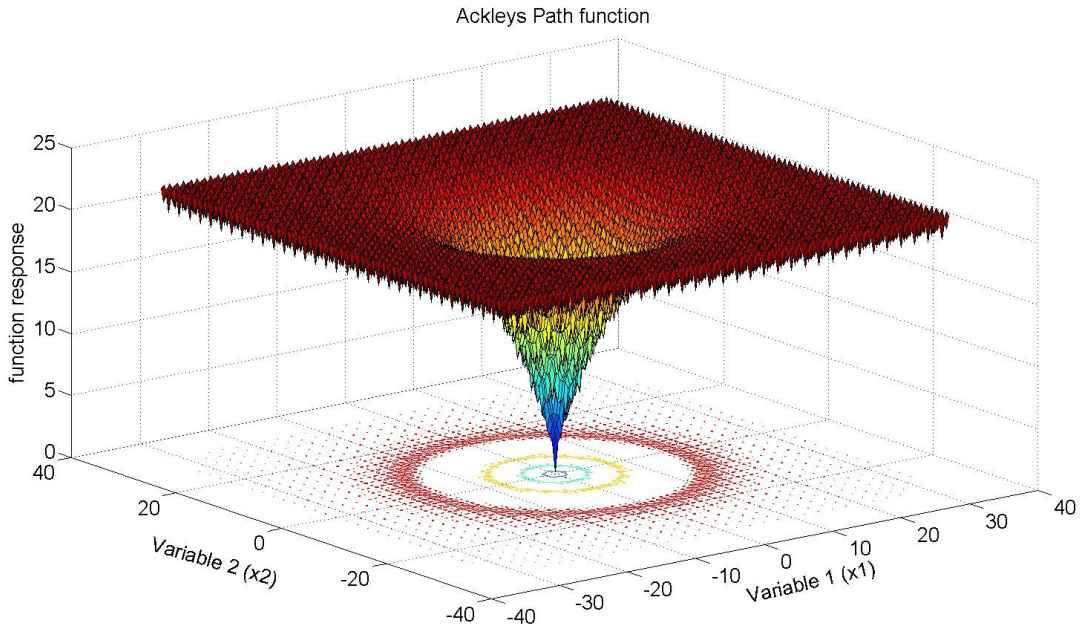

Figure 6.1 Surface plot of Ackley's Path Function with two variables

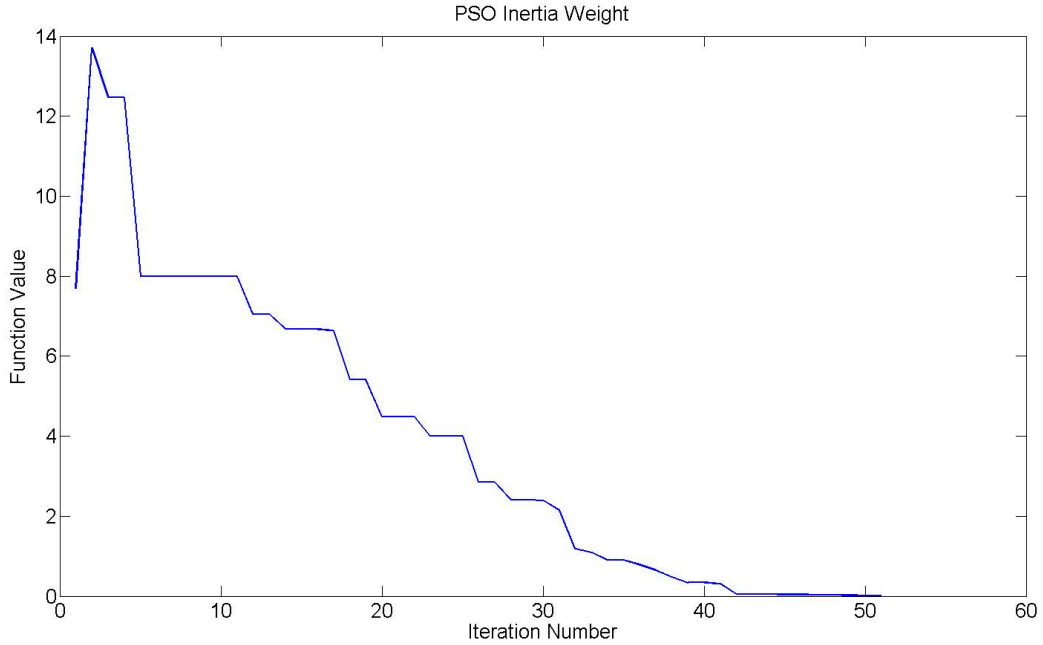

Figure 6.2 Evolution of the function value vs iteration number for the Ackley's path function

Similar tests were performed in optimizing the Rastrigen's function, Eq. (6.2). The surface plot of this function is shown in Figure 6.3 and the variable range is listed in Table 6.2. The present PSO was able to find the global minimum in 74 iterations. The above results indicated that the present PSO algorithm was implemented correctly. The next step is to integrate PSO with engine testing as will be discussed in the next chapter.

$$f(x) = 10.n + \sum_{i=1}^{n}(x_i^2 - 10.\cos(2.\pi.x_i) \qquad (6.2)$$

(n is the number of variables)

Table 6.2 Variable ranges and global minimum for Rastrigin Function

Variable Name	Variable Range		g min	f(x) at g min
X1	-5.12	5.12	0	
X2	-5.12	5.12	0	0

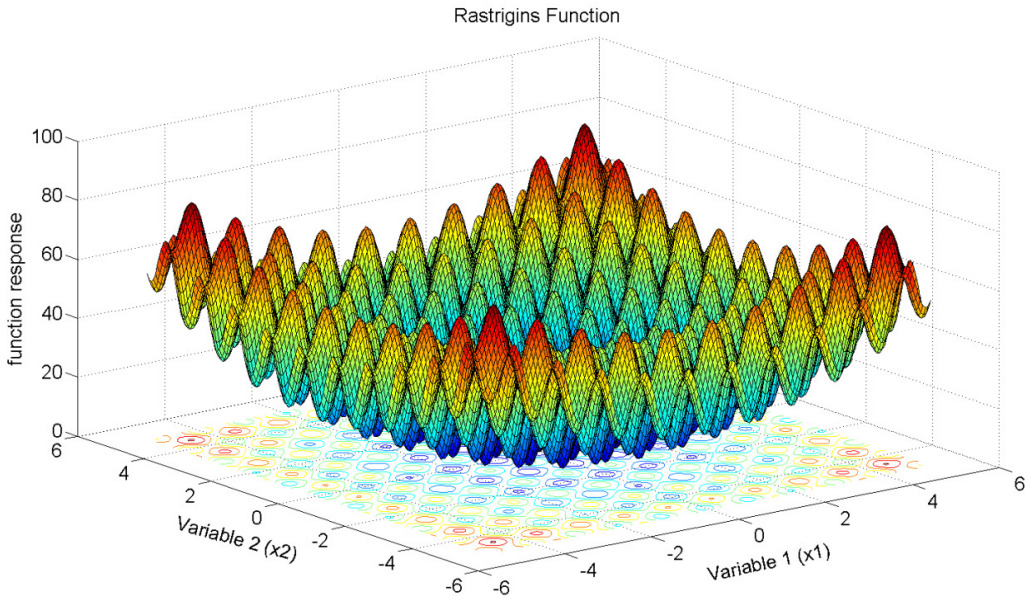

Figure 6.3 Surface plot of Rastrigin's function with two variables

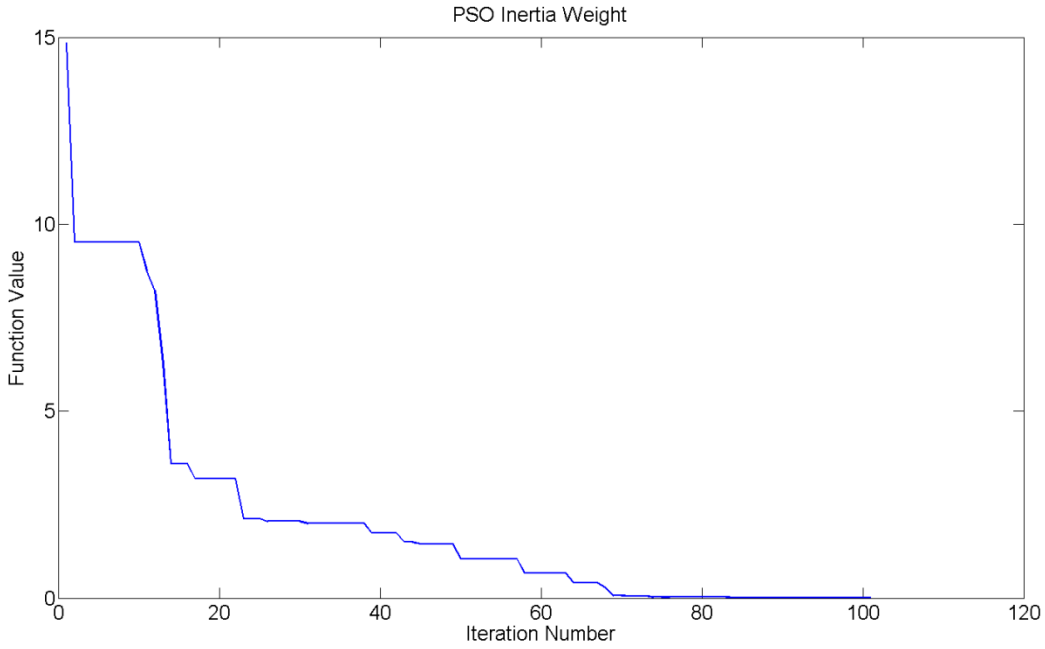

Figure 6.4 Evolution of the function value vs iteration number for the Rastrigin's function

The following sections explain the present engine optimization study via experiment and simulation. In all cases, the baseline injectors (6X133X800) were used. Total fuel injection was kept at 50 mg/stroke. All experiments and simulations were performed at 1400 rpm and 150 MPa injection pressure.

6.2 Single Injection Optimization

In the single injection optimization, three variables were used as independent variables including EGR, start of injection (SOI), and injection pressure. The merit function shown in Eq. (6.3) was used to calculate the fitness of each experiment.

$$f(x) = Fitness = \frac{1000}{(\frac{NO_x+HC}{(NO_x+HC)_t})^2+(\frac{Soot}{Soot_t})^2+\frac{BSFC}{BSFC_t}} \qquad (6.3)$$

Tier 4 mandates for the present class of non-road diesel engines (56 to 130 kW) used in this study were used as the target. Table 6.3 lists the emissions targets together with the chosen BSFC. The CO emissions were not included in the fitness function in this initial test.

Table 6.3. Targets used for NOx, HC, PM, and BSFC

Emissions	Target (g/kW-h)
NOx_t	0.4
HC_t	0.19
CO_t	5
PM_t	0.02
$BSFC_t$	220

The resolution for each variable was defined prior to the start of the experiments individually. The ranges and resolutions of the variables are given in Table 6.4.

Table 6.4. Range and resolution of design variables

Variable	Lower Limit	Upper Limit	Resolution
EGR %	0	35	1
SOI (ATDC)	-20	5	1
Injection Pressure (MPa)	130	180	5

From the previous experimental testing, it was found that combustion was not stable at EGR levels higher than 35% at very late injection timings. Hence the upper limit of EGR was taken as 35%. To ensure proper exploration throughout the design space, the number of particles (experiments) in each iteration was chosen to be twice the number of design variables. As a result, for the single injection optimization, there were six experiments in each iteration.

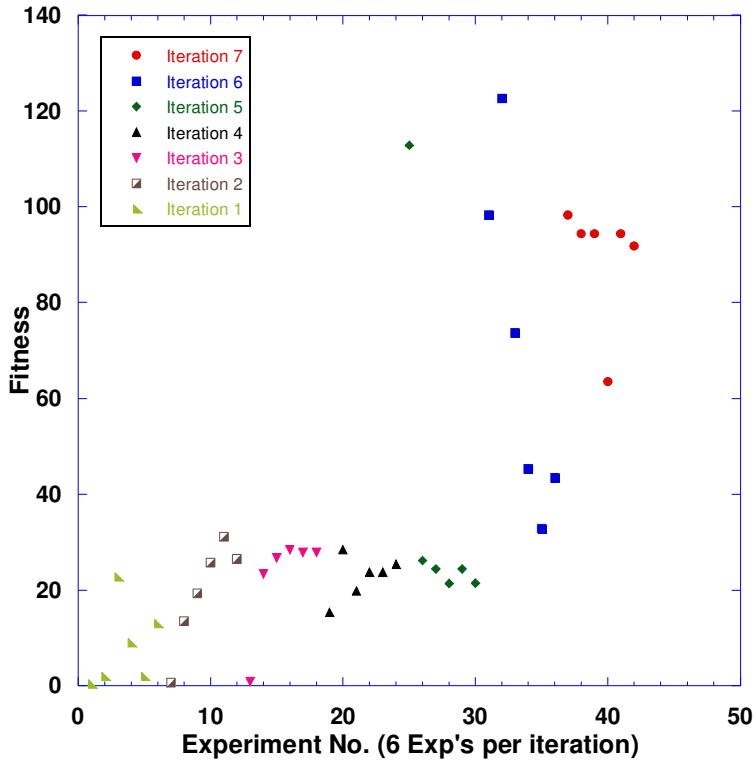

Figure 6.5 Fitness values of all the experiments

Figure 6.5 shows the evolution of the fitness value with respect to the experiment number. As mentioned above, each iteration (i.e., generation) had six experiments whose fitness values are shown by an individual label. Operating conditions for the first iteration were generated randomly, and the maximum fitness was 23 with the operating conditions of 19% EGR, 5 ATDC SOI, and 150 MPa injection pressure. In the second iteration, the maximum fitness increased to 31. The fitness value was relatively small even after five iterations. Though SOI and injection pressure were stabilized, the EGR was still low (Figure 6.7). It can be seen that as soon as the EGR value increased after the fifth iteration, the fitness value also increased. When the EGR was higher than 31%, the HC and BSFC values increased leading to a reduction in fitness.

Evolutions of NOx, PM, HC, and BSFC are shown in Figure 6.6. From Eq. (6.3), it can be noted that the expressions containing NOx, HC and PM are squared. This relation increases the penalty on the fitness function when NOx, HC, and PM emissions increase. The fitness function value in Figure 6.5 increased as the values of NOx, PM reduced. In the sixth iteration (experiment No. 32), a maximum fitness value of 122 has reached. The operating conditions at this point were 31% EGR, 1 ATDC SOI, and 155 MPa injection pressure. The emission values at this point are given in Table 6.5.

Table 6.5 Final results for single injection optimization

Emission	**Data (*g/kW-h*)**
NOx	1.174
HC	0.223
PM	0.0196
BSFC	231

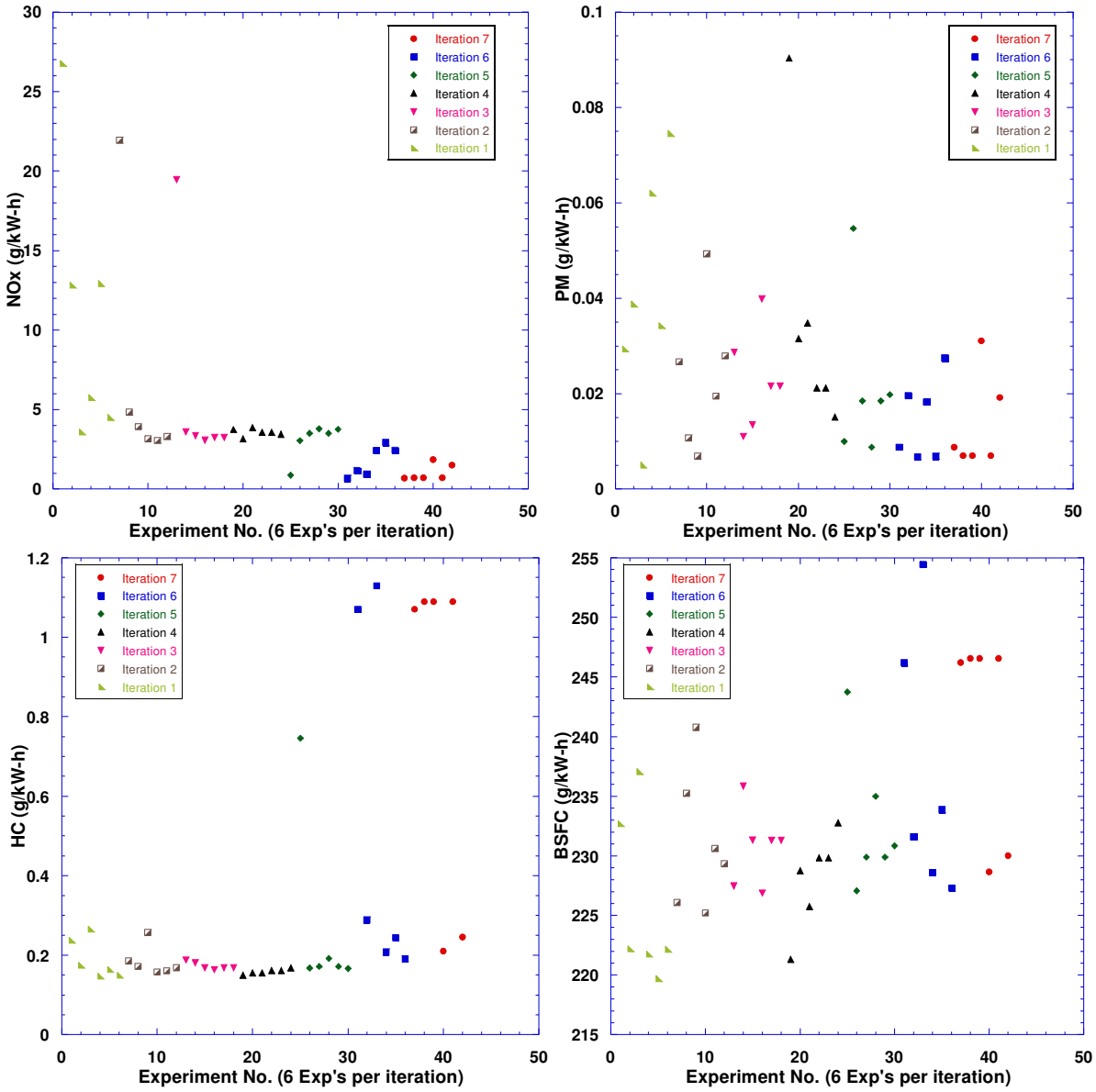

Figure 6.6 Evolution of NOx, PM, HC, and BSFC

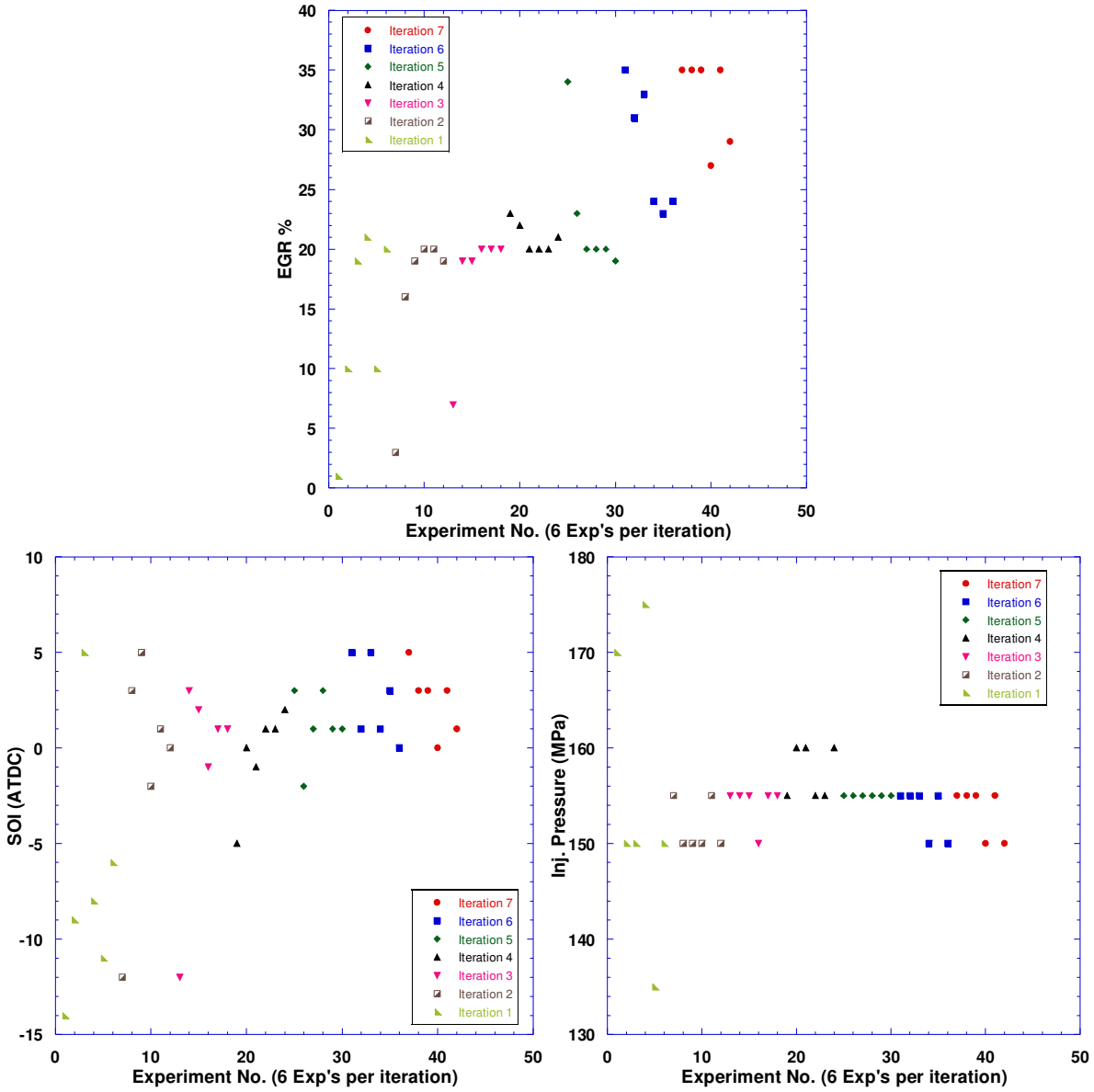

Figure 6.7 Evolution of design variables

From the previous experience, it appeared that the simultaneous reduction of NOx and PM was possible at high EGR levels and late SOI. Comparisons of Figures 6.5, 6.6, and 6.7 revealed that as the EGR level increased and SOI moved near TDC, both NOx and PM emissions could be reduced. As expected, BSFC was increased as the EGR increased. The injection pressure did not have a significant effect on the fitness function value for the given operating range.

The fitness value was reduced in the seventh iteration as the EGR was increased and SOI was further retarded. While the NOx and PM were reduced further with increased EGR and retarded SOI, HC was increased to 1.1 g/kW-h which was nearly 5.5 times the target. Further, due to the retarded SOI, the BSFC value was increased to 247.

6.3 Double Injection Optimization

Double injection optimization is divided into three parts. In the first two parts, the intake temperature was kept constant at 23 ºC. In the third part, the intake temperature was increased to 40 ºC to observe the effect of intake temperature on emissions. As the EGR mixes with the intake air before entering the cylinder, the temperature of the mixture varies depending on the amount of EGR. To avoid the problem of variable intake temperature, an EGR cooler was used to cool the intake air to the desired level.

6.3.1 Intake temperature 23 ºC (without HC and CO in fitness function)

Double injection strategies have shown potential to reduce PM emissions by undergoing relatively homogeneous pre-mixed combustion without the increase in NOx emissions. In this strategy, a small amount of pilot fuel is injected prior to the main combustion. Important variables in the double injection strategy that could affect the emissions are pilot injection timing, main injection timing, and fuel allocation in the pilot injection. A graphical representation of double injection strategy is shown in Figure 6.8. As these variables greatly affect the emissions, it is important to optimize them for low emissions. However, it is very time consuming to test all the experimental combinations to determine the optimal operating conditions. Thus, PSO was used to reduce the time for testing and to effectively find the optimum using the double injection strategy.

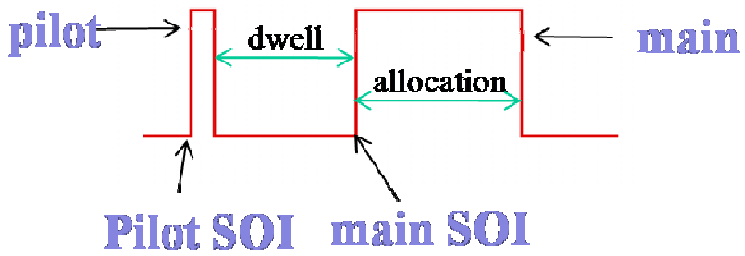

Figure 6.8 Schematic of double injection profile

An injection profile with two injections at different timings is shown in Figure 6.8. The area under the square for respective injection events indicates the percentage of total fuel injected, eg., fuel allocation. The dwell time between two injections also greatly affects the emissions. Therefore, four design variables, namely main SOI, pilot SOI, pilot fuel percentage, and EGR level, were chosen for optimization in this study. The ranges of variables are given in Table 6.6.

Table 6.6 Range and resolution of design variables

Variable	Lower	Upper	Resolution
EGR %	0	38	1
Main SOI	-5	5	1
Pilot SOI (ATDC)	-15	-55	1
Pilot %	5	50	1

The upper limit of EGR was increased to 38%. Pilot fuel can preheat the contents of the cylinder mixture and thus can enable the use of higher EGR levels without causing any combustion instability. The main injection limits were chosen between -5 and 5 ATDC as previous studies indicated that very early main injections with pilot injection could result in very high NOx and PM emissions. It also ensured that there was reasonable time lapse between the pilot injection and main injection events. Pilot fuel limits were chosen between 5 and 50%. Once the fuel was injected in the pilot injection, the remaining of the 50 mg/stroke

of fuel was injected in the main injection. Lower limit of the pilot injection was taken as 5% of the total fuel injected. This was chosen as experimental accuracy below this level is not guaranteed.

$$Fitness = \frac{1000}{(\frac{NO_x}{(NO_x)_t})^2+(\frac{Soot}{Soot_t})^2+\frac{BSFC}{BSFC_t}} \quad (6.4)$$

The merit function shown in the Eq. (6.4) was used to determine the fitness value. HC and CO emissions were not used in the fitness function. Tier 4 emissions were used as the target emissions. The BSFC target was changed to 250 to reduce the penalty for not meeting the BSFC target. The number of experiments in each iteration was increased to eight to account for the increase in the number of design variables. This enabled the PSO to search the design space thoroughly without going through too many iterations.

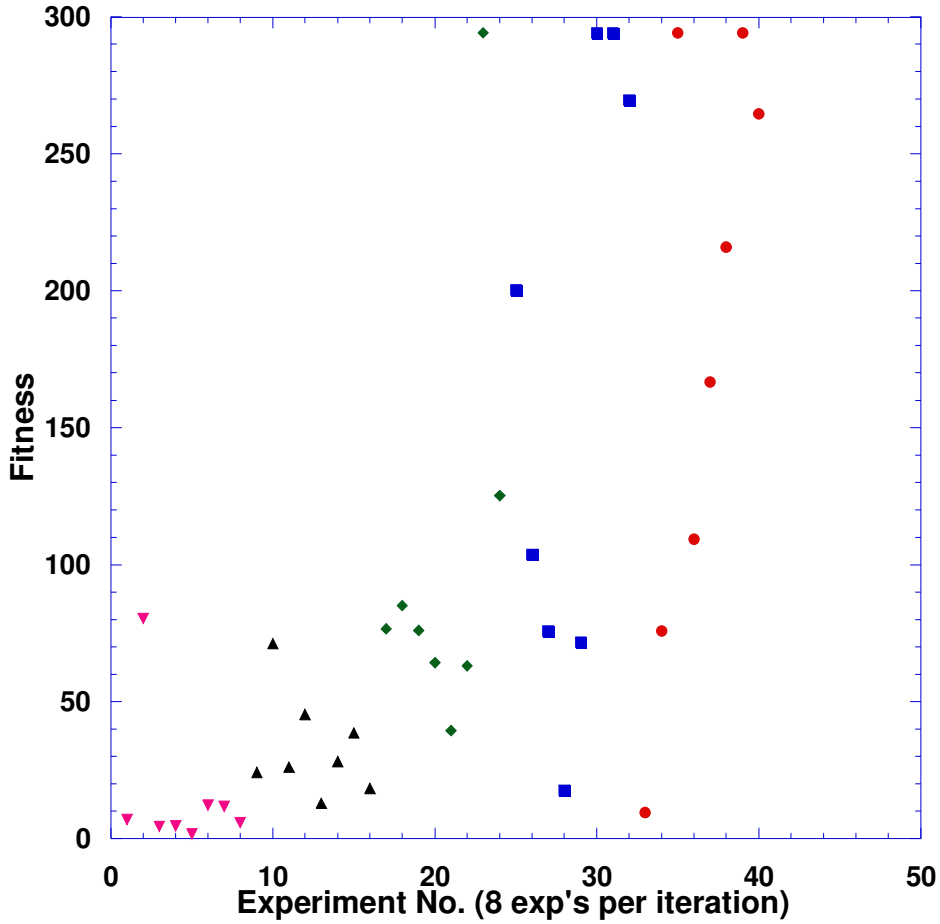

Figure 6.9 Fitness values of all experiments with double injections (intake temperature 23 ºC)

The evolution of the fitness value for double injection optimization is shown in Figure 6.9. The fitness value for seven experiments was less than 10 in the first iteration. This indicated poor random starting points for the optimization. The optimization, however, was continued to the next iteration. The fitness value for the next two iterations was below 100. At this stage, the optimization moved towards late injections which led to the reduction in PM emissions. However, the NOx emissions for the experiment with the highest fitness in the second iteration was approximately around three times the Tier 4 limit. This seriously reduced the fitness value. In iteration 3, the EGR was increased to 37% while moving the main SOI to 4 ATDC leading to a fitness value of 294. The operating conditions at this point

were 37% EGR, 4 ATDC main SOI, -17 ATDC pilot SOI and 5 % pilot. The data at this point were 0.32, 0.026, and 255 g/kW-h for NOx, PM, and BSFC respectively. No increase in the fitness value was observed when the optimization was continued for two more iterations.

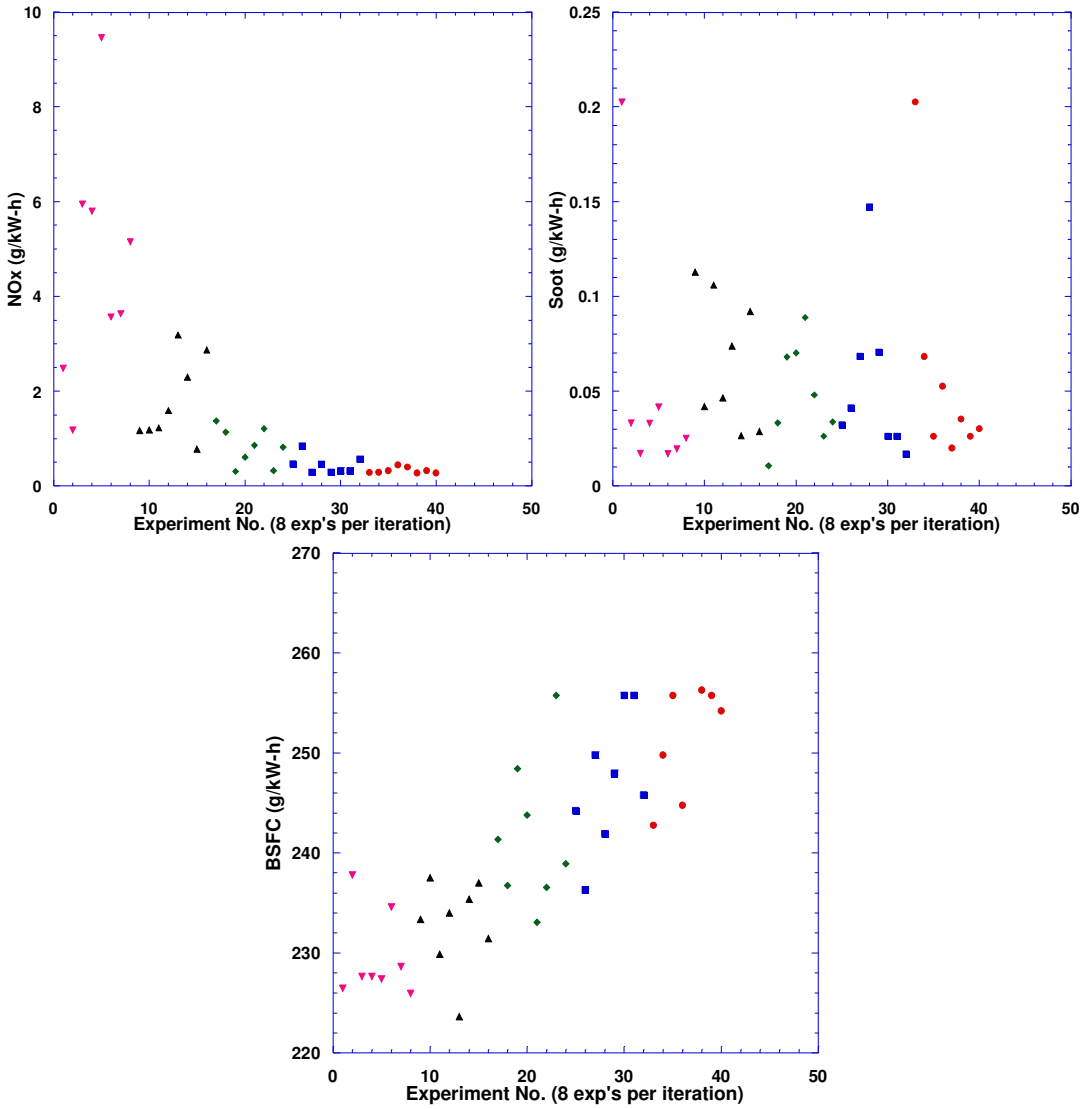

Figure 6.10 Evolution of NOx, PM, and BSFC values

Evolution of NOx, PM, and BSFC values are shown in Figure 6.10. The BSFC values increased along with the fitness values. As mentioned earlier, high EGR levels and late injections led to the reduction of the NOx and PM emissions. High EGR levels and late

injections are known to increase BSFC. With the use of multi-objective fitness function, a drastic increase in BSFC was avoided.

Comparison of NOx and PM emissions with Tier 4 mandates is given in Figure 6.11. Only few data points near the Tier 4 box are shown in this figure. The best experiment in the optimization came very close towards meeting the Tier 4 mandates. It should be noted that the fuel injectors used in this study were designed to meet Tier 2 mandates.

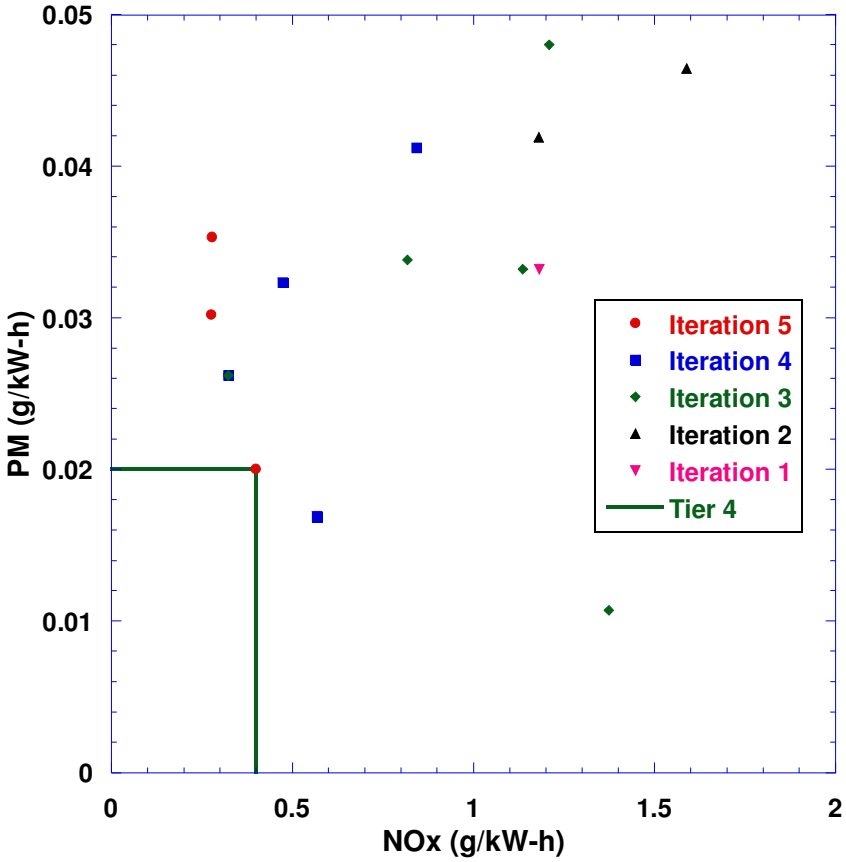

Figure 6.11 Comparison of NOx and PM emissions with Tier 4 emissions

6.3.2 Intake temperature 23 ºC (with HC and CO)

This section describes the double injection optimization at 23 ºC intake temperature with HC and CO emissions included in the fitness function. The fitness function used is given in Eq. (6.5). The fitness value will reach 200 when all the emissions targets are met.

$$f(x) = Fitness = \frac{1000}{(\frac{NO_x}{(NO_x)_t})^2+(\frac{Soot}{Soot_t})^2+\frac{HC}{HC_t}+\frac{CO}{CO_t}+\frac{BSFC}{BSFC_t}} \quad (6.5)$$

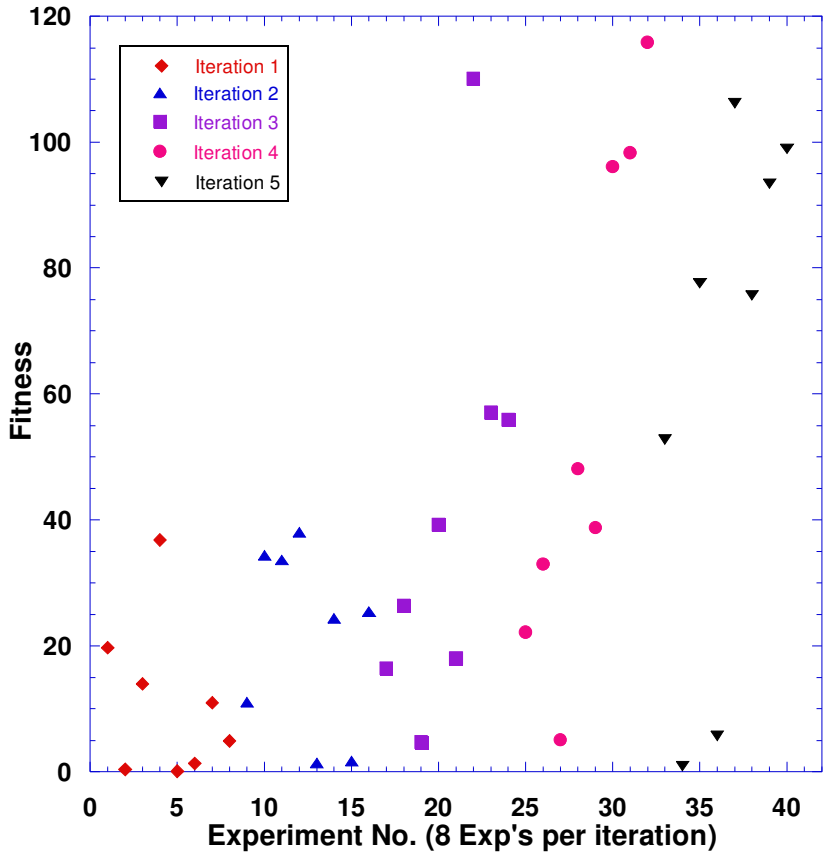

Figure 6.12 Fitness values of all experiments with double injections (intake temperature 23 ºC)

The evolution of the fitness function is given in Figure 6.12. A maximum fitness of 116 was achieved in the fourth iteration. Similar trends were observed to those in the previous section. High EGR levels with late main injections were found to be favorable towards reducing the four emissions included in the fitness function. Though trends were the same, there were some differences in the optimal point when HC and CO were included in the fitness function. The comparison of optimal points and emissions of both cases is given in Table 6.7.

Table 6.7 Comparison of optimal point operating conditions and emissions

Variable	Without HC and CO	With HC and CO
Main SOI (ATDC)	4	4
Pilot SOI (ATDC)	-17	-23
EGR %	37	34
Pilot %	5	5
NOx (g/kW-h)	0.32	0.37
Soot (g/kW-h)	0.026	0.018
HC (g/kW-h)	0.989	0.76
CO (g/kW-h)	10.76	9.59
BSFC (g/kW-h)	255	255

Both optimal points differed in the EGR rate and pilot SOI. When HC and CO were not included, the EGR rate was allowed to reach 37%. This indicates that HC and CO may have noticeable effects on reducing the fitness value for EGR values higher than 34%. It is also evident from the comparison of the HC and CO emissions in both cases. While HC was 0.989 g/kW-h at 37% EGR, it was only 0.76 g/kW-h at 34% EGR. With the target value of 0.19 g/kW-h, the resulting HC emissions were one order of magnitude higher for 37% EGR. This would have reduced the fitness value significantly if the HC was included in the fitness function.

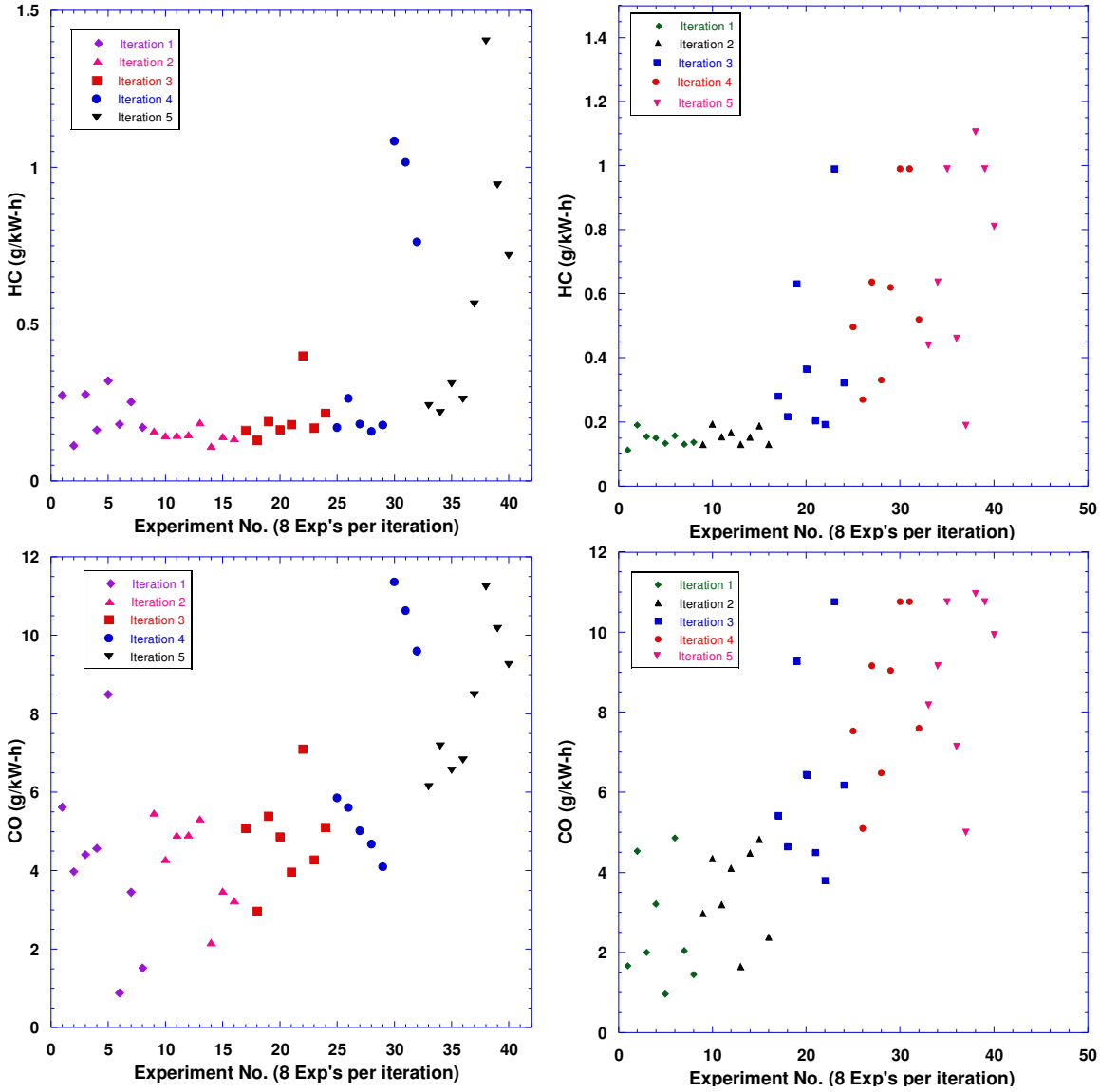

Figure 6.13 Comparison of CO and HC emissions. On the right the fitness function included HC and CO. On the left, HC and CO emissions were not included in the fitness function.

Figure 6.13 shows the comparison of CO and HC emissions. On the right, the fitness function included the CO and HC emissions. On the left, CO and HC emissions were not included. Similar trends were observed in both cases. As the number of iterations increased, the optimization pointed towards late main injections and high EGR levels. With the increase

in EGR levels, the CO and HC emissions increased. The magnitudes of scales for both cases were similar.

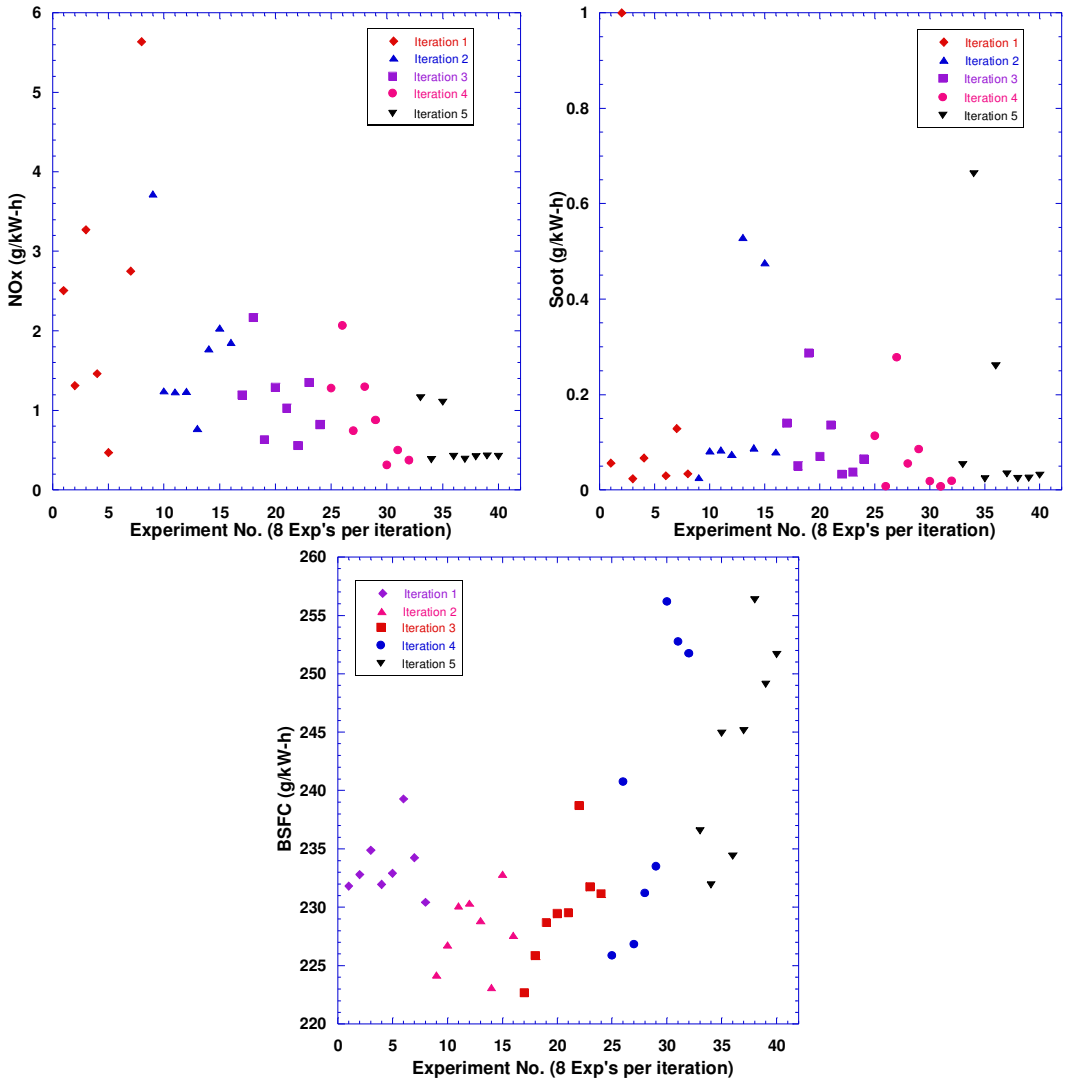

Figure 6.14 Evolution of NOx, PM, and BSFC values

Figure 6.14 shows the evolution of NOx, PM, and BSFC values. Similar levels of NOx, soot, and BSFC were observed. Comparison of NOx and soot emissions with Tier 4 emissions is given in Figure 6.15. it can be seen that iteration 4 was able to produce favorable soot and NOx emissions.

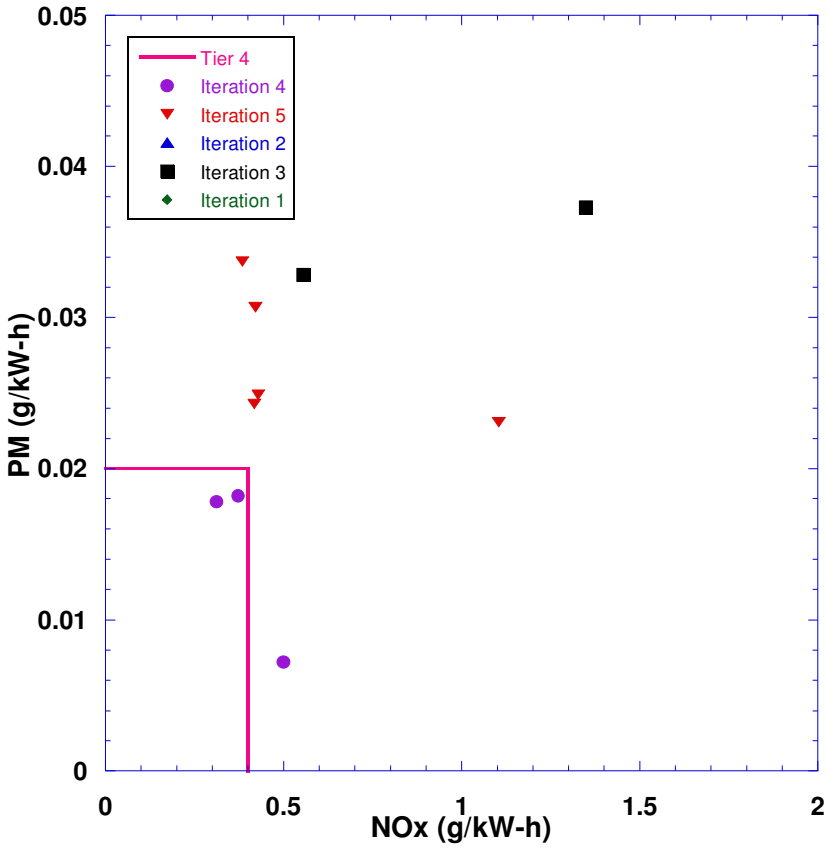

Figure 6.15 Comparison of NOx and PM emissions with Tier 4 emissions

6.3.3 Intake temperature 40 ºC

As the PM emissions are sensitive to the intake temperature, optimization was performed at another intake temperature to observe the changes in the optimum point. In this section, intake temperature for the experiments was kept at 40 ºC. The design variables and their ranges chosen for this optimization are given in Table 6.6. Tier 4 mandates given in Table 6.3 were used as targets. The fitness function was modified to include the HC and CO emissions. Eq. (6.6) shows the merit function used to calculate the fitness value.

$$f(x) = Fitness = \frac{1000}{(\frac{NO_x}{(NO_x)_t})^2+(\frac{Soot}{Soot_t})^2+\frac{HC}{HC_t}+\frac{CO}{CO_t}+\frac{BSFC}{BSFC_t}} \qquad (6.6)$$

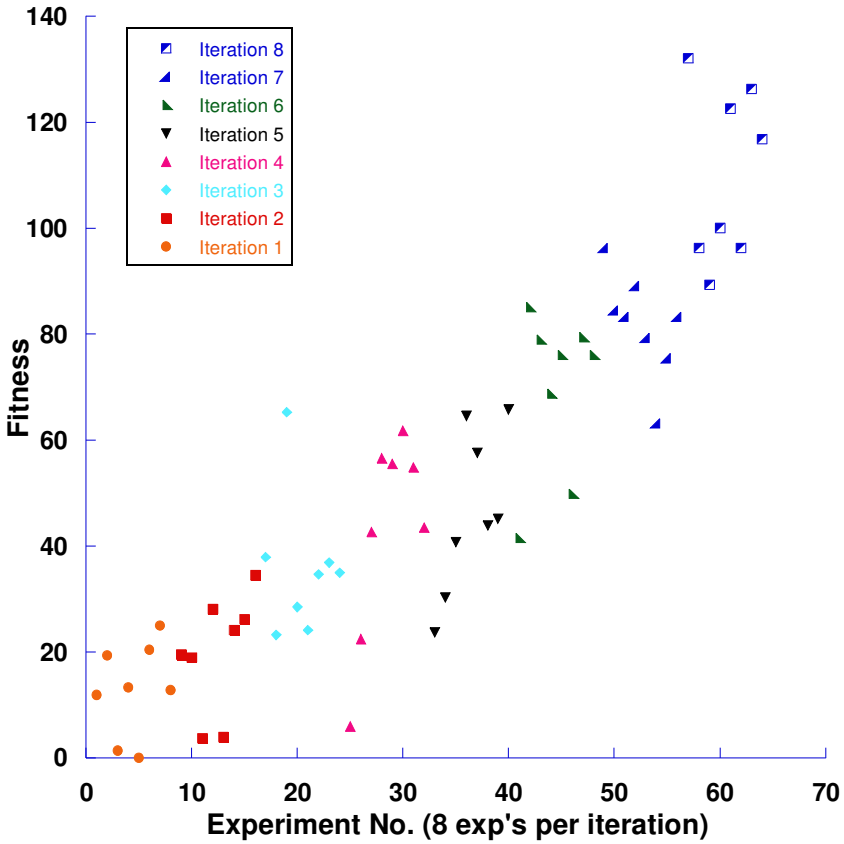

Figure 6.16 Fitness values of all experiments with double injections optimization (intake temperature 40 ºC)

After 8 iterations (64 experiments) a maximum fitness value of 132 was achieved in the eighth iteration. The operating conditions at this point were 34% EGR, 5 ATDC main SOI, -24 ATDC pilot SOI, and 5% pilot fuel. The emissions at this point are given in Table 6.8.

Table 6.8 Final results for double injection optimization with intake temperature 40 ºC

Emission	Data (g/kW-h)
NOx	0.41
PM	0.0092
CO	8.51
HC	0.678
BSFC	249

The fitness values was relatively low despite being close to Tier 4 mandates for NOx, PM, and BSFC emissions. The exhaust CO and HC emissions were believed to cause significant reduction in the fitness function value. It can be noticed from Table 6.8 that CO was about 1.5 times of the Tier 4 mandate and the HC close to 3.5 times the mandate. HC and CO emissions usually increase with the use of high EGR levels. Note that it is less difficult to remove HC and CO from the exhaust than to remove NOx and PM.

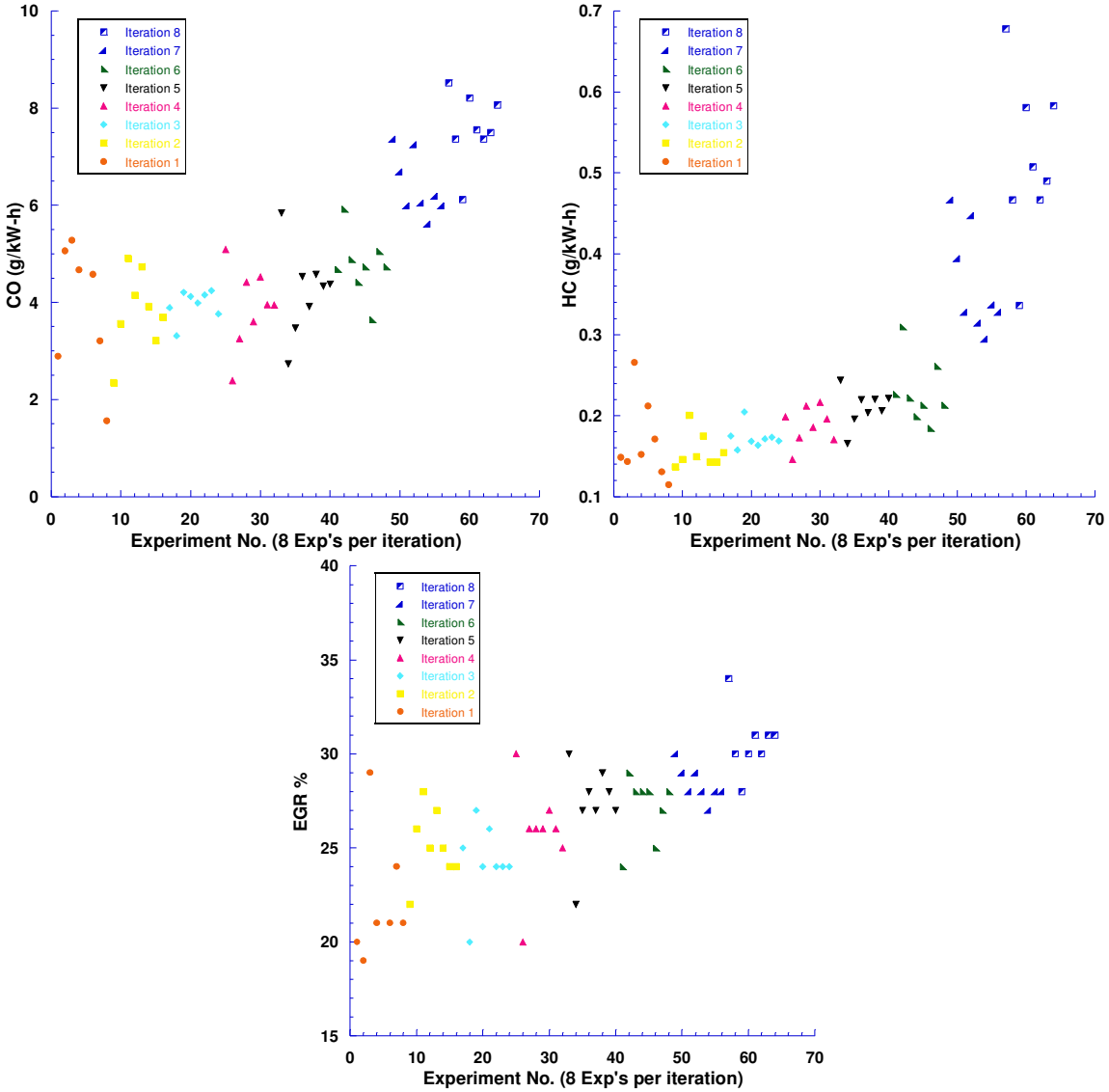

Figure 6.17 Evolution of CO, HC emissions and EGR level

Figure 6.17 shows the evolution of HC, CO emissions and EGR levels. It clearly shows that CO and HC emissions increased in parallel with the increase in the EGR level. Figure 6.18 compares cylinder pressure and HRR of two experimental cases (Case 2 & 3) in the first iteration with those of an experimental case (Case 63) in iteration 8. The fitness values of Case 2 and Case 3 were 19 and 1, respectively. The top figure compares Case 2 with Case 63 (fitness 126). It can be seen that the peak cylinder pressure of Case 63 was much lower than that of Case 2. Due to early release of pilot fuel in case 2(14% pilot at -32 ATDC), noticeable amount of combustion occurred, resulting in a slightly higher cylinder pressure at TDC. For Case 63, due to very small pilot and late main injection, combustion occurred late in the cycle. Further, with the use of high EGR, the phasing of the combustion (start of ignition) has been delayed. All these factors contributed to the lower NOx and PM emissions.

In the bottom figure, for Case 3, though the EGR rate was comparable to that of Case 63, the pilot fuel was too high. As 35% of the total fuel is injected at -35 ATDC, the combustion has split into two separate parts which was evident from Figure 6.18. A significant amount of fuel was injected at -35 ATDC, ignition of pilot fuel took place at around -20 ATDC. This led to very high cylinder pressure for Case 3. PM emission was relatively high for Case 3. It is thought that combustion of the pilot fuel produced high amount of soot due to low temperature and the soot was not able to be oxidized during the main combustion stage.

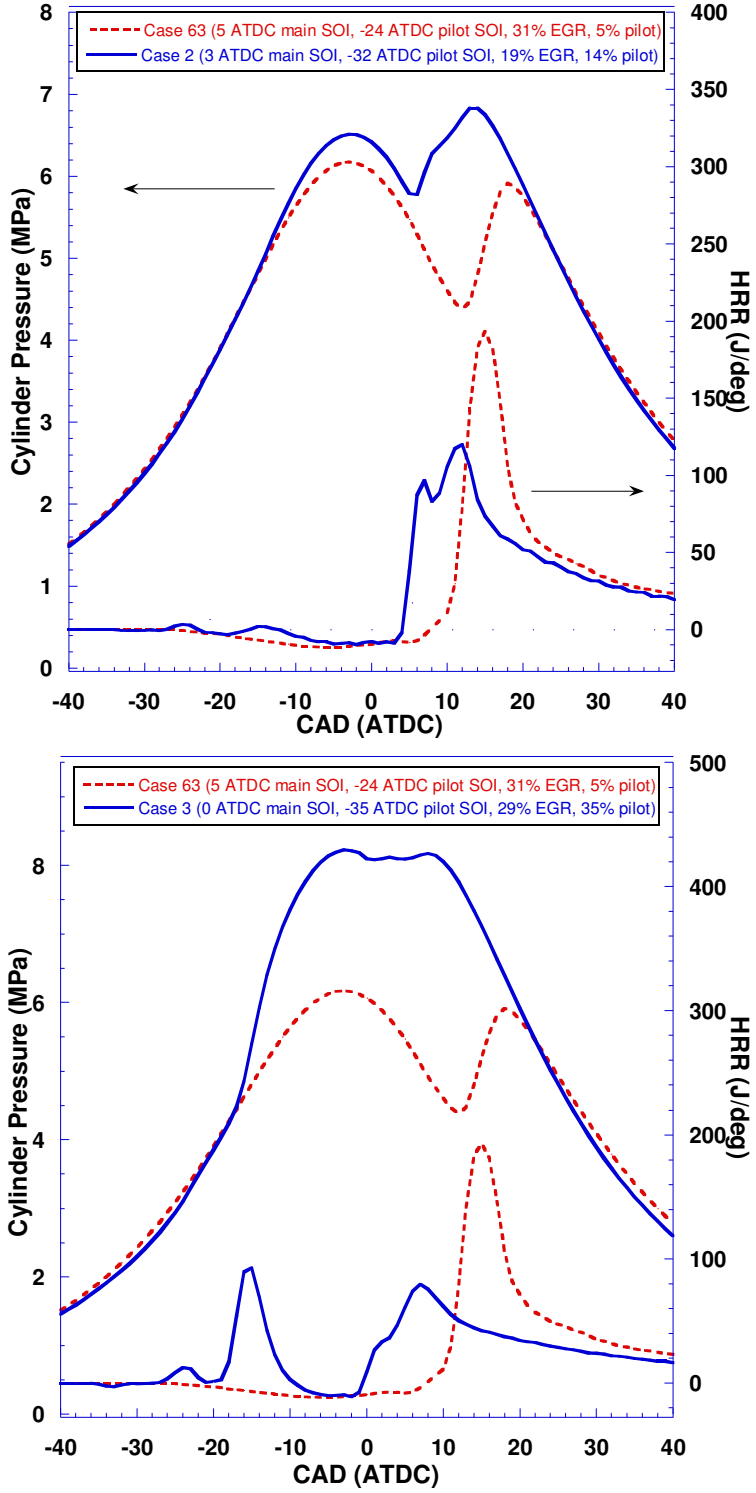

Figure 6.18 Comparison of cylinder pressure and HRR of experiments in the first iteration with that of experiments in last iteration

6.3.4 Sensitivity Study Based on the Optimum

As mentioned above, there is some randomness involved in the PSO methodology. Randomness is included in the PSO to ensure that design space is properly explored by the algorithm. Due to this randomness, it is possible that the optimum found by the PSO requires further refinement. Refinement of the optimum was performed by running experiments in the vicinity of the optimum. The experimental operating conditions performed in this section are given in Table 6.9. In the following sensitivity study, one variable was swept while the other variables remained at their optimum values.

Table 6.9 Operating conditions used in the refinement of the optimum

Variable	Values
EGR %	30,32,**34**,35,36
Main SOI (ATDC)	2,3,4,**5**
Pilot SOI (ATDC)	-27,**-24**,-21
Pilot %	10,7,**5**,3

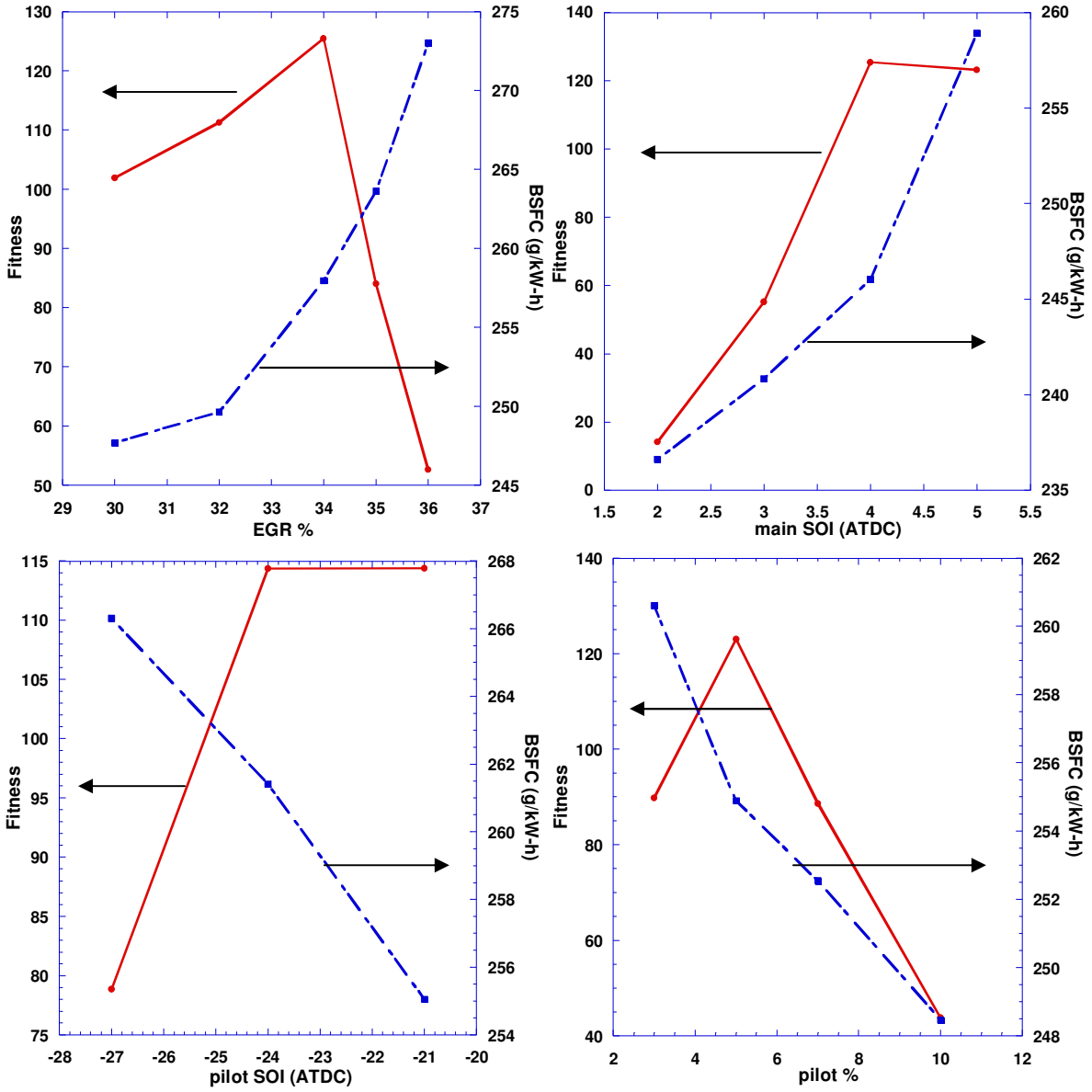

Figure 6.19 Comparison of fitness values and BSFC from sensitivity study

Figure 6.19 shows the comparison of the fitness values and BSFC of the variables studied. The solid line in each of these plots shows the fitness values and the dotted line represents the BSFC data. The variable tested is given on the x-axis. It can be observed that the fitness value found by PSO in the previous section was the highest most of the time. The fitness value was slightly higher at 4 ATDC SOI as opposed to the 5 ATDC previously found

by the PSO. Overall, it was found that a significant amount of refinement is not required to find a better operating condition after PSO search.

6.4 Application of PSO to Engine Simulations

In the previous section, application of PSO to engine experiments was explained. Though it showed a good promise of reducing the emissions, the experiments were often limited by hardware and the optimization could also be expensive. For example, with the current experimental setup, it is very time consuming to adjust the intake temperature to the required level. Additionally, preparing laboratory for test will take significant time and resources. For this reason, and to automate the process of optimization, PSO was integrated with an engine simulation code to optimize the engine operating conditions. The present simulation code, is capable of performing 3-D in-cylinder spray combustion calculations using advanced physical and chemistry models. The code is based on KIVA-3V with many updated physical and chemistry models [28].

The major models included RNG k-ε turbulence, spray atomization, drop-wall impingement, wall heat transfer, piston-ring crevice flow, autoignition, turbulent combustion, soot and NOx emissions models. This code was used for the optimization as a significant amount of research has been done in model development and validation [28].

6.4.1 Implementation of PSO

One of the most difficult tasks of this numerical optimization was to make sure that PSO and KIVA work together. Two separate programs for PSO and KIVA were written and were controlled using a shell script written in the bash scripting language, while the rest of PSO was written in Fortran95 and compiled using Intel Fortran compiler.

Input variables for the PSO program were saved in two files. The file psoparam.txt contained algorithm parameters. The parameters and their descriptions are given below.

```
1       6       ! nd – Number of design variables
2       2.0     ! c1 – PSO Parameter
3       2.0     ! c2 – PSO Parameter
4       0.5     !w – Weighting Factor
5       1       ! npart – Number of particles in each iteration
6       3       ! convmeth – Convergence test method
```

The sixth variable, convergence method, was used to determine if the optimization has reached the convergence. Three types of convergence criteria were defined and were used as needed. They included a clustering check, a value check, and a generation count check. In the input file, psoparam.txt, one of these three criteria can be selected with the appropriate *convmeth* value. A 1 checks only the clustering, a 2 the value, and 3 the iteration count. Any other value will have the effect of checking every single convergence criteria and exiting as soon as one of the three criteria is met.

The first criterion (clustering) is satisfied if more than a half of the particles have a fitness value within 1% of the current global best. The reason for specifying a half the particles is that individual particles in any given iteration may be randomly accelerated to a region very far away from the equilibrium solution, but most of the particles will converge around a single solution. The second check (value) is for the fitness value. If the fitness value of the Gbest reaches 200, then the program is terminated. The third check (iteration count) is for the number of iterations. This check is similar to the fail-safe in the shell script (limiting the number of generations to 10 which is user defined). Once a certain number of iterations

have been reached, this criterion calls an exit. This number is flexible and was put in place to avoid the code from running for an infinite amount of time.

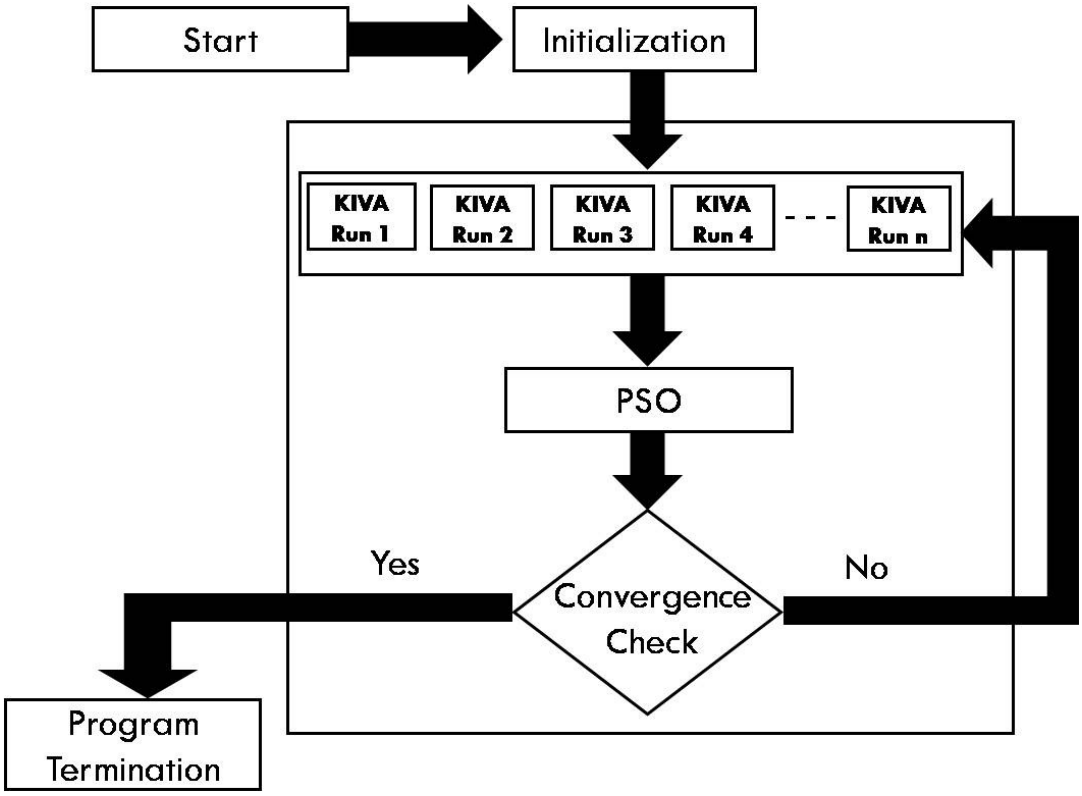

Figure 6.20 Flow chart for the optimization of emissions using PSO and KIVA

Figure 6.20 gives the outline of the entire program. The start and termination of the program are done by the shell script. Under the control of the shell script, the PSO program initiates the randomly generated operating conditions. In the next step, it inserts the generated operating conditions into the input files for KIVA. A copy of the original input files for the KIVA (read-only) is used to modify the input as necessary. Additional subroutines are used to generate injection profile and intake air constituents which are necessary inputs for KIVA. Once the input files for KIVA are generated, they are pasted into separate directories along with the KIVA binary executable file. For example, if there are 10 simulations (particles) in each iteration, then 10 directories will be created and files necessary for the simulation will

be placed into the folder. The KIVA program was modified to suppress the creation of any output files but *thermo.dat*, which consists of the emissions data used by the *emis_eval* subroutine to calculate the fitness value of that simulation. These values are cataloged into an output file which would be used by the PSO program to create the operating conditions for the next iteration.

6.4.2 Fitness Function

Despite that a similar fitness to that mentioned in the previous sections was used to calculate the fitness value, there were minor modifications. Input files for KIVA were modified to run the engine simulation from intake valve closure (IVC) to exhaust valve open (EVO). This was put in place to reduce the computation time of the simulations. This makes the calculation of BSFC very difficult and possibly inaccurate. As the BSFC is not calculated, the emissions can be only calculated in g/kg-f. However, using these units would leave the BSFC out of the fitness equation. Mean Effective Pressure (MEP), which is the ratio of work over unit swept volume, was used as an indicator of the engine's efficiency. The Tier 4 targets were converted to "gram of emissions per kg of fuel" (g/kg-f) to be able to use in the modified fitness function.

6.4.3 Model Validation

Engine experiments performed on a John Deere 4045 diesel engine mentioned in Table 3.1 were used for model validation. The simulations were compared with the experimental results at various SOI and EGR levels. Comparisons of experimental and simulation results for 0, 15 and 30% EGR levels at SOIs between -20 and 5 ATDC for 150 MPa injection pressure are shown in Figure 6.21. Solid lines represent the experimental

results and the dotted lines represent the simulation results. It can be noted that when SOI was near TDC, both experimental simulation results match well for both NOx and PM emissions. For NOx emissions, when the SOI was earlier than -10 ATDC, the difference in emissions was relatively high. Nonetheless, the model was able to capture the trend of engine performance with respect to various operating conditions.

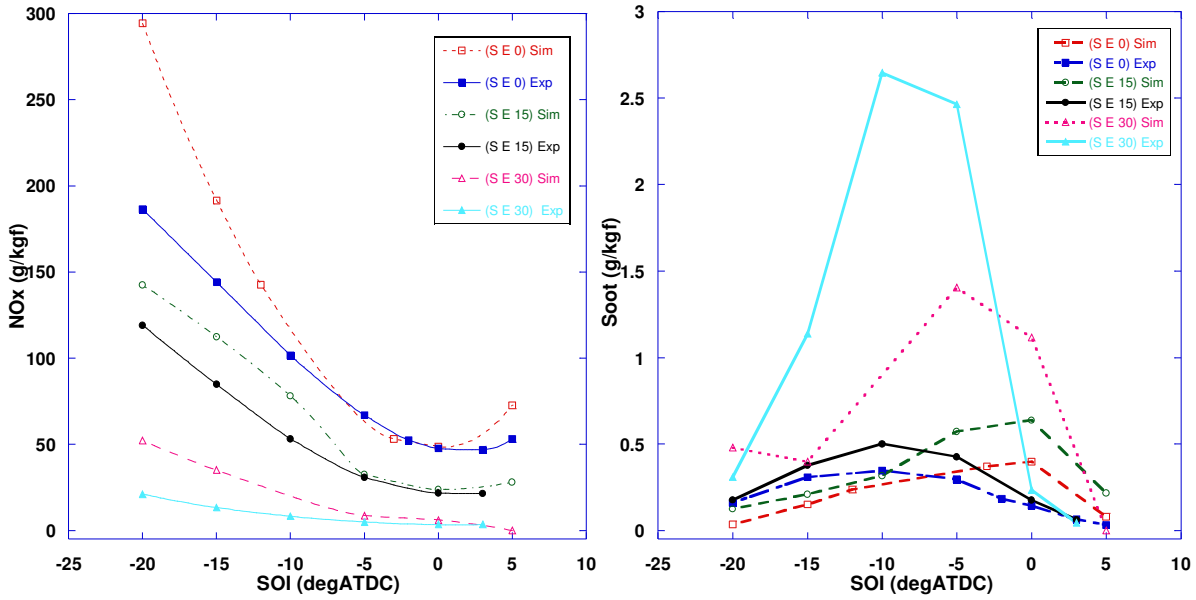

Figure 6.21 Comparison of NOx and PM emissions at 0, 15 and 30% EGR levels at various SOIs

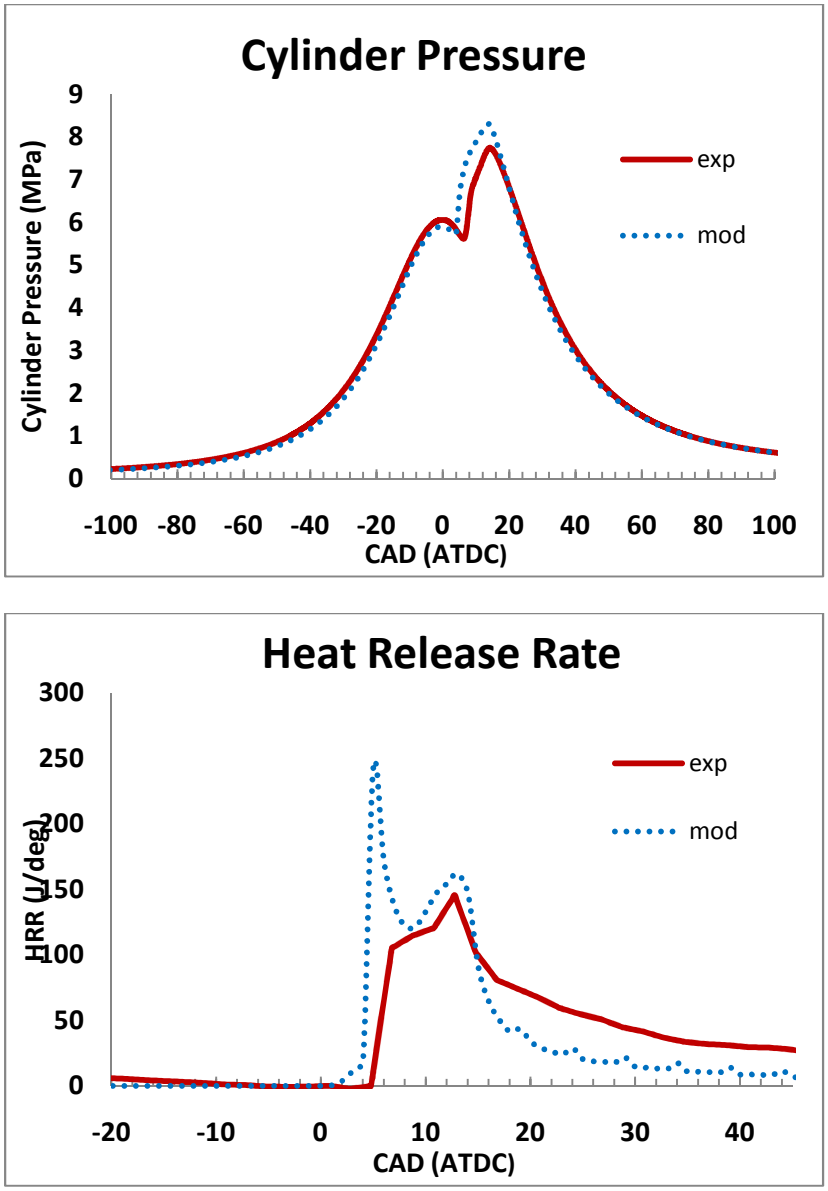

Figure 6.22 Comparison of cylinder pressure and heat release rate for 150 MPa, 0 SOI, and 0% EGR

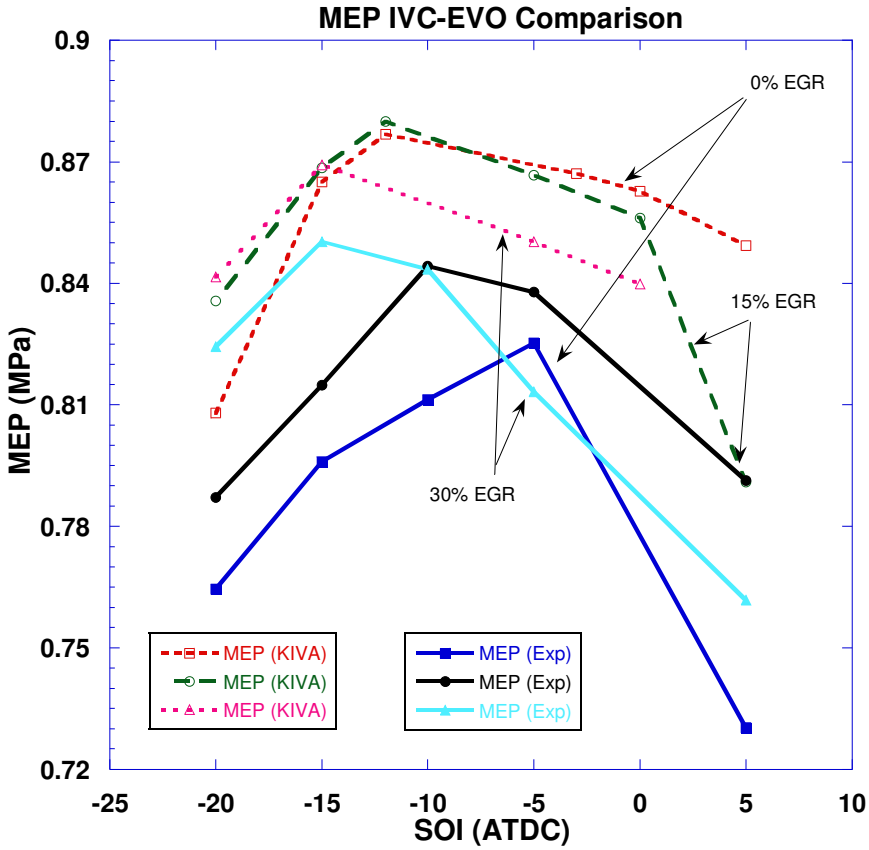

Figure 6.23 Comparison of mean effective pressures at 0, 15, and 30% EGR levels

Validation of cylinder pressure and heat release rate is shown in Figure 6.22. The cylinder pressures matched reasonably well for the baseline case. Comparison of mean effective pressures for various start of injections at 0, 15 and 30% EGR levels are shown in Figure 6.23. At all EGR levels, the simulations predicted the trends accurately.

6.4.4 Single Injection Results

Engine operating parameters used in single injection optimization are shown in Table 6.10.

Table 6.10 Range and resolution of design variables

Variable	LL	UL	Resolution
SOI (ATDC)	-21	5	2
EGR (%)	0	60	2
Injection Pressure (MPa)	120	240	10
Initial Temp. at IVC (K)	300	400	10

The fitness function used in this optimization is given in Eq. (6.7). MEP was not used in the fitness function. The targets for NOx, PM, CO, and HC were 2, 0.1, 20, 0.78 g/kg-f , respectively.

$$Fitness = \frac{1000}{(\frac{NO_x}{(NO_x)_t})^2+(\frac{Soot}{Soot_t})^2+(\frac{CO}{CO_t})+(\frac{HC}{HC_t})} \qquad (6.7)$$

The fitness values of all simulations are given in Figure 6.24. Each iteration consisted of 8 experiments. Each iteration is denoted by a separate symbol. It can be seen that the fitness values increased with progress in iteration number. Some simulations stopped before reaching EVO. These simulations stopped well before the combustion phase which led to almost zero emissions. This led to a drastic increase in the fitness value leading the optimization recognize this conditions as Gbest and Pbest. To avoid this problem, every simulation was checked to see if it has reached the EVO (118 ATDC). If any simulation has not reached the EVO, then such simulation was given a negative fitness value to avoid being recognized as a good case. Simulations with negative fitness values can also be seen Figure 6.24.

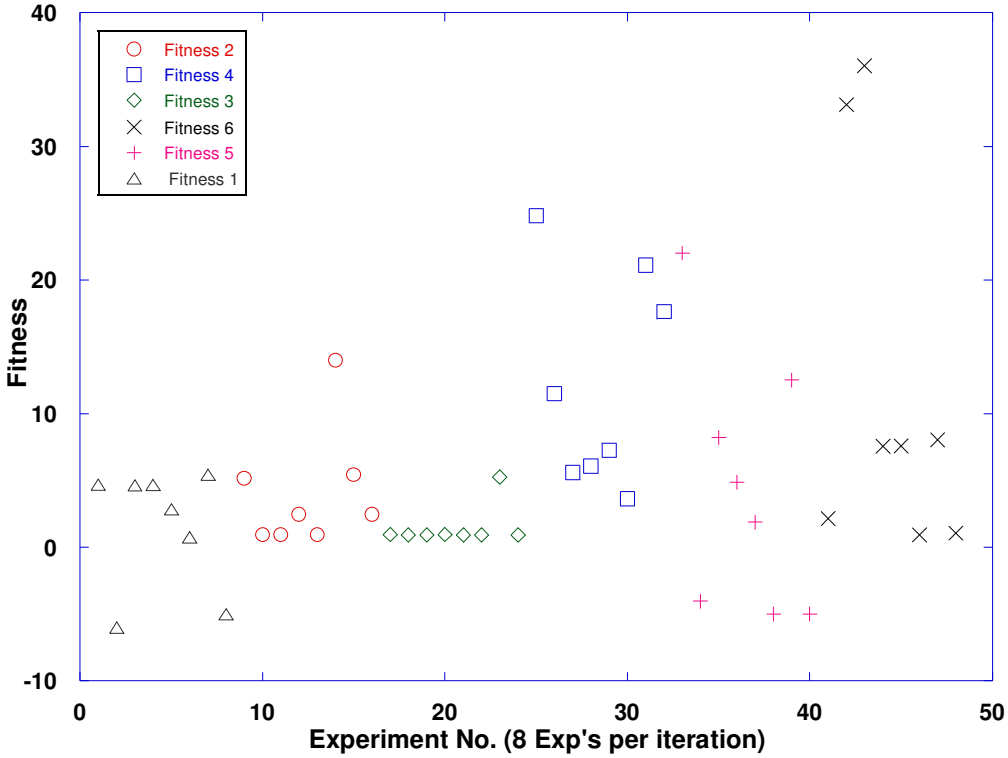

Figure 6.24 Fitness values of all the experiments

It can be seen that in the iteration 6, two simulations reached fitness values of 33 and 36. The operating conditions for these simulations are: -3 ATDC SOI, 44% EGR, 180 MPa injection pressure, 310 K intake temperature, and 3 ATDC SOI, 32% EGR, 120 MPa injection pressure, 340 K intake temperature, respectively. The emissions for the latter point were 8.99, 0.27, 0.02, and 6.75 g/kg-f for NOx, PM, HC, and CO, respectively. The NOx emission were over-predicted at this point which has led the fitness to go down to 36. However, the optimization has correctly pointed out a high EGR level and late SOI.

Both the results mentioned in above pointed to high EGR levels, near TDC injection timing to reduce overall emissions which is consistent with the experimental results. They also pointed towards reasonably high injection pressures to increase the fitness function.

Note that initial temperature was the temperature at IVC and it is higher than the actual intake manifold temperature observed in the experiment.

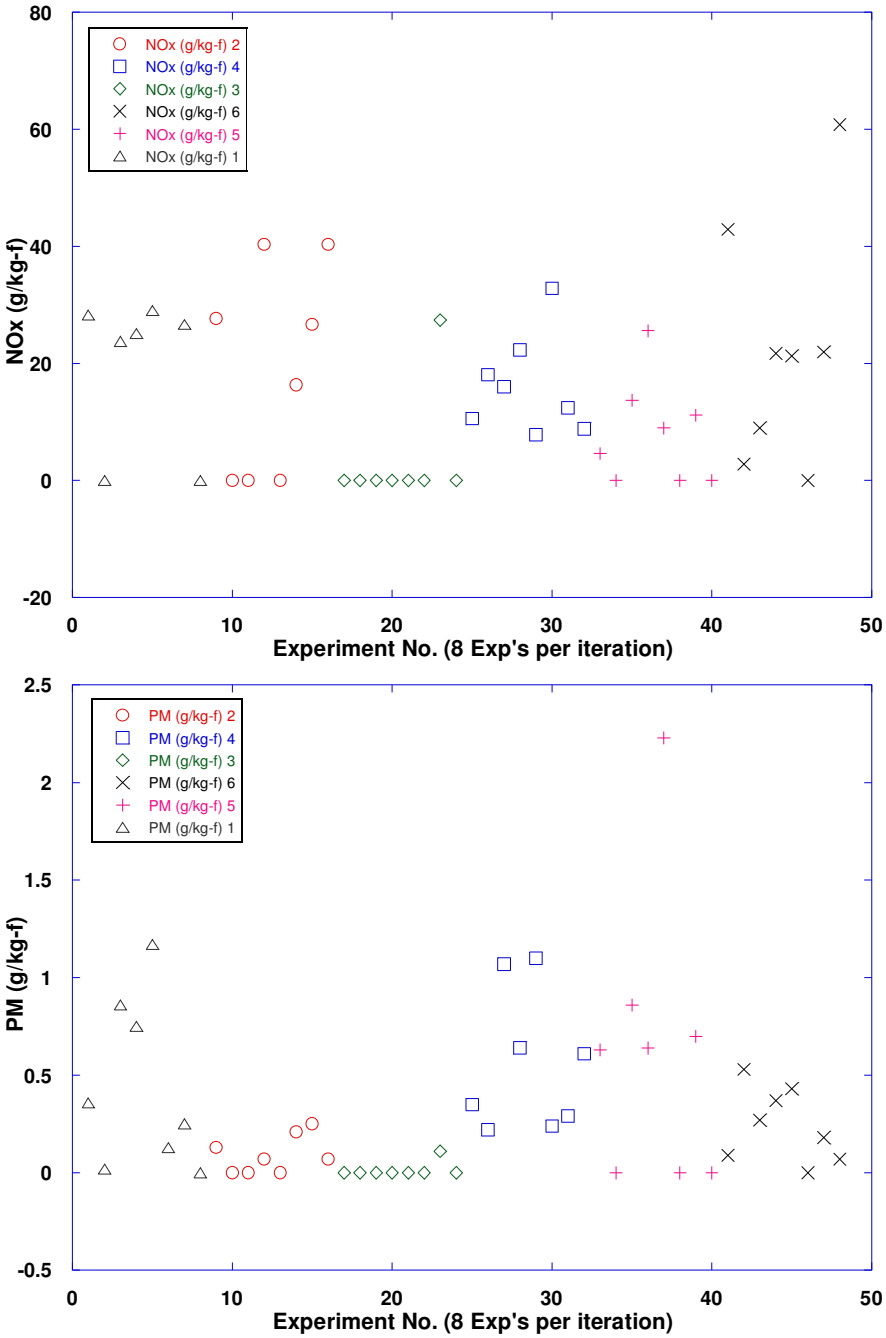

Figure 6.25 Evolution of NOx and PM emissions

Figure 6.25 shows the evolution of NOx and PM emissions. It can be seen that some simulations produced zero or near zero NOx and PM emissions. These points refer to the simulations that failed to run all the way through the EVO. Barring the failed simulations, the NOx and PM emissions clearly reduced as iterations increased.

6.4.5 Double Injection Results

Various design variables used in double injection optimization are shown in Table 6.11. A temperature of 350 K at IVC was used in all simulations. The lower limit of the main SOI was changed from -20 ATDC to -5 ATDC to avoid the overlap of pilot and main injection events. The EGR upper limit was also changed from 60% to 35% to avoid failed simulations.

Table 6.11 Range and resolution of design variables

Variable	LL	UL	Resolution
mSOI (ATDC)	-5	5	1
pSOI (ATDC)	-34	-15	3
Pilotf (%)	5	50	5
EGR (%)	0	35	1
Injection Pressure (MPa)	120	220	20

CO and HC emissions were not included in the fitness function in this study as it was found that the simulation did not predict these emissions well. The new fitness function used is given in Eq. (6.8).

$$Fitness = \frac{1000}{(\frac{NO_x}{(NO_x)_t})^2+(\frac{Soot}{Soot_t})^2+\frac{MEP_t}{MEP}} \qquad (6.8)$$

The targets for NOx and PM were 2 and 0.1 g/kg-f, respectively. The target for MEP was 0.8 MPa. The target for MEP was chosen as 0.8 MPa after examining several engine cycles whose experimental BSFC values were around 250 g/kW-h (the target for the BSFC in

the previous section). As high MEP values are desirable, the expression related to MEP in the fitness function is inverted.

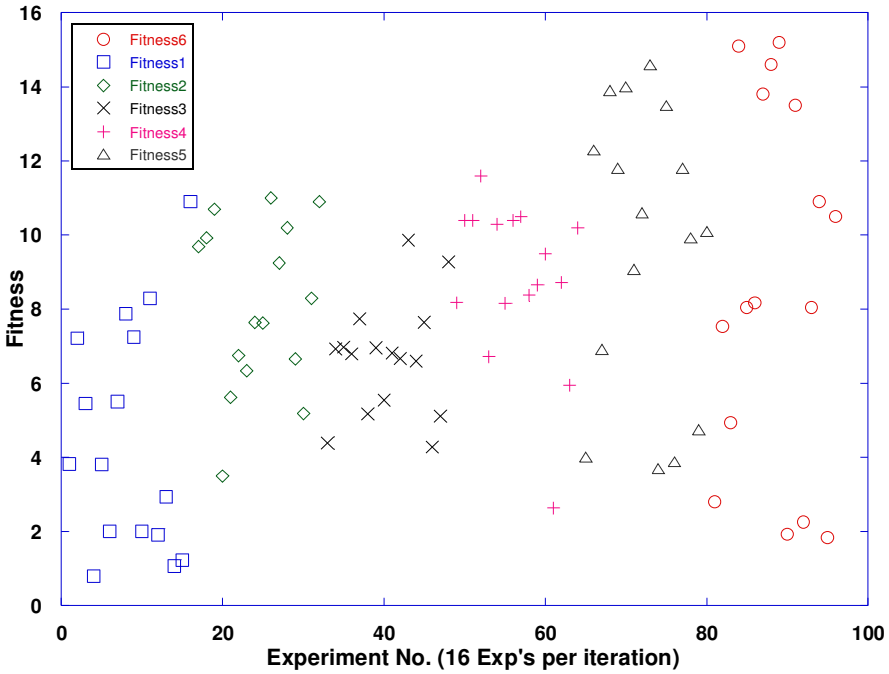

Figure 6.26 Fitness values of all the experiments

Fitness values for all simulations are shown in Figure 6.26. Sixteen simulations were run in each iteration. It can be observed that the fitness values improved with the iteration number. The fitness value was not as high as expected. The maximum fitness observed was 15.18 in iteration 6. The operating conditions at this point were 5 ATDC main SOI, -34 ATDC pilot SOI, 5% pilot fuel, 22% EGR, and 220 MPa injection pressure. Maximum fitness value was significantly lower compared to the experimental results due to the higher NOx and PM levels predicted by simulation at similar operating conditions. Though simulations using higher EGR levels were also performed during optimization, the PM values increased significantly leading to reduction in the fitness values.

Table 6.12 Operating conditions and emission results for iteration 6.

Case No.	mSOI (ATDC)	pSOI (ATDC)	pilot %	EGR %	inj_p (MPa)	Intake Temp (K)	NOx (g/kg-f)	PM (g/kg-f)	MEP (Mpa)	Fitness
1	5	-26	20	0	180	350	37.150	0.343	0.895	2.796
2	5	-34	20	13	220	350	20.950	0.471	0.902	7.531
3	5	-33	20	8	220	350	27.290	0.393	0.903	4.938
4	5	-34	5	20	220	350	9.972	0.635	0.860	15.140
5	5	-34	5	35	220	350	2.720	1.102	0.844	8.049
6	5	-34	5	10	220	350	20.260	0.435	0.868	8.168
7	5	-34	5	22	200	350	7.730	0.753	0.850	13.790
8	5	-34	5	21	220	350	9.227	0.682	0.858	14.560
9	5	-34	5	22	220	350	8.641	0.680	0.859	15.180
10	4	-34	10	1	220	350	45.300	0.236	0.908	1.925
11	5	-34	10	26	220	350	7.714	0.762	0.877	13.540
12	4	-34	10	1	180	350	41.630	0.297	0.899	2.257
13	5	-34	5	35	220	350	2.720	1.102	0.844	8.049
14	5	-33	5	13	200	350	15.790	0.532	0.860	10.920
15	3	-30	25	0	220	350	46.110	0.339	0.911	1.838
16	5	-33	20	30	220	350	5.160	0.939	0.890	10.450

The operating conditions and emissions results for the sixth iteration are given in Table 6.12. It can be noted from Case 5 that at a high EGR of 35%, though the NOx was lower, the PM emission was relatively high leading to a lower fitness value. This has led the optimization to choose lower EGR levels for the optimum.

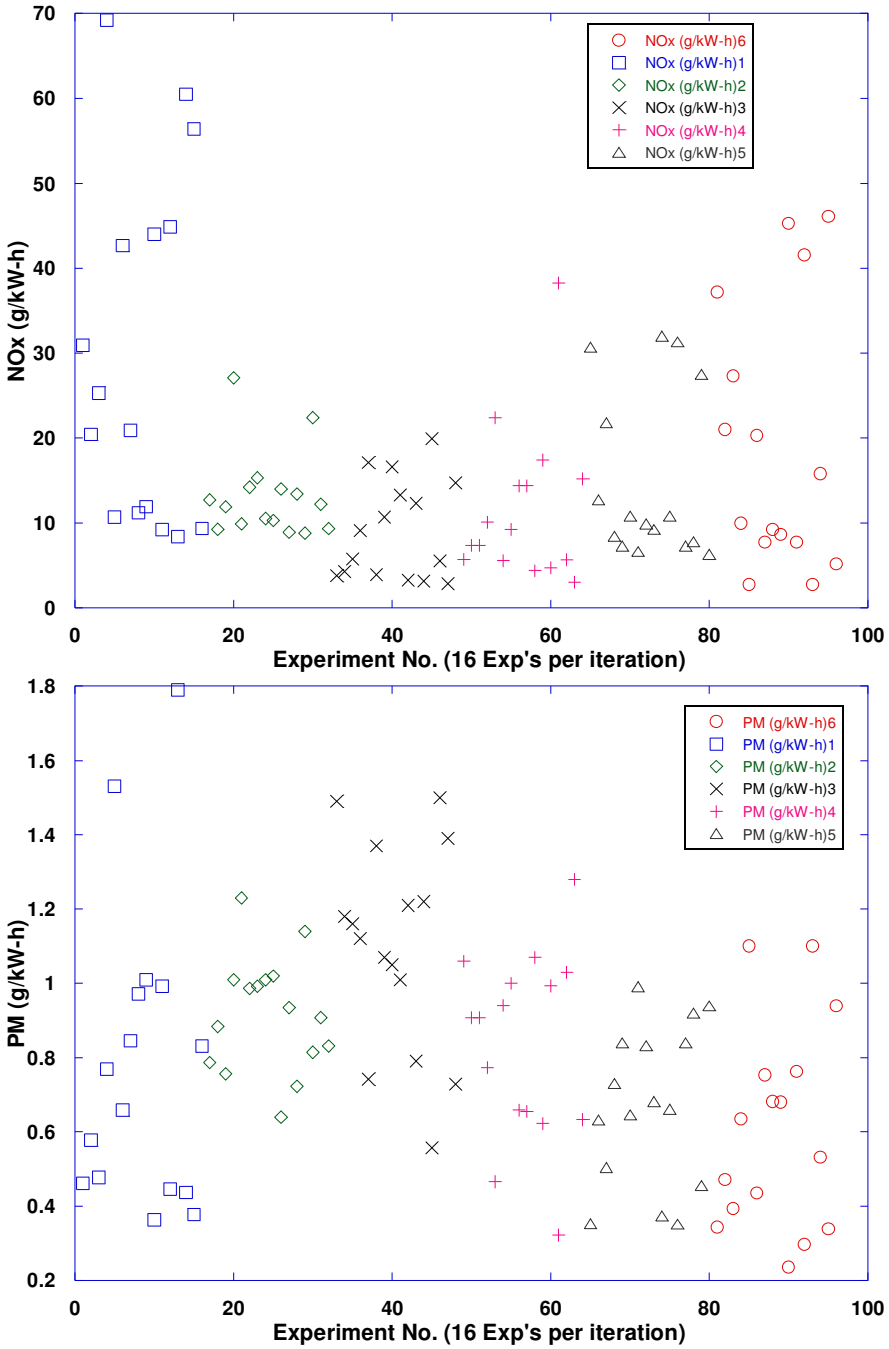

Figure 6.27 Evolution of NOx and PM emissions

Figure 6.27 shows the evolution of NOx and PM emissions. Both NOx and PM emissions were clearly reduced in iteration 6 over their levels in iteration 1. With the SOI near or after TDC, both NOx and PM have reduced considerably. However, the difference

between the simulation with the highest and lowest emissions is pretty high compared to the experimental results.

In summary, the present PSO algorithm was coupled with a 3-D engine simulation code for numerical optimization of engine performance. The trends in engine operating variables predicted by the optimization were consistent with those by the experimental results. Comparisons of operating conditions with experimental and numerical optimization are given in Table 6.13.

Table 6.13 Comparison of optimal operating conditions of experiments and simulations

Variable	Experimental	Numerical
Main SOI (ATDC)	4	5
Pilot SOI (ATDC)	-17	-34
EGR %	37	22
Pilot %	5	5

It can be seen that the numerical optimization also predicted the late main injections, high EGR levels for the reduction of emissions. It is worth noting that as the CFD model itself becomes more accurate in the future, the usefulness of numerical optimization will be greatly increased.

CHAPTER 7. CONCLUSIONS AND RECOMMENDATIONS

7.1 Strategies for Low Emissions

This study investigated diesel engine emissions characteristics under various injection conditions with different nozzle geometries. Several injectors with different flow number, geometry, and number of nozzles were tested.

With high EGR, low temperature combustion for simultaneous PM and NOx reductions can be achieved by two different injection strategies, namely 1) single injection using a late SOI, and 2) double injection using an early, small pilot injection with a late main injection.

For single injections at high EGR levels (around 30%), when the injection pressure is increased from 100 to 150 MPa, the late SOI limit can be extended from 0 to 5 ATDC. However, an injection pressure of 200 MPa does not further extend the late SOI limit beyond 5 ATDC. A high injection pressure can reduce PM emissions under the conventional SOI range (e.g., –20 to –5 ATDC) but does not provide further PM reduction for SOI at 5 ATDC.

For double injection conditions with 30% EGR, favorable PM and NOx emissions can be obtained by injecting 15% pilot fuel at an early timing (e.g., –30 ATDC) with a main SOI of 5 ATDC. When the injection pressure is increased from 150 to 180 MPa, the pilot SOI can be advanced to –40 ATDC for further PM reduction while maintaining a stable engine operation.

A converging nozzle with a K-factor of 3 allows the use of higher injection pressures due to a better flow coefficient. However, the benefits in overall emission reduction by using the present converging nozzles were not significant under the conditions tested in this study.

Injectors with lower flow numbers were able to produce low emissions at high EGR (>35%) and injection pressures (200 MPa) without delaying the SOI past TDC to prevent efficiency deterioration. Despite that the baseline (6X133X800), 10-hole (10X133X800), and convergent nozzle (6X133X800, K=3) injectors were able to produce low emissions, the engine efficiency was reduced at EGR levels higher than 30%.

The small nozzles in the 10–hole injector can produce small fuel drops for better atomization and mixing to reduce PM emissions. Better air utilization by using more nozzle holes (i.e. 10 holes) can also contribute to the reduction in NOx and PM emissions. However, the 16-hole injector produced relatively high PM emissions because the nozzles are crowded causing poor air utilization.

Reducing the flow number from 800 to 500 and 480 increased the maximum EGR that could be used without noticeable loss in engine efficiency. The low flow number injector also has the potential to further reduce NOx and PM emissions at 0 ATDC SOI. In the mean time, the BSFC can be maintained at a reasonable level.

7.2 Engine Optimization Using PSO

The PSO algorithm was implemented and tested for possible errors and was found to work correctly in optimizing sample mathematical functions. This was achieved by slightly modifying the code to find the global minimum of the test functions mentioned in Section 6.1. The code was able to find the global minimum satisfactorily.

The PSO algorithm was then integrated with engine testing to explore low emissions operating conditions. Both single-injection and double-injection strategies were optimized. To reduce multiple emissions simultaneously, a merit function was used. The merit function

was taken as a performance indicator. BSFC was also included in the merit function to ensure the fuel efficiency was taken into account.

In the single injection optimization, three variables, SOI, EGR, and injection presence, were optimized. Baseline injectors (6X133X800) were used during these experiments. The optimum operating conditions found were 31% EGR, 1 ATDC SOI, and 155 MPa injection pressure. The emissions at this point were 1.174 g/kW-h for NOx, 0.223 g/kW-h for HC, 0.0196 g/kW-h for PM, and 231 g/kW-h of BSFC. The optimum point was found in 7 iterations or 42 experiments.

In the double injection optimization, the optimization was performed at two different intake temperatures (23ºC and 40ºC) as intake temperature has a significant effect on engine emissions. Four design variables, main SOI, pilot SOI, pilot fuel amount, and EGR, were tested. The optimum for the low intake temperature optimization required 40 experiments or five iterations. The optimum was found at 37% EGR, 4 ATDC main SOI, -17 ATDC pilot SOI, and 5% pilot. The emissions at this point were 0.32, 0.026, 255 g/kW-h for NOx, PM, and BSFC, respectively. For the high intake temperature optimization, 64 experiments (8 iterations) were necessary to find the optimum. The optimum was found at 34% EGR, 5 ATDC main SOI, -24 ATDC pilot SOI, and 5% pilot fuel. The emissions at this point were 0.41, 0.0092, 8.51, 0.678, 249 g/kW-h for NOx, PM, CO, HC, BSFC, respectively. In both cases, optimization pointed to a very low pilot fuel which might have extended the main SOI from 1 ATDC in single injection cases to 4 ATDC for low intake temperature and 5 ATDC for high intake temperature optimizations. The optimization also successfully found that very high levels of EGR were useful in reducing both NOx and PM simultaneously. The

optimization has also correctly pointed out that the pilot SOI could not be too early as they may lead to very high PM emissions.

The PSO optimization was also integrated with an engine simulation code for numerical optimization. Both single injection and double injection optimizations were performed. In the single injection optimization, eight simulations were performed in each iteration. The optimum was found at 3 ATDC SOI, 32% EGR, 120 MPa injection pressure, and 340 K initial in-cylinder temperature at intake valve closure.

In the double injection optimization, the optimum was found at 5 ATDC main SOI, -34 ATDC pilot SOI, 5% pilot fuel, 22% EGR, and 220 MPa injection pressure. While EGR seemed low, trends for main SOI, injection pressure, and pilot fuel amount were correctly predicted. The numerical optimization was able to predict similar operating conditions to those in experimental testing. The PSO algorithm developed in this study was shown to be able to explore the optimal engine operating conditions effectively via both experiments and modeling.

7.3 Recommendations

The first recommendation is to optimize the low flow number injectors that have shown promise in reducing the engine emissions. Due to their differing characteristics, the low flow number injectors would have different and more favorable optimal conditions. It is expected that these injectors would increase the operating range of the given engine.

The second recommendation is to calibrate the engine simulation code for the low flow number injectors. Currently, the calibration is performed manually by observing the effect of various model constants and adjusting them accordingly. This process not only is

time consuming but also takes significant amount of human effort. In the future, perhaps PSO can be applied to the process of model calibration to automatically adjust the model constant. Once the calibrations are completed, the optimization can be applied to the simulations for new injectors. Additionally, a wide range of operating conditions can be included in the optimization to achieve enhanced performance and even lower emissions.

REFERENCES

1. DOT. 2008; Available from: http://www.fhwa.dot.gov/ohim/onh00/bar4.htm.
2. Ferguson, C.R. and A.T. Kirkpatrick, *Internal Combustion Engines*. 2000: John Wiley.
3. Exxon, M., *Annual Energy Outlook*. 2005.
4. Cohen, A.J. and M.W.P. Higgins, *Diesel Exhaust. A Critical Analysis of Emissions, Exposure, and Health Effects*. 1995, Health Effects Institute.
5. Bhatia, R.P., P. Lopipero, and A.H. Smith, *Diesel exhaust exposure and lung cancer.* Epidemiology, 1998. **9**(1): p. 84-91.
6. Godowitch, J.M., et al., *Modeling assessment of point source NOx emission reductions on ozone air quality in the eastern United States.* Atmospheric environment, 2008. **42**: p. 87-100.
7. Needham, J.R., D.M. Doyle, and A.J. Nicol, *The Low NOx truck engine*, in *SAE Paper*. 1991.
8. Senecal, P.K. and R.D. Reitz, *Simultaneous Reduction of Engine Emissions and Fuel Consumption Using Genetic Algorithms and Multi-Dimensional Spray and Combustion Modeling*, in *SAE Paper*. 2000.
9. Dieselnet. *Emission Standards: USA: Nonroad Diesel Engines*. 2008; Available from: http://www.dieselnet.com/standards/us/nonroad.php#tier3.
10. Miles, P.C., et al., *Rate-Limiting Processes in Late-Injection, Low-Temperature Diesel Combustion Regimes*, in *Proc. THIESEL 2004 Conference*. 2004. p. 429-447.
11. Heywood, J.B., *Internal combustion engine fundamentals*. 1988: McGraw-Hill.
12. Kamimoto, T. and M. Bae, *High combustion temperature for the reduction of particulate in diesel engines*, in *SAE*. 1988. p. 880423.

13. Ladommatos, N., S. Abdelhalim, and H. Zhao, *The effects of exhaust gas recirculation on diesel combustion and emissions.* Int. J Engine Research, 2000. **1**(1): p. 107-126.
14. Ladommatos, N., et al., *Effects of EGR on heat release in diesel combustion*, in *SAE Paper*. 1998. p. 980184.
15. Klingbeil, A.E., *Particulate and NOx reduction in a heavy-duty diesel engine using high levels of EGR and very early or very late start of injection*, in *Mechanical Engineering*. 2002, University of Wisconsin - Madison: Madison.
16. Klingbeil, A.E., H.R. Juneja, and R.D. Reitz, *Premixed diesel combustion analysis in a heavy duty diesel engine*, in *SAE Paper*. 2003. p. 2003-01-0341.
17. Pickett, L.M. and D.L. Siebers, *Non-Sooting, Low Flame Temperature Mixing-Controlled DI Diesel Combustion*, in *SAE Paper*. 2004. p. 2004-01-1399.
18. Minato, A., T. Tanaka, and T. Nishimura, *Investigation of Premixed Lean Diesel Combustion with Ultra High Pressure Injection*, in *SAE Paper*. 2005. p. 2005-01-0914.
19. Shimazaki, N., T. Tsurushima, and T. Nishimura, *Dual Mode Combustion Concept with Premixed Diesel Combustion by Direct Injection near Top Dead Center*, in *SAE Paper*. 2003. p. 2003-01-0742.
20. Karra, P. and S.-C. Kong, *Diesel Emission Characteristics Using High Injection Pressure with Converging Nozzles in a Medium-Duty Engine*, in *SAE Paper*. 2008. p. 2008-01-1085.
21. Montgomery, D.T., et al., *Effect of Injector Nozzle Hole size and Number of Spray Characteristics and the Performance of a Heavy-Duty D.I. Diesel Engine*, in *SAE Paper*. 1996. p. 962002.

22. Su, T.F., et al., *Effects of Injection Pressure and Nozzle Geometry on Spray SMD and D.I. Diesel Emissions*, in *SAE Paper*. 1995. p. 952360.

23. Bergwerk, W., *Flow Pattern in Diesel Nozzle Spray Holes.* Proc. Inst. Mech. Eng. , 1959. **173**: p. 655-660.

24. Arcoumanis, C. and M. Gavaises, *Linking Nozzle Flow with Spray Characteristics in a Diesel Fuel Injection System, Atomization and Sprays.* 1998. **8**: p. 307-347.

25. Tamaki, N., K. Nishida, and H. Hiroyasu, *Promotion of the Atomization of a liquid Jet by Cavitation in a Nozzle Hole.* Proc. ILASS, 1998. **98**: p. 218-223.

26. Challen, B. and R. Baranescu, *Diesel engine reference book 2nd edition*. 1999: Butterworth Heinemann.

27. Chaves, H., et al., *Experimental Study of Cavitation in the Nozzle Hole of Diesel Injectors Using Transparent Nozzles*, in *SAE Paper*. 1995. p. 950290.

28. Kong, S.-C., Y. Sun, and R.D. Reitz, *Modeling Diesel Spray Flame Lift-Off, Sooting Tendency and NOx Emissions Using Detailed Chemistry with Phenomenological Soot Models.* ASME J. Eng. Gas Turbines Power, 2007. **129**: p. 245-251.

29. He, L. and F. Ruiz, *Effect of Cavitation on Flow and Turbulence in Plain Orifices for High-Speed Atomization.* Atomization and Sprays. **5**: p. 569-584.

30. Knox-Kelecy, A.L. and P.V. Farrell, *Internal Flow in a Scale Model of a Diesel Fuel Injector nozzle*, in *SAE Paper*. 1992. p. 922308.

31. Nurick, W.H., *Orifice Cavitation and Its Effects on Spray Mixing.* J. Fluids Eng, 1976. **98**: p. 681-687.

32. Benajes, J., et al., *Analysis of Influence of Diesel Nozzle Geometry in the Injection Rate Characteristic.* J. Fluids Eng., 2004. **126**: p. 63-71.

33. Desantes, J., et al., *Experimental characterization of outflow for different diesel nozzle geometries*, in *SAE Paper*. 2005. p. 2005-01-2120.

34. Montgomery, D.T. and R.D. Reitz, *Six-Mode Cycle Evaluation of the Effect of EGR and Multiple Injections on Particulate and NO_x Emissions from a D.I. Diesel Engine*, in *SAE Paper*. 1996. p. 960316.

35. Pierpont, D.A., *An Experimental Study of the Effect of Injection Parameters and EGR on D.I. Diesel Emissions and Performance*, in *Mechanical Engineering*. 1994, University of Wisconsin: Madison.

36. Pierpont, D.A., D.T. Montgomery, and R.D. Reitz, *Reducing Particulate and NO_x Using Multiple Injections and EGR in a D.I. Diesel*, in *SAE Paper*. 1995. p. 950217.

37. Benajes, J., S. Lalina, and J.M. Garcia, *Influence of Pre-and Post-Injection on the Performance and Pollutant Emissions in a HD Diesel Engine*, in *SAE Paper*. 2001. p. 2001-01-0526.

38. Kreyszig, E., *Advanced Engineering Mathematics*. 8 ed. 1998: Wiley.

39. Thiel, M.P., A.E. Klingbeil, and R.D. Reitz, *Experimental Optimization of Heavy-Duty Diesel Engine Using Automated Genetic Algorithms*, in *SAE Paper*. 2002. p. 2002-01-0960.

40. Box, G.E.P. and N.R. Draper, *Response surfaces, mixtures, and ridge analyses*. 2007: Wiley.

41. Box, G.E.P. and N.R. Draper, *Empirical Model-Building and Response Surfaces*. 1986: Wiley.

42. Box, G.E.P. and P.Y.T. Liu, *Statistics as a Catalyst to Learning by Scientific Method Part I - An Example.* J. of Quality Technology, 1999. **31**: p. 1.

43. Montgomery, D.C., *Design and Analysis of Experiments*. 4 ed. 1996: Wiley.

44. Montgomery, D.T., *An Investigation Into Optimization of Heavy-Duty Diesel Engine Operating Parameters When Using Multiple Injections and EGR*. 2000, University of Wisconsin: Madison.

45. Montgomery, D.T. and R.D. Reitz, *Optimization of Heavy-Duty Diesel Engine Operating Parameters Using a Response Surface Method*, in *SAE Paper*. 2000. p. 2000-01-1962.

46. Goldberg, D.E., *Genetic Algorithms In Search, Optimization and Machine Learning*. 1989: Addison-Wesley.

47. Pilley, A.D., et al., *Design of Experiments for Optimization of Engines to Meet Future Emissions Targets*, in *27th Int. Symposium on Automotive Technology and Automation*. 1994.

48. Thiel, M.P., *Application of automated experiments to the optimization of a heavy-duty direct injected diesel engine for the simultaneous reduction of NOx and particulate emissions*, in *Mechanical Engineering*. 2001, University of Wisconsin-Madison: Wisconsin.

49. Liechty, M.P., *Optimization of heavy-duty diesel engine operating parameters at high speed and medium load using μ-genetic algorithms*, in *Mechanical Engineering*. 2004, University of Wisconsin, Madison: Wisconsin.

50. Kennedy, J. and R. Eberhart, *Particel Swarm Optimization.* IEEE, 1995. **95**: p. 1942-1948.

51. Davis, L., *Handbook of Genetic Algorithms*. 1991, NY: Van Nostrand Reinhold.

52. Heppner, F. and U. Grenander, *A stochastic nonlinear model for coordinated bird flocks. In S . Krasner, Ed., The Ubiquity of Chaos.* AAAS Publications, 1990.

53. Reynolds, C.W., *Flocks, herds and schools: a distributed behavioral model.* Computer Graphics, 1987. **21**(4): p. 25-34.

54. Shi, Y. and R. Eberhart, *A Modified Particle Swarm Optimizer*, in *Proceedings of the 1998 IEEE International conference on Evolutionary Computation*. 1998: Piscataway, NJ. p. 69-73.

55. Shi, Y. and R. Eberhart, *Parameter Selection in Particle Swarm Optimization*, in *Proceedings of the 7th International Conference on Evolutionary Programming*. 1998. p. 591-600.

56. Kim, M., R.D. Reitz, and S.-C. Kong, *Modeling Early Injection Processes in HSDI Diesel Engines*, in *SAE Paper*. 2006. p. 2006-01-0056.

57. Kitamura, T., T. Ito, and H. Fujimoto, *Mechanism of smokeless diesel combustion with oxygenated fuels based on the dependence of the equivalence ratio and temperature on soot particle formation.* Int J Engine Research, 2002. **3**(4): p. 223-248.